Report No. CER-826
Part II
Copy No. 17

PART II

FINAL ENGINEERING REPORT
ON
WIND TUNNEL TEST STUDY (U)

1 June 1958

DA-44-177-TC-448 P.O. DEE-10017

Covering Period from 1 April to 16 May 1958

COLLINS AERONAUTICAL RESEARCH LABORATORY
A. M. Lippisch, Director
Cedar Rapids, Iowa

71

A PUBLICATION OF

THE AERONAUTICAL RESEARCH LABORATORY

COLLINS RADIO COMPANY

Cedar Rapids, Iowa

Printed in the United States of America

FINAL ENGINEERING REPORT
ON
WIND TUNNEL TEST STUDY

1. INTRODUCTION.

This report presents the results of the work done by the Collins Aeronautical Research Laboratory on the Chrysler aerial research vehicle during the period from 1 April 1958 to the termination of contract date, 16 May 1958.

This report, together with Part I of the final report, covering the period of 25 January 1958 through 31 March 1958, represents the results of all the experimental work done on the Chrysler aerial research vehicle. Insofar as the experimental apparatus and the test procedures described in Part I were typical of the work in both periods, this information is not repeated in this report.

The complete list of symbols is included in paragraph 2 of this report.

The test results have been arranged in three sections and the discussion of these results appears in the body of this report in the following order:

(a) Devices to reduce the nose up pitching moment in forward flight.

(b) Determination of trim points, and stability and control work.

(c) Miscellaneous tests.

During all of the testing in this report the original control vanes were in position #2 (see figure 4 in Part I). In all of the drawings appearing in this report the forward end of the model is to the left of the figure; the forward end is to the right in all of the photographs.

Figures 1 and 2 in the first part of section 5 are detailed sketches of the equipment, applicable to the full scale, used on the model to obtain the final set of performance data. This arrangement of trim and control devices represents only one of several possible arrangements, any one of which may be a practical solution to the general performance problem.

Figures 57-65 present the results of the flow visualization studies made on several different configurations. The smoke does not present as complete a picture as is desirable, but does allow some general conclusions to be drawn from the position of the streamlines.

2. IDENTIFICATION OF SYMBOLS.

The symbols used in this report may be identified by referring to the following list.

Symbol	Dimensions	Definition
C	lb	Side force
$C_C = \frac{C}{\rho u^2 S}$		Side force coefficient in hovering
$C_D = \frac{D}{\rho u^2 S}$		Drag coefficient in hovering
$C_L = \frac{L}{\rho u^2 S}$		Lift coefficient in hovering
$C_l = \frac{L'}{\rho u^2 S d}$		Rolling moment coefficient in hovering
$C_m = \frac{M'}{\rho u^2 S d}$		Pitching moment coefficient in hovering
$C_n = \frac{N'}{u^2 S d}$		Yawing moment coefficient in hovering
D	lb	Drag
$K_D = \frac{D}{q_o S}$		Drag coefficient for forward flight
$K_L = \frac{L}{q_o S}$		Lift coefficient for forward flight
$K_N = \frac{N}{q_o S}$		Normal force coefficient for forward flight
$K_l = \frac{L'}{q_o S}$		Rolling moment coefficient for forward flight
$K_m = \frac{M'}{q_o S}$		Pitching moment coefficient for forward flight
L	lb	Lift

Symbol	Dimensions	Definition
L'	lb/ft	Rolling moment
M'	lb/ft	Pitching moment
N	lb	Normal force
N'	lb/ft	Yawing moment
S	ft^2	Area of the two shrouds combined measured in the plane of the propellers
d	ft	Diameter of the shrouds measured in the plane of the propeller
e	ft	Distance of the normal force from the C.G. (+ forward)
n	RPM	Revolutions per minute of the propellers
n'	RPS	Revolutions per second
q_o	lb/ft^2 and kg/m^2	Dynamic pressure of the air from wind tunnel (measured)
q_1	lb/ft^2 kg/m^2	Dynamic pressure of the slip stream of the propeller
r	ft	Radial distance from propeller axis to blade section
u	ft/s	Propeller tip speed
v_o	ft/s	Tunnel speed reduced to standard sea level condition
v_a	ft/s	Axial air speed through propeller
v_T	ft/s	Tangental velocity of blade section of propeller
θ	degrees	Angle of pitch of the model
α	degrees	Effective angle of attack of a section of the propeller
δ	degrees	Deflection angle of the vanes
δ_c	degrees	Angle of cascade (See figure 2)
δ_L	degrees	Angle of louvers (+ upward from plane of inlet)
δ_F	degrees	Angle of flap (+ upward from plane of inlet)

Symbol	Dimensions	Definition
ϑ	degrees	Angle between the chord of the propeller blade section and the plane of rotation
ϑ_0	degrees	Angle of blade setting of the propeller at the hub
ρ	lb s^2/ft^4	Air density during the test
ϕ	degrees	Effective pitch angle of the propeller
ω	radians/s	Angular velocity of the propeller

3. DISCUSSION OF TEST RESULTS.

3.1 DEVICES TO TRIM NOSE UP PITCHING MOMENT IN FORWARD FLIGHT.

This section of the report deals with the work directed toward reducing the forward shift of the center of pressure during the transition from hovering to forward flight. This shift in the center of pressure is expressed in figure 5 as Δ e/d. In this expression e is the location of the normal force forward(+) or aft (-) of the c.g., and d is the propeller diameter. The ideal solution to this problem (disregarding its effect upon the stability) would have been a stationary device which made Δ e/d = 0 with a minimum reduction in operating efficiency.

The effect of the various devices on the operating efficiency of the model is expressed in the tables as $\frac{LIFT^{3/2}}{WATT}$. This term, which can be derived from momentum theory, is a measure of the efficiency of a given configuration in hovering flight.

The configurations shown in figure 3 were tested during the period in which the original inlets were being replaced by the new inlets. These configurations represent various arrangements of four different shroud inlets: (1) no inlet, (2) 7/8" cylinder, (3) original inlet, (4) new inlet. A detailed cross section of each of these four inlets is shown in figure 4. The results of the tests are presented in table form in figure 5. In all the subsequent tests the new inlets had been permanently attached.

The configurations shown in figure 6 represent the first efforts to attempt to reduce the e/d shift by a device above the inlet plane. The results of these tests are presented in table form in figure 5. While these configurations did little to reduce the e/d shift in the fixed position, the tests showed that a shape similar to that in figure 6-(4) could prove to be a very effective method of pitch control if the angle or position of the flap could be varied during flight.

The next attempts at reducing the nose up moment were those illustrated in figure 7. These devices represent various arrangements of sheet metal cylinders placed so that the inside wall of the cylinder was flush with the inside wall of the shroud. These cylinders represent essentially an inlet extension. The original cylinder in figure 7-(1) was constructed so that the upper edge was 3" above the inlet. This cylinder was then cut in two which provided two tapered cylinders, each with the minimum edge height flush with the inlet and the maximum edge height 2-1/2" above the inlet. Several photos were taken of the configurations used during these tests and appear in figures 8 through 14. The corresponding results for these configurations are presented in figure 5.

Figures 15, 16 and 17 represent one of the first attempts to determine the effects of the external air flow in reducing e/d shift for extended fuselage plan forms. The results of these tests shown in figure 5 were encouraging and indicated that the configuration shown in figure 15-(2), with some modifications, might provide a zero e/d shift.

Figure 18 represents a number of configurations of which some are similar to ones already tested, others are new approaches. Figures 19 and 20 are photographs of the configurations in figure 18-(1) and (8) respectively. The configurations shown in figure 18 all included a set of ten cascade vanes downstream of the impeller in the front shroud. For a more detailed view of the cascades see figures 1 and 2.

The first set of runs (figure 18-(1)) was obtained by reducing the nose extension in 1" increments. The first of these runs was a duplication of the runs for which figure 15-(2) was the configuration. See figure 5 for results.

The runs illustrated by figure 18-(2), (3) and (4) were all variations of a previous run (see figure 6-(1)) in which the domed plate was 1/2" above the inlet. The results of these runs are presented in figure 5.

In figure 18-(5) the large nose plate was placed as it had been before (see figure 18-(1)), however, the radius "R" in this case was increased to 11-1/2". This test was run because a plot of $\Delta e/d$ for various extension increments (see figure 21) had shown that a 6" extension should make the e/d shift from hovering to forward flight (-20° pitch) go negative. This theory was borne out in the ensuing tests (see figure 5).

The line of reasoning that had been followed in all of the previous tests was based on the thought that if a device could be found which would provide a zero e/d shift between the hovering case and the forward flight case*, the problem of the large nose up pitching moment would be solved. Since the configuration last mentioned above (figure 18-(5)) yielded not only a zero shift but a negative shift in e/d between these two points, there was strong feeling at the time that this configuration was the solution to the problem. However, spot checks of the value of e/d at various other pitch angles indicated that this optimism was not well-founded. The configuration tested was similar to that shown on figure 18-(5); however, 1" had been removed from the sides of the plates. (See figure 18-(6)). The results of this series of tests are shown in figure 22 (the lower curve). The large variation of e/d with θ immediately indicated a very undesirable situation. This variation together with the fact that there was a large portion of the curve which maintained a strong destabilizing tendency led to the decision that this plate had to be altered in order to perform satisfactorily.

The other two configurations shown in figure 18-(6) were then tested through the range of pitch angles. The results of these tests (figure 22) were not more promising. Figure 18-(7) represents the configuration tested to determine the absolute maximum nose down moment which could be obtained by a combination of three previously tested configurations (flat plate

*A typical attitude representative of the forward flight case had been arbitrarily chosen as a pitch angle of -20°.

above inlet, 6" flat plate extension on nose, and cascade set at 45°). The results of this test are plotted in figure 23. The configuration shown in figure 18-(8) was spot checked at hovering and at 20° pitch angle to determine the effects of the fuselage on moment, lift, etc. The results of this test are shown in figure 5.

The final attempt at reducing the nose up tendency was the configuration shown in figures 24 and 25. The results of these tests are plotted in figure 26.

3.2 BASIC PERFORMANCE, AND STABILITY AND CONTROL WORK.

The object of the runs described in this section of the report was to obtain basic performance and stability and control data for preselected configurations. A summary of the pertinent information contained in the three subparagraphs of this section is listed in table I below.

TABLE I. SUMMARY OF PARAGRAPH 3.2

Title	Performance Work (D=0)	Moment Control	Power Req'd Data*	Cascade	Stability Work
3.2.1 Performance and Stability of New Shrouds	Yes	No	Yes	No	Yes
3.2.2 Performance of New Shrouds with Moment Control	Yes	Yes	Yes	No	No
3.2.3 Performance and Stability and Control of New Shrouds w/Cascades	Yes	Yes	No Yes	Front & Rear Front only	No Yes

*Refers to several runs, for the particular configuration, in which the lift was maintained constant and the power required for steady horizontal flight was measured.

The new inlets were installed on the shrouds permanently for these and all subsequent runs. Also the outer shape of the shrouds had been faired in to provide a clean external flow (figure 27). The control vanes had been placed in position #2 and remained in the undeflected state during all of the runs in this section.

3.2.1 PERFORMANCE AND STABILITY OF NEW SHROUDS.

The work in this area was performed in order to evaluate the effect a new inlet had on the performance and stability of the model. (See figure 27-(1).) The tests to obtain the performance data were run first. The data were obtained by measuring the lift, side force and moments for the condition of D = 0 for any one pitch angle and tunnel speed setting. The performance data were obtained for a range of pitch angles from 0° to -37.5°. The power required to maintain a constant value of lift at each of these angles was then obtained (figure 28). Using these performance data as reference points, the stability data were obtained for two increments on each side of each of these points. The results of this work are plotted in figures 29 through 33. For a more thorough discussion of the method of obtaining the performance and stability data refer to Part I of the final report, paragraph 4.

In the final phase of this area, the work was concerned with recording performance and power required data for the abreast configurations. (See figure 27-(2).) No stability work was done for this configuration. The results are plotted in figure 34. It should be noted here how the power required curve for the abreast attitude falls below that of the tandem attitude.

3.2.2 PERFORMANCE OF NEW SHROUDS WITH MOMENT CONTROL.

The work discussed in this section represents the first time that performance data had been obtained under trim conditions (M = 0). Since previous investigations had suggested that a fairly large, flat plate placed above the shroud inlet could possibly be used to trim the pitching moment to zero in forward flight, the effectiveness of this configuration was tested during the first part of the work in this section. The angle of the plate was adjusted at each pitch angle to a setting at which the pitching moment became zero. It was felt at this time that such a vane might represent a possible pitch control scheme. A drawing which represents typical attitudes of the model with the pitch control vane set to trim the moment is shown in figure 35. The plate proved to be successful in reducing the pitching moment to zero at all attitudes. The results of this series of runs are plotted in figure 36.

At this time, a pitch control system which appeared to be closer to a practical solution than the flat plate was designed and constructed. This system contained four 3/4 inch louvers cut out of a plan form which was identical to the flat plate tried above. Each of the louvers was hinged at the trailing edge and could be adjusted to any angle. The whole system was placed 1/2" above the inlet plane as the previous plate had been, and each louver was adjusted to comparable angles through all the tests. Figure 37 shows the model at typical attitudes with the louvers adjusted to produce M = 0 in each case. Performance data for the trim case were obtained with this configuration and appear in figure 38. A point of interest here is that the individual louvers had to be set to approximately the same angle as the single flat plate in order to zero out the moment at each pitch angle.

3.2.3 PERFORMANCE AND STABILITY AND CONTROL OF NEW SHROUDS WITH CASCADES.

The configuration tested in this phase included a set of cascade vanes, ten in each shroud, which were designed to deflect the flow 30° in the neutral position. A detail drawing of these vanes appears in figure 2.

The first series of points was obtained by adjusting the cascades in both shrouds to the undeflected position (δ_c = -6°), adjusting the pitch control louvers until M = 0, and running the tunnel speed up until D = 0. The pitch control louvers had been augmented by one more louver for these and the succeeding tests. See figure 39-(1) for a typical setting. Data were obtained through the full range of pitch angles from 0° to 37.5°. Next, the cascade angle was readjusted to δ_c = +15° and the trim performance data again determined. At the end of these last runs it was apparent that due to the strong nose up moment produced by the two cascades, the set of five pitch control louvers would not be sufficient to control the moments on the model so that further testing with this configuration was halted. A drawing of a typical model attitude during these runs appears in figure 39-(2). Figure 40 shows the variation of δ_L and K_L vs. θ for the trim conditions and the two different cascade settings. Figure 41 shows the effectiveness of the louver deflection for pitch control at a typical attitude.

The next series of runs was made to determine the performance points (D = 0), with no attempt to trim the model (M = 0), through the full range of pitch angles for each of three different cascade settings (δ_c = -6°, +15°, +45°). A drawing of the three cascade angle settings for these runs appears in figure 42. The results of these tests appear in figure 43.

At the conclusion of the testing discussed above, it was decided to remove the cascade from the rear shroud as a compromise between an increase in the deflection angle for one case and a decrease in the pitching up moment in the other case. A series of runs were then performed identical to the preceding series, the only difference being that the cascade in the rear had been removed. The plot of these results is shown in figure 44.

The final performance and stability and control work was performed on a configuration which represented a combination of schemes in addition to the basic shroud design, each of which served a specific function: (1) the fuselage, necessary to provide cargo and pilot compartments, (2) the cascade in the front shroud, necessary to reduce the angle at which a prototype may cruise at a given velocity, and (3) the control louvers, necessary to trim the pitching moment to zero at any attitude and further, to provide continuous pitch control.

This configuration represents a layout which could be used in the prototype to make it flyable. A photograph of the model with the configuration which contained all of the above schemes, and for which the rest of the stability and performance data in this section were obtained is shown in figure 45. The louvers on the rear shroud were added to duplicate a system which may be necessary to control the full scale in hovering. These louvers remained stationary with δ_L = 90° during all the testing.

The performance points were determined first based on a flight program which would follow in this order: (1) hover and/or vertical flight to sufficient altitude, (2) gradual increase in cascade angle from -6° to +45° still maintaining zero pitch angle, (3) finally increase pitch angle until maximum forward speed is attained. The results of these trim performance points are presented in figure 46. This graph presents all performance data, including power data, versus tunnel speed as the abscissa, and represents the transition flight program outlined

above. (It should be pointed out here that it was necessary to [illegible] that the overall efficiency of the electrical motors remained constant in order to pres[illegible]ver data as shown. This was felt justified within reasonable limits for such small variation in input power.)

The stability work for this configuration was run around three of the above performance points. Data were obtained for the variation of coefficients with both pitch angle (θ) and forward speed (V_o). The results of these tests are plotted in figures 47 and 48.

4. MISCELLANEOUS TESTS.

The tests included in this section in most cases were run as points of specialized interest developed during the scheduled testing program and, therefore, are presented in chronological order and not necessarily in the order of significance.

4.1 VARIATION OF MOMENT WITH VELOCITY.

This series of runs was made with the model in the horizontal $\theta = 0°$ attitude, with no additional devices on the model, and roll and pitch vanes in neutral position. The propeller speed was held constant and the tunnel speed was varied from 0 to 30.8 feet per second. This test was desired to observe the variation of pitching moment in the hovering attitude with the wind speed. The results of this test are plotted in figure 49.

4.2 MOMENT CONTROL WITH PROPELLERS.

The purpose of this test was to determine the practicability of adjusting the propellers to obtain zero pitching moment at a high forward speed and pitching attitude and then using the flat plate pitch control vane above the rear inlet to zero out the pitching moment in the hovering attitude. The pitch of the front propeller was adjusted to 26.75° at the hub, this allowed the moment at $\theta = 30°$ with no additional control device added to become negative as shown in table 2 below. The model was then set in the hovering attitude and the 3" flat plate added 1/2" above the rear shroud to attempt to reduce the moment to zero. A drawing of the arrangement for the hovering case is shown in figure 50-(1). This particular plate was not quite large enough to completely remove the moment. The plate was then lowered to 1/4" above the shroud inlet, resulting in a small decrease in moment. The significant data obtained from this test are included in table 2.

TABLE 2. RESULTS OF DIFFERENTIAL PROP PITCH TESTS

Data Point	θ	δ_L	Height Above Inlet	n	Drag	e/d	$\frac{P_{flt}}{P}$ Hover At 1600 Kg	$\frac{P_{(8)}}{P}$ With no Control
(1)	(2)	(3)	(4)	(5)	(6)	(7)	(8)	(9)
571	-30°	Not on	Not on	6755	0	-.065	.85	.95
572	0°	0°	1/2"	6600	-42 gm	-.040	N.A.	---
573	0°	0°	1/4"	7075	-39 gm	-.025	1.00	1.22

4.3 ADDITIONAL POWER FOR CONTROL.

The purpose of this test was to obtain data on the additional power required to provide 50% more control than that necessary to trim out the model at -25° angle of pitch. The 50% additional control was to be obtained at the same propeller speed and tunnel speed as those occurring at the trim condition. The moment which occurred on the model at -25° pitch with no pitch control at 1.60 kg of lift and zero drag was +0.35 ft/lb.* The model was placed at -25° pitch and the 3" flat plate placed above the front inlet at $\delta_F = 0$. The propeller and tunnel speed were run up until the lift equalled 1.60 kg and the drag was zero. The pitching moment was approximately zero under these conditions. The power was recorded for this configuration. Then a 1" extension was added on the rear of the 3" flap to provide for approximately 50% more nose down control than that occurring in the trim case. The tunnel and propeller speed were both adjusted to the same setting as those previously determined from the trim case. At these settings, the power was again recorded. A summary of the important information obtained in these runs appears in table 3. A sketch of the configuration tested appears on figure 50-(2).

*Estimated from previous tests.

TABLE 3. RESULTS OF 50% OVERCONTROL TESTS

Data Point	Lift (kg)	Moment (ft/lb)	Drag (kg)	Power (watts)	n	V_o (ft/s)	Configurations
Esti-mated	1.60	+.35	0	345	---	19.7	Plain new shrouds No controls.
591	1.60	0	0	386	6450	19.0	Same as above with 3" flat plate 1/2" above front inlet.
592	1.51	-.15	.034	386	6450	19	Same as above with 4" flat plate 1/2" above front inlet.

4.4 GROUND EFFECTS.

This series of runs was performed to determine the effect the presence of the ground made on the lift of the model. The model had no trim devices attached, and the cascade in the front shroud was adjusted to the zero deflection position (δ_c = -6°). All the data were obtained for the hovering case. The ground was simulated by a 4' x 8' sheet of 3/4-inch plywood approximately centered below the model. (See figure 51.) The results of this test appear in dimensionless form in figure 52. The large flat extended fuselage was added to obtain the data for data point 735. A photograph of the test arrangement for this run appears in figure 53.

4.5 ROLL VANE EFFECTIVENESS.

The purpose of this test program was to determine the roll vane effectiveness (the vanes being in position #2) for the final model configuration. The first series of runs was performed with forward speed. The pitch angle was -10°, the cascade setting was δ_c = +45°, the louvers above the front inlet were set at δ_L = 19° so that M = 0 , and the fuselage with wind shield was attached. The tunnel and propeller speeds were set at the values which yielded D = 0 and L = 1.60 kg. The roll vanes were then deflected positively from 0° in 10° increments. The results of these tests are plotted in figure 54.

The second series of runs was performed in the hovering attitude. The cascade in the front shroud, and the fuselage with wind shield had been removed for this test. All that remained attached to the model were the new shrouds and the roll vanes. This series of runs represents

the only vane effectiveness tests in which comparisons could be made between results with the original shrouds and with the new shrouds. The results of these runs appear in figure 55.

4.6 C_L VARIATION WITH PROPELLER SPEED.

This test was performed to determine how the lift coefficient for the hovering case varied with the propeller speed through a wide range of speeds. The model contained no vanes or control devices of any kind during these runs. The low speed was 2000 rpm and the speed was increased in 1000 rpm increments to a top speed of 7000 rpm, representing an increase in speed of 350%. The results of this test are plotted in figure 56.

4.7 FLOW VISUALIZATION STUDIES.

Photographs obtained from the smoke flow visualization studies appear in figures 57 - 65. These studies were made on three basic configurations, each one at three different attitudes. Table 4 lists the important data pertaining to each model attitude and configuration.

TABLE 4. SUMMARY OF DATA FOR FLOW VISUALIZATION PHOTOS

Fig. No.	θ	Cascade Angle	Louver Angle	V_o (ft/sec)	n	Drag	Moment
57	0	-6°	---	0	---	0	70
58	-10	-6°	---	9.3	5910	0	70
59	-30	-6°	---	14.3	4330	0	70
60	0	-6°	+68°	0	6090	0	0
61	-10	-6°	+32°	9.3	6090	0	0
62	-30	-6°	+18°	14.3	4380	0	0
63	0	+45°	---	9.3	6260	0	70
64	-10	+45°	---	14.3	5810	0	70
65	-30	+45°	---	21.7	4860	0	70

5. ILLUSTRATIONS.

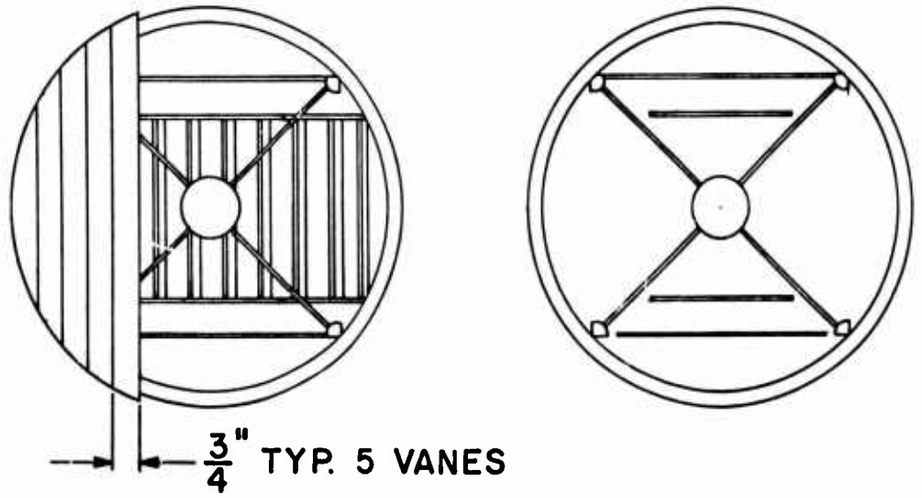

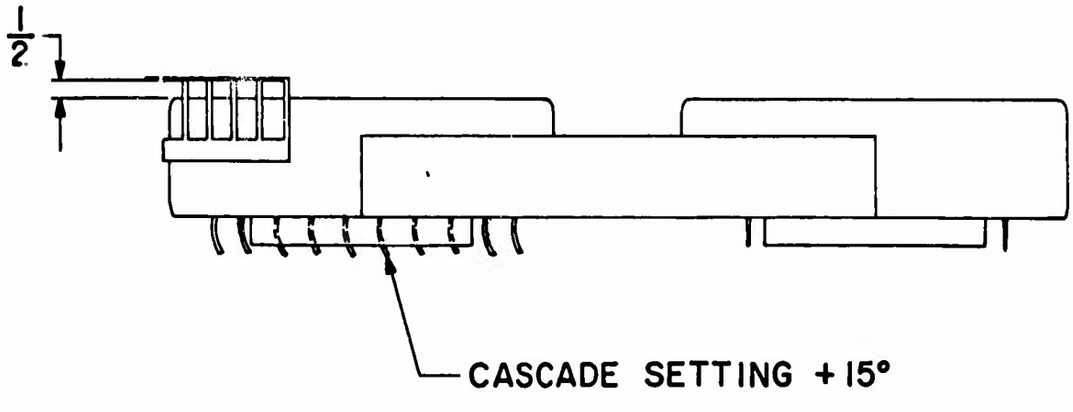

Figure 1. Detail Drawing of Louvers and Roll Vanes

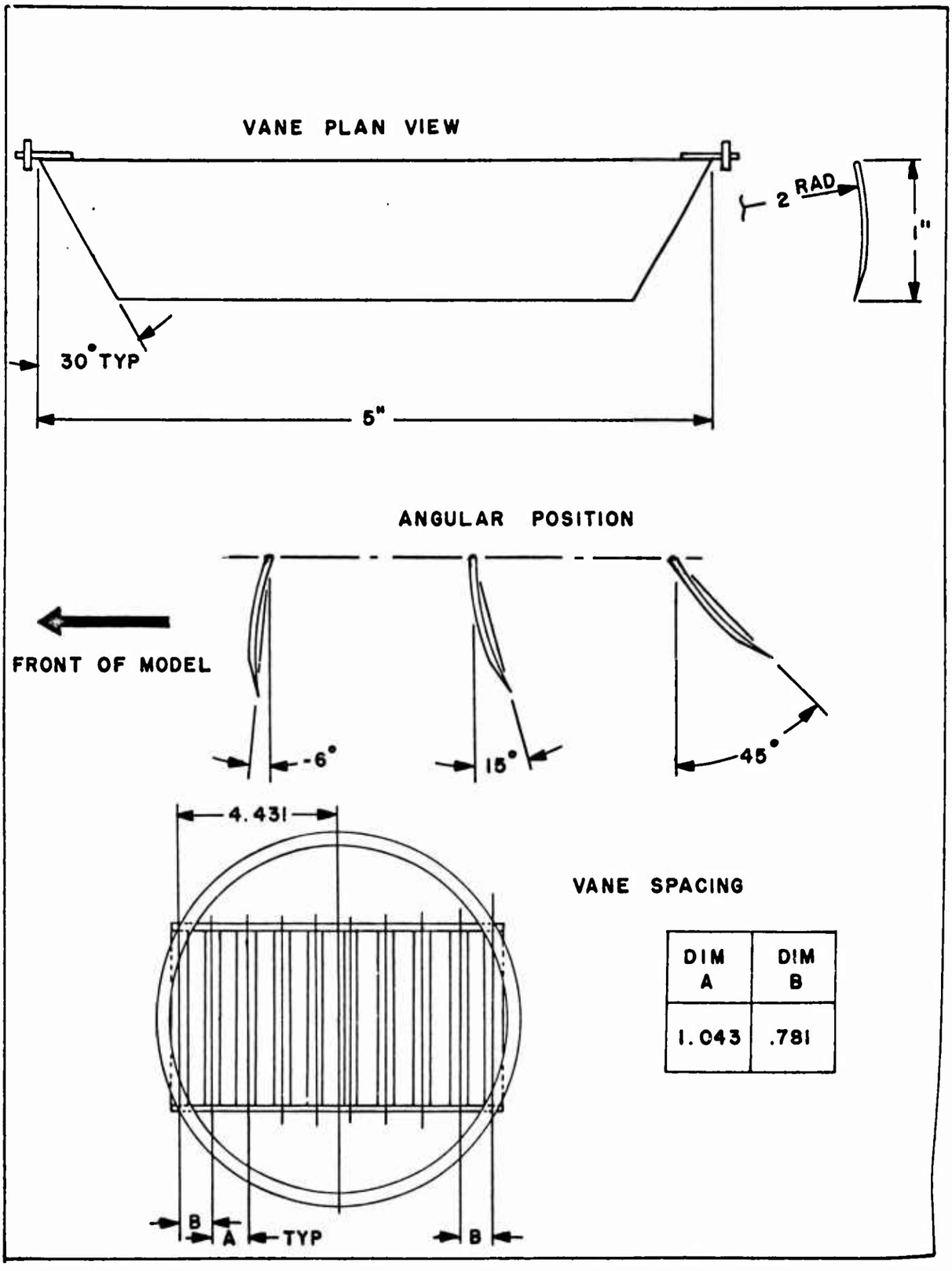

Figure 2. Detail Drawing of Cascades

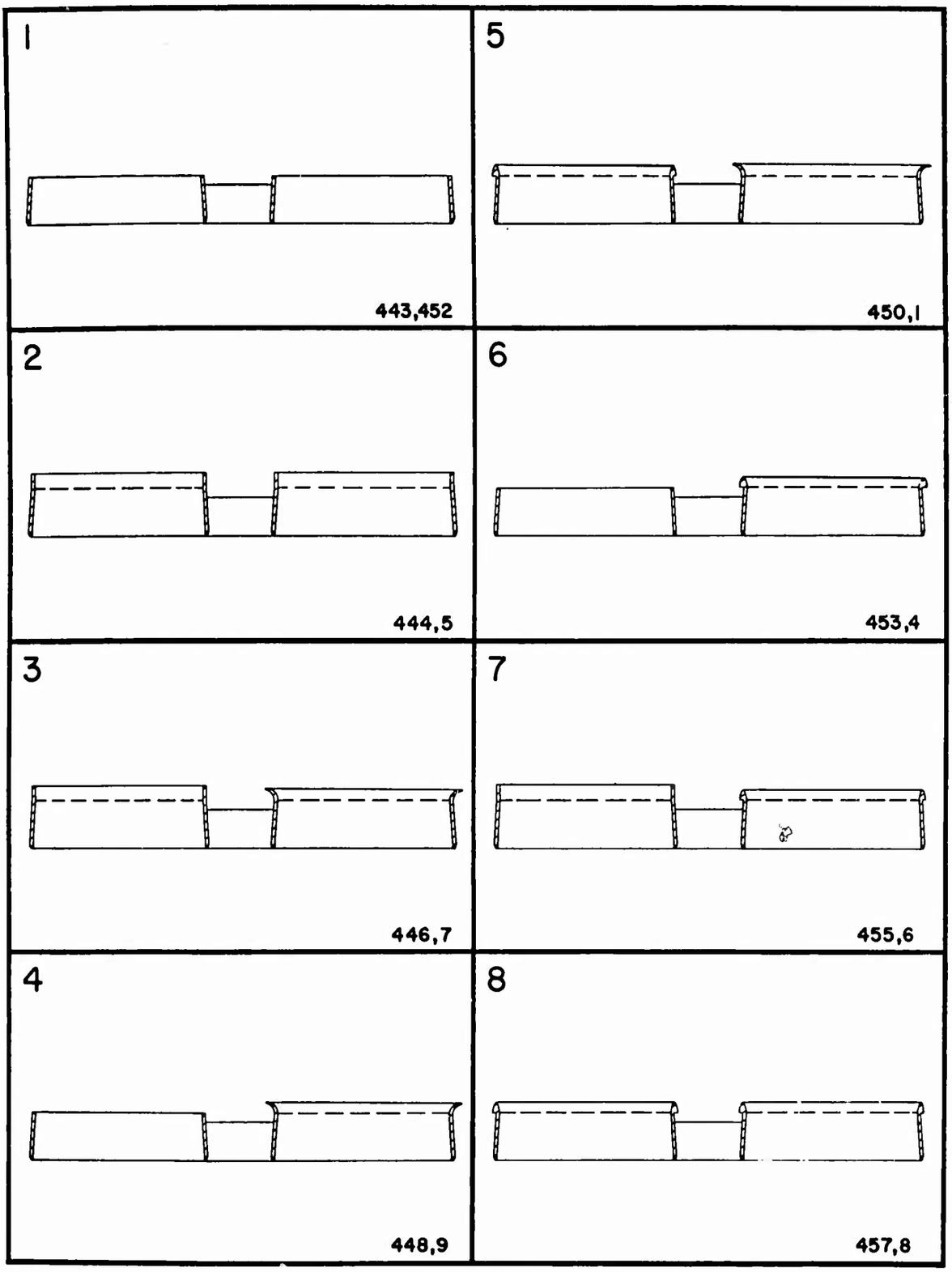

Figure 3. Drawings of Various Inlet Geometries Tested

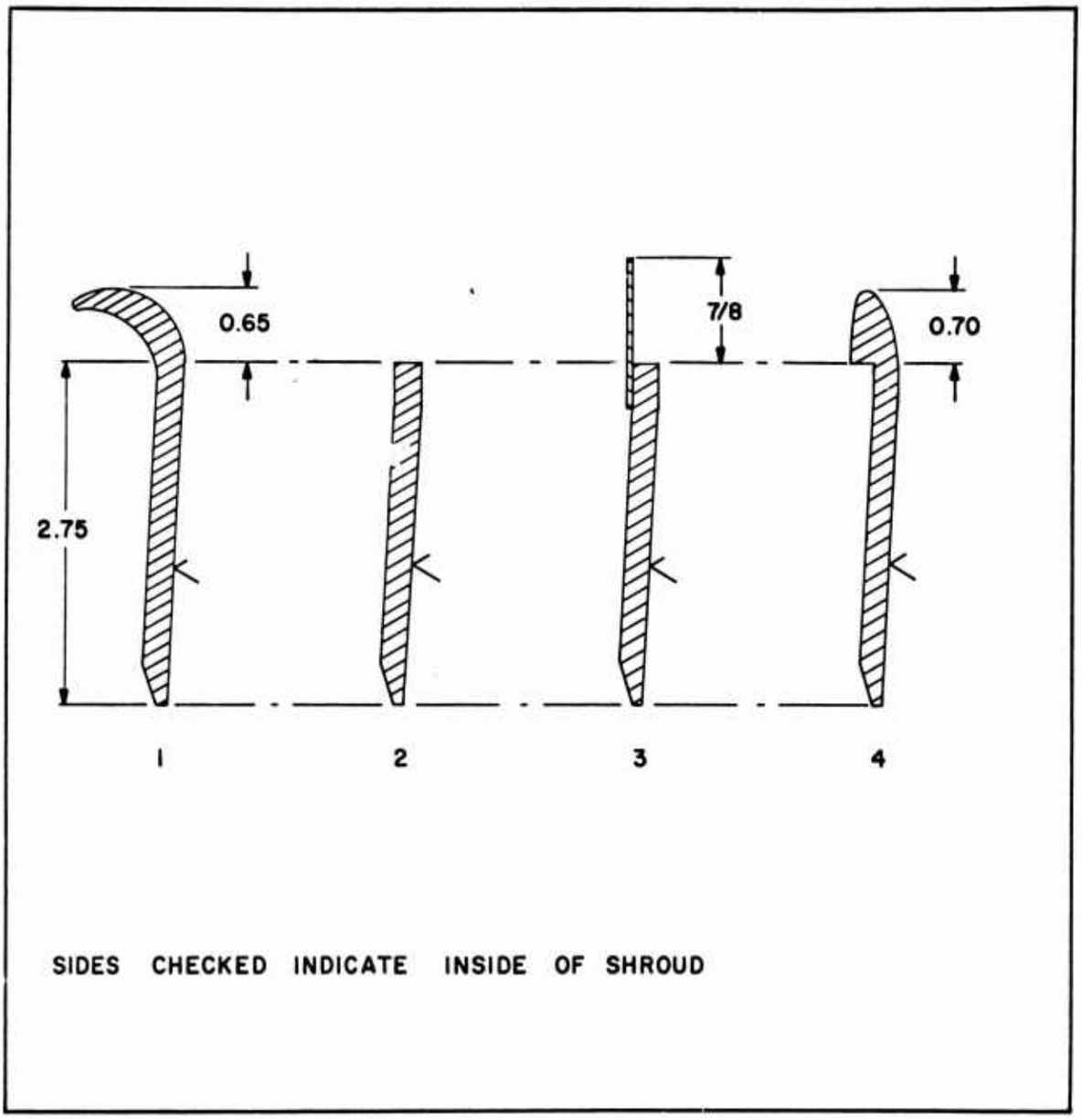

Figure 4. Detail Drawings of Inlets Tested in Figure 3

FIGURE No.	DATA POINT	θ (°)	n (rpm)	q_o (kg/m²)	LIFT (kg)	POWER INPUT (watts)	$\frac{L^{3/2}}{P}$	e/d	Δ e/d
3-(1)	452	0	6395	0	1.609	374	5.45×10^{-3}	+.009)	+.038
	443	-20	6395	1.95	1.594	376	5.38 " "	+.047)	
3-(2)	444	0	6580	0	1.611	381	5.38 " "	+.0068)	+.1037
	445	-20	6470	1.37	1.603	385	5.25 " "	+.1105)	
3-(3)	446	0	6210	0	1.592	321	6.25 " "	-.0804)	+.1364
	447	-20	6250	1.32	1.604	338	6.04 " "	+.056)	
3-(4)	448	0	6160	0	1.602	325	6.25 " "	-.055)	+.1047
	449	-20	6230	1.60	1.605	341	6.00 " "	+.0497)	
3-(5)	450	0	6020	0	1.603	298	6.80 " "	-.0168)	+.1258
	451	-20	6090	1.40	1.599	320	6.30 " "	+.109)	
3-(6)	453	0	6230	0	1.602	345	5.88 " "	-.046)	+.095
	454	-20	6265	1.57	1.604	350	5.81 " "	+.049)	
3-(7)	455	0	6300	0	1.603	342	5.92 " "	-.054)	+.121
	456	-20	6300	1.30	1.600	350	5.79 " "	+.067)	
3-(8)	457	0	6070	0	1.598	312	6.50 " "	+.0015)	+.1045
	458	-20	6105	1.38	1.602	324	6.25 " "	+.106)	
6-(1)	460	0	5000	0	.902			-.211)	+.096
	459	-20	5000	.63	.877			-.115)	
6-(2)	461	0	5000	0	.926			-.125)	+.065
	462	-20	5000	.68	.917			-.06)	
6-(3)	463	0	5000	0	.936	189	4.80×10^{-3}	-.143)	+.083
	464	-20	5000	.68	.917	191	4.58 " "	-.066)	
6-(4)	465	0	5000	0	.921	191	4.63 " "	-.185)	+.142
	466	-20	5000	.72	.931	191	4.70 " "	-.043)	
"	467	0	5000	0	.924	191	4.65 " "	-.177)	+.134
	468	-20	5000	.72	.923	187	4.74 " "	-.043)	
"	470	0	5000	0	.936	186	4.88 " "	-.162)	+.139
	469	-20	5000	.73	.925	186	4.81 " "	-.043)	
"	471	0	5000	0	.958	186	5.05 " "	-.113)	+.094
	472	-20	5000	.74	.951	186	5.00 " "	-.019)	
6-(5)	474	0	5000	0	.950	186	5.00 " "	-.124)	+.097
	473	-20	5000	.74	.942	188	4.85 " "	-.027)	
6-(6)	476	0	5000	0	.942	186	4.90 " "	-.138)	+.099
	477	-20	5000	.65	.920	186	4.74 " "	-.039)	
6-(7)	480	0	5000	0	1.014	183	5.57 " "	-.065)	+.120
	481	-20	5000		1.003	186	5.38 " "	+.055)	
7-(1)	522	0	5000	0	1.004	210	4.79×10^{-3}	-.082)	+.166
	523	-20	5000	.70	1.006	211	4.79 " "	+.084)	
7-(2)		0	(See 522)					)	
	524	-20	5000	.70	1.012	214	4.76 " "	+.194)	+.112
7-(3)	525	0	5000	0	.966	199	4.76 " "	-.105)	
	526	-20	5000	.70	.983	203	4.81 " "	+.05)	+.110
7-(4)		0	(Assumed symmetrical in hovering)					)	
	527	-20	5000	.70	.912	204	4.28 " "	+.196)	+.196

Figure 5. Tabulation of Data (Sheet 1 of 2 Sheets)

FIGURE No.	DATA POINT	θ (°)	n (rpm)	q_o (kg/m^2)	LIFT (kg)	POWER INPUT (watts)	$\frac{L^{3/2}}{P}$	e/d	Δ e/d
7-(5)		0	(See 525)						
	528	-20	5000	.70	.971	202	4.74 " "	+.236)	+.341
7-(6)	529	0	5000	0	.905	205	4.20 " "	+.063)	
	530	-20	5000	.70	.896	206	4.12 " "	+.246)	+.183
7-(7)		0	(Assumed symmetrical)						
	531	-20	5000	.70	.906	216	4.00 " "	+.133)	+.133
7-(8)	532	0	5000	0	.891	212	3.96 " "	-.098)	
	533	-20	5000	.70	.922	216	4.10 " "	+.079)	+.177
7-(9)	534	0	5000	0	.968	208	4.58 " "	+.008)	
	535	-20	5000	.70	.979	200	4.85 " "	+.125)	+.133
15-(1)	537	0	5000	0	1.107	200	5.85 " "	+.001)	
	536	-20	5000	.70	1.022	208	4.95 " "	+.060)	+.059
15-(2)	538	0	5000	0	1.089	200	5.68 " "	+.003)	
	539	-20	5000	.70	1.031	207	5.05 " "	+.047)	+.044
15-(3)	540	0	5000	0	1.141	199	6.14 " "	-.003)	
	541	-20	5000	.70	1.005	207	4.85 " "	+.120)	+.123
18-(1)	665	0	6090	.50	1.477	323	5.55 " "	+.051)	
	666	-20	6090	2.36	1.275	322	4.46 " "	-.045)	-.096
"	667	0	6090	0	1.621	319	6.45 " "	-.002)	
	668	-20	6090	1.23	1.513	321	5.79 " "	+.044)	+.046
"	669	-20	6090	1.25	1.525	321	5.85 " "	+.067	
"	670	-20	6090	1.30	1.545	321	6.00 " "	+.079	
18-(2)	671	0	6090	0	1.304	321	4.65 " "	+.190)	
	673	-20	6090	1.35	1.308	321	4.65 " "	+.243)	+.053
18-(3)	674	-20	6090	1.03	1.230	318	4.29×10^{-3}	-.109	
"	677	0	6090	0	1.383	329	4.92 " "	-.138)	
	678	-20	6090	.99	1.312	323	4.65 " "	-.078)	+.060
"	679	0	6090	0	1.451	330	5.26 " "	-.119)	
	680	-20	6090	1.00	1.356	331	4.81 " "	-.054)	+.065
"	682	0	6090	0	1.507	324	5.71 " "	-.063)	
	681	-20	6090	1.12	1.449	332	5.24 " "	+.021)	+.084
18-(4)	675	0	6090	0	1.343	334	4.65 " "	+.136)	
	676	-20	6090	1.20	1.347	338	4.83 " "	+.005)	-.131
18-(5)	683	0	6090	0	1.644	321	6.58 " "	+.010)	
	684	-22.5	6090	1.40	1.466	324	5.50 " "	-.280)	-.290
18-(6)	697	0	6090	0	1.631	310	6.72 " "	-.015)	
	698	-20	6090	1.31	1.534	317	6.00 " "	+.104)	+.119

Figure 5. Tabulation of Data (Sheet 2 of 2 Sheets)

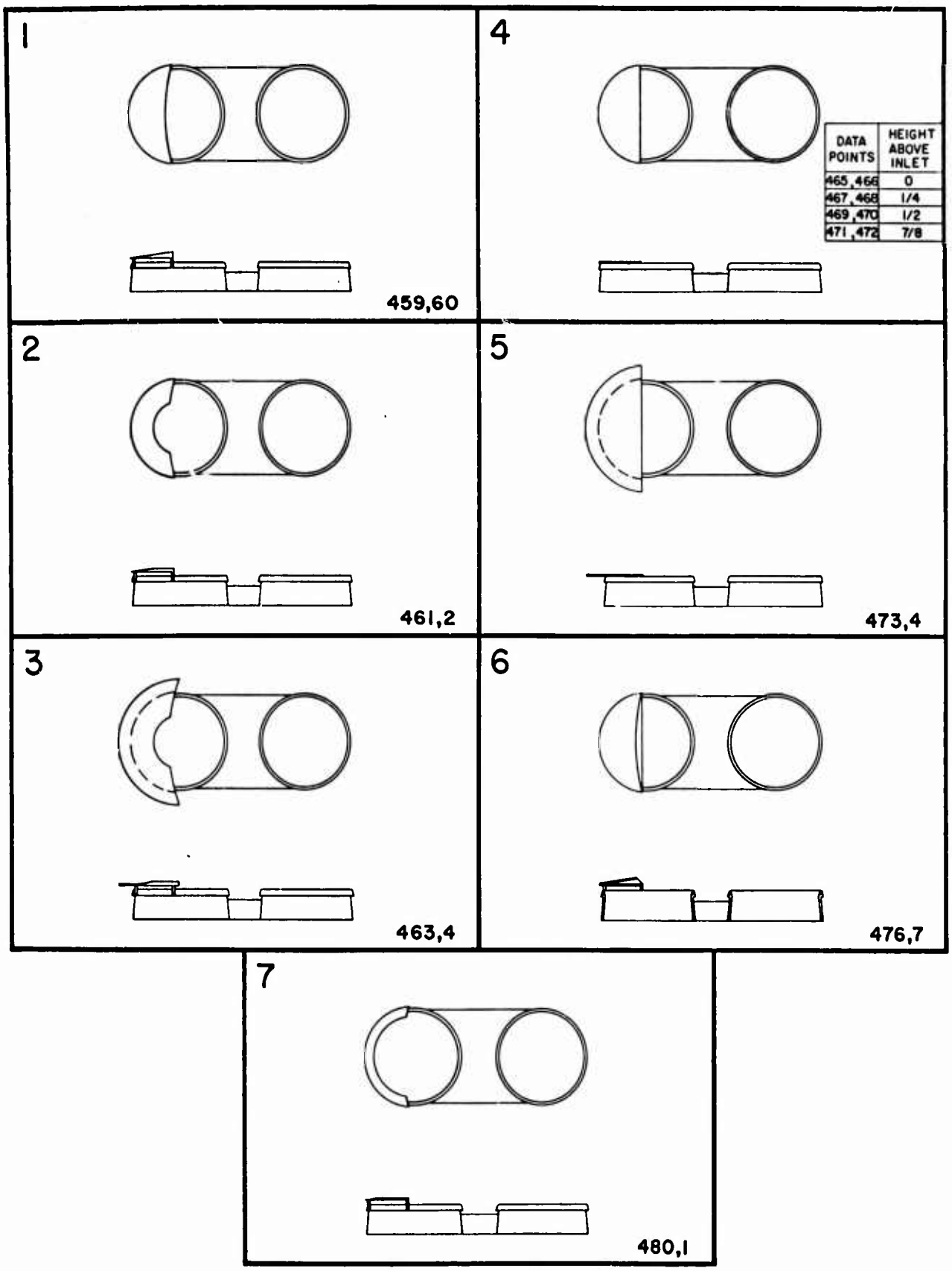

Figure 6. Schematic Drawings of Moment Reducers Tested

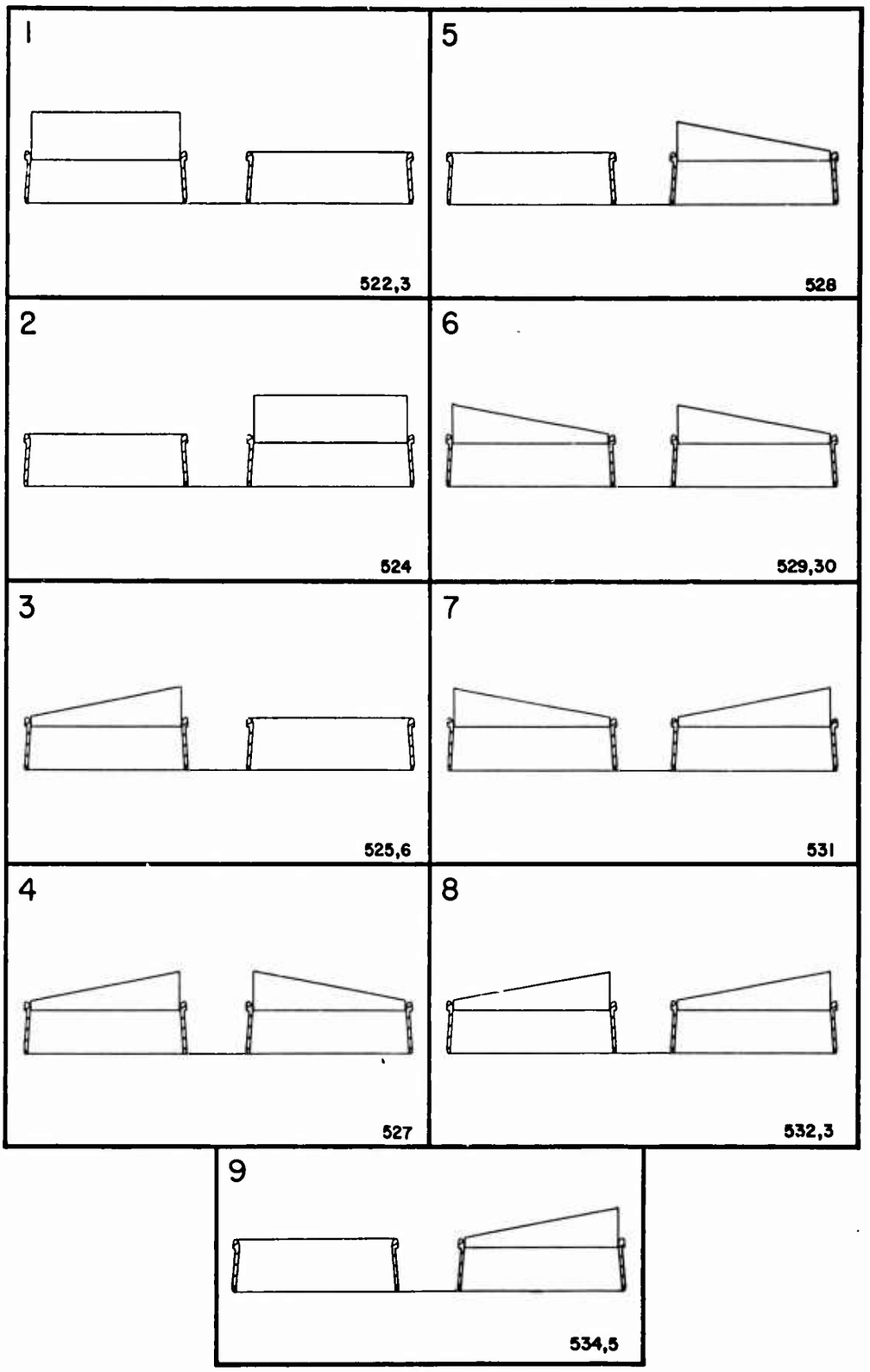

Figure 7. Schematic Drawings of Various Cylindrical Inlets Tested

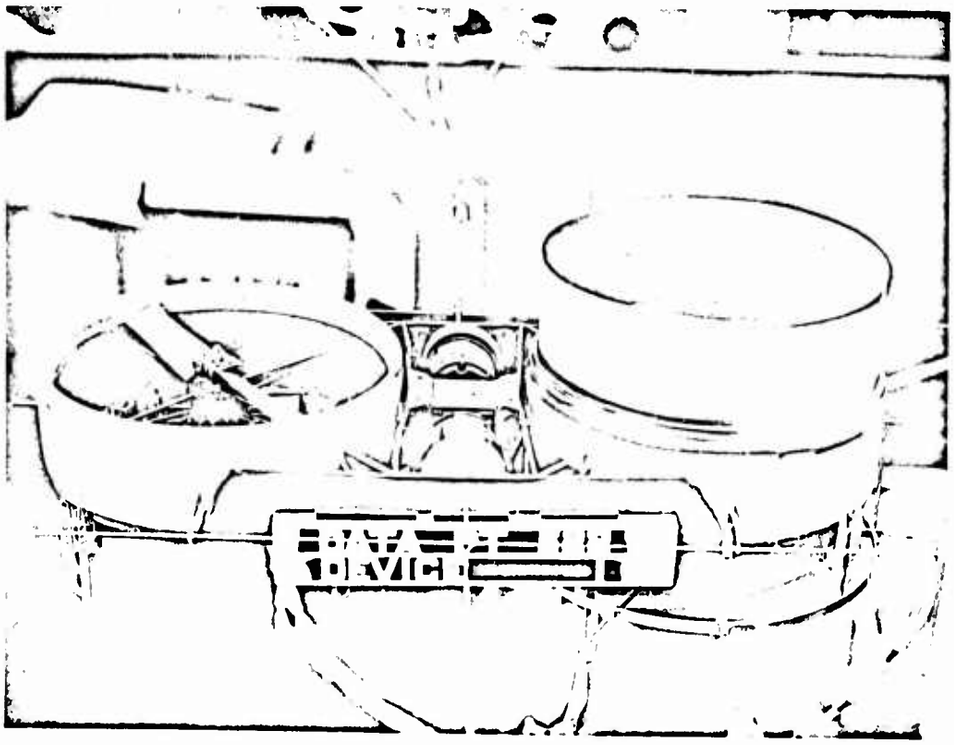

Figure 8. Photograph of Configuration Drawn in Figure 7-(1)

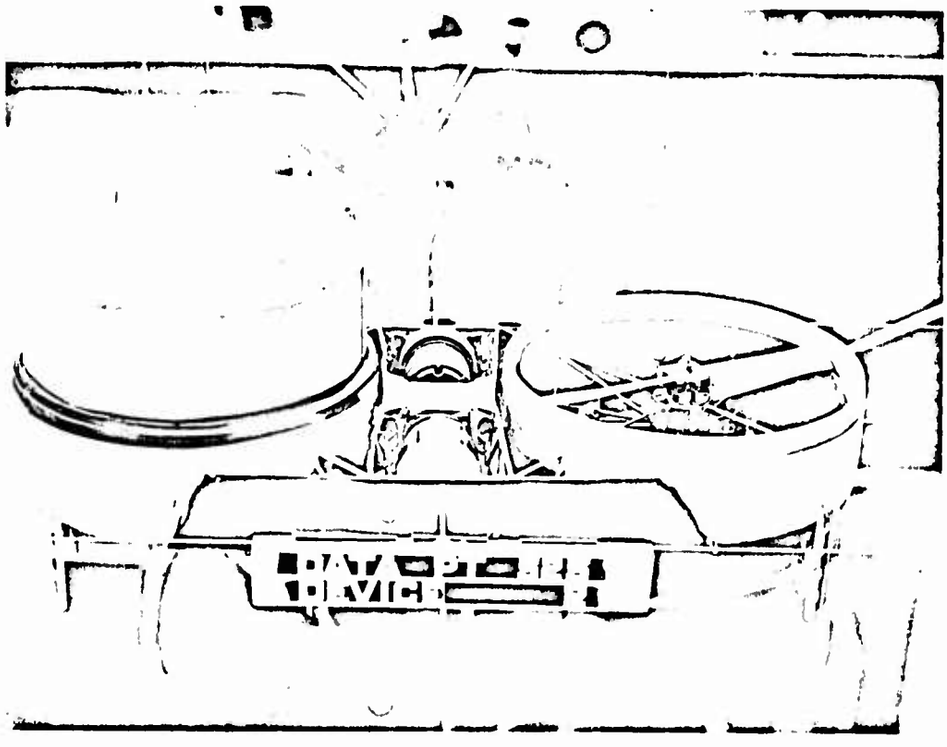

Figure 9. Photograph of Configuration Drawn in Figure 7-(2)

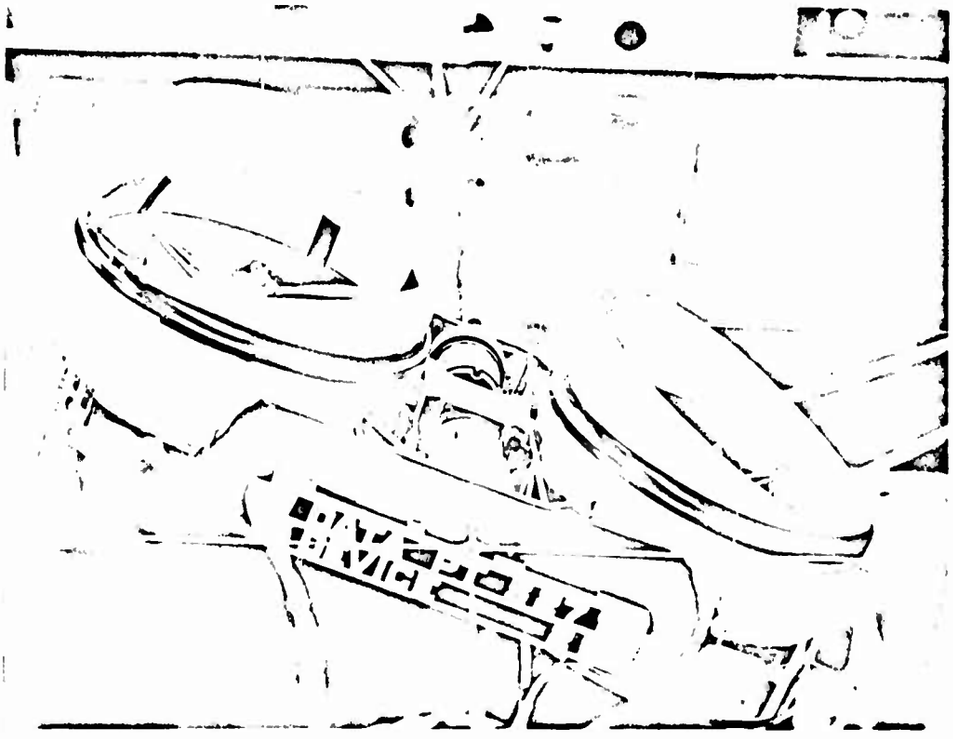

Figure 10. Photograph of Configuration Drawn in Figure 7-(4)

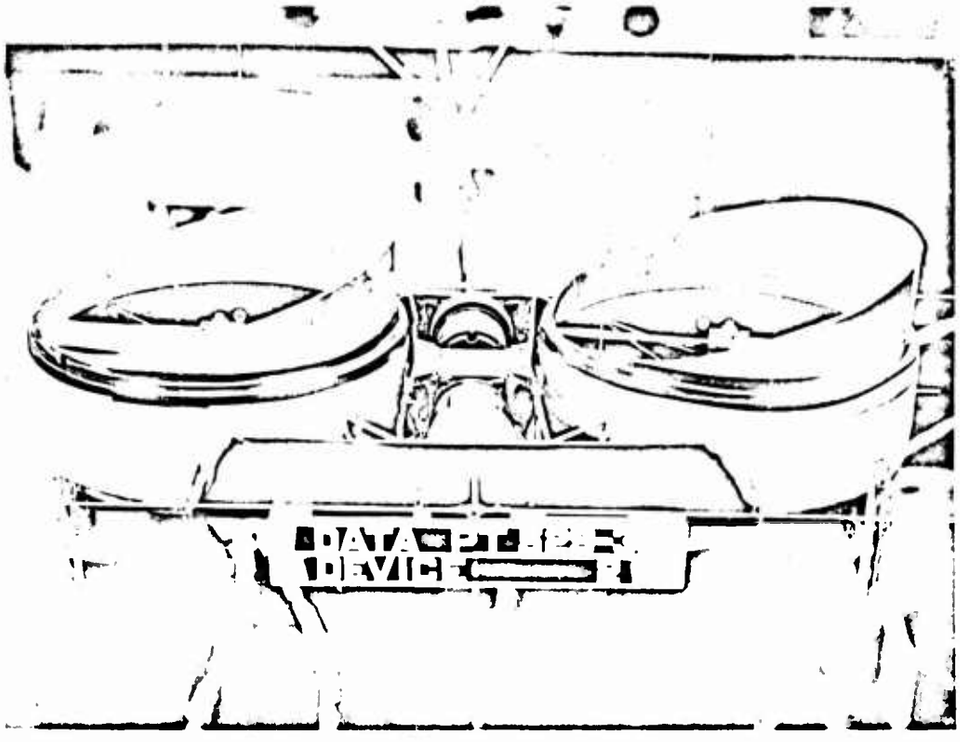

Figure 11. Photograph of Configuration Drawn in Figure 7-(6)

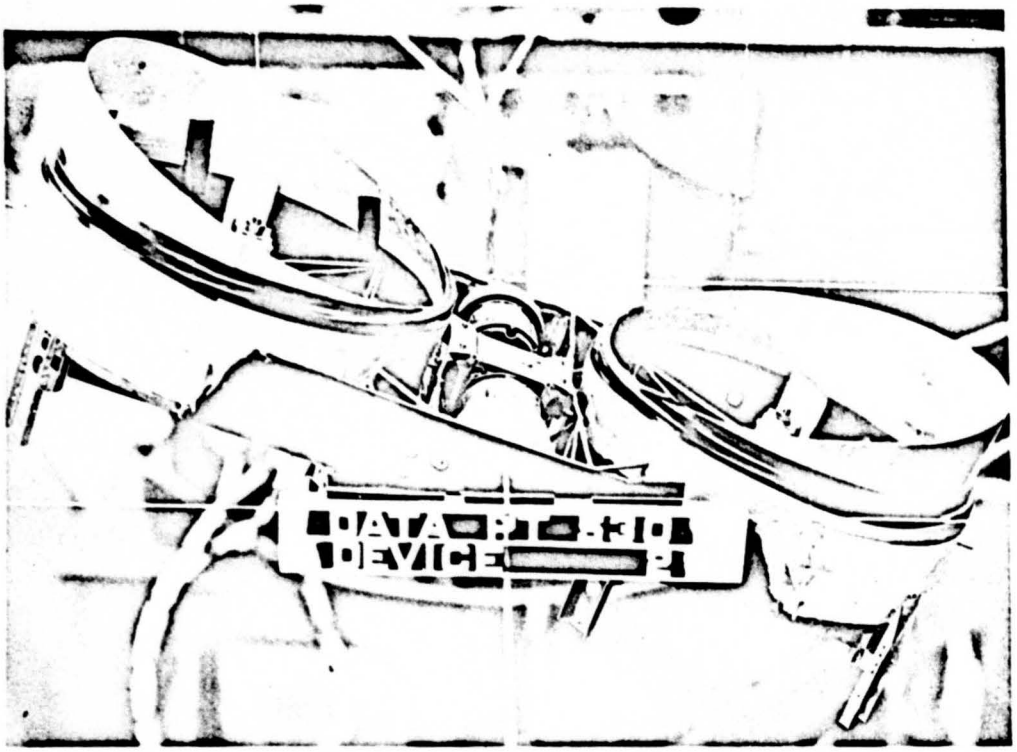

Figure 12. Photograph of Configuration Drawn in Figure 7-(7)

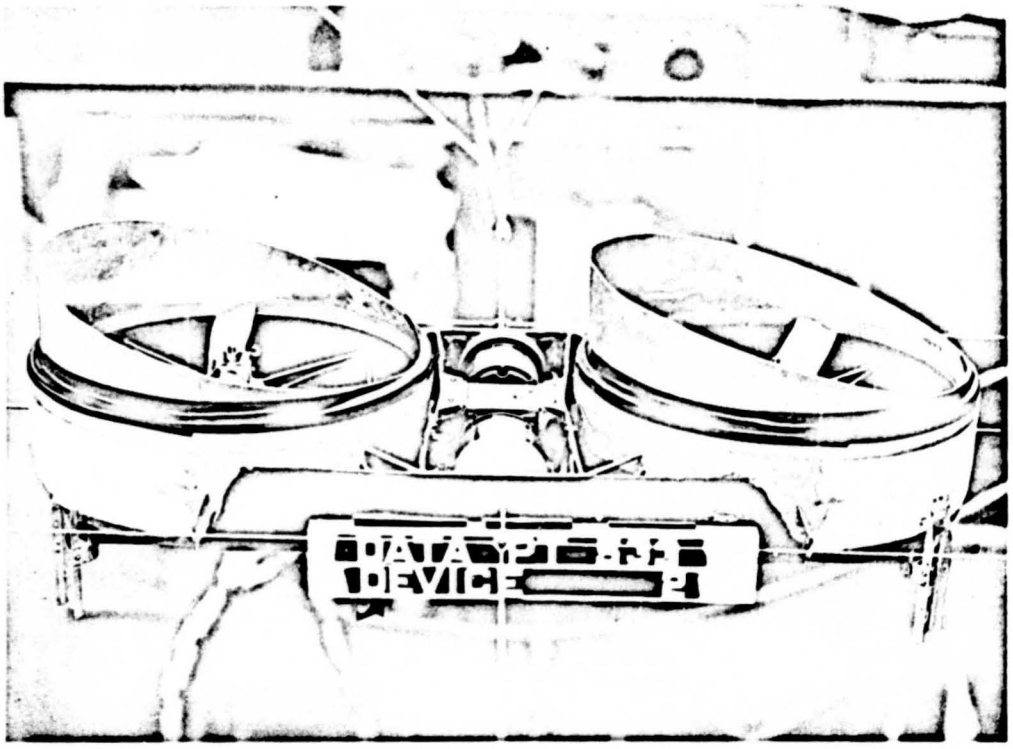

Figure 13. Photograph of Configuration Drawn in Figure 7-(8)

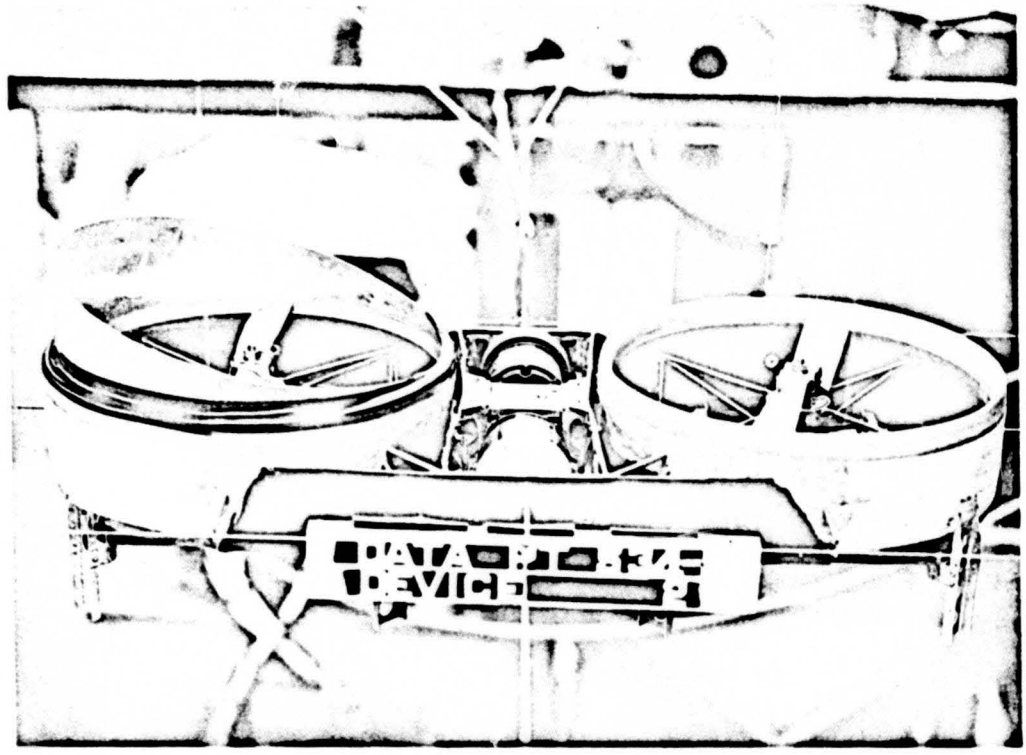

Figure 14. Photograph of Configuration Drawn in Figure 7-(9)

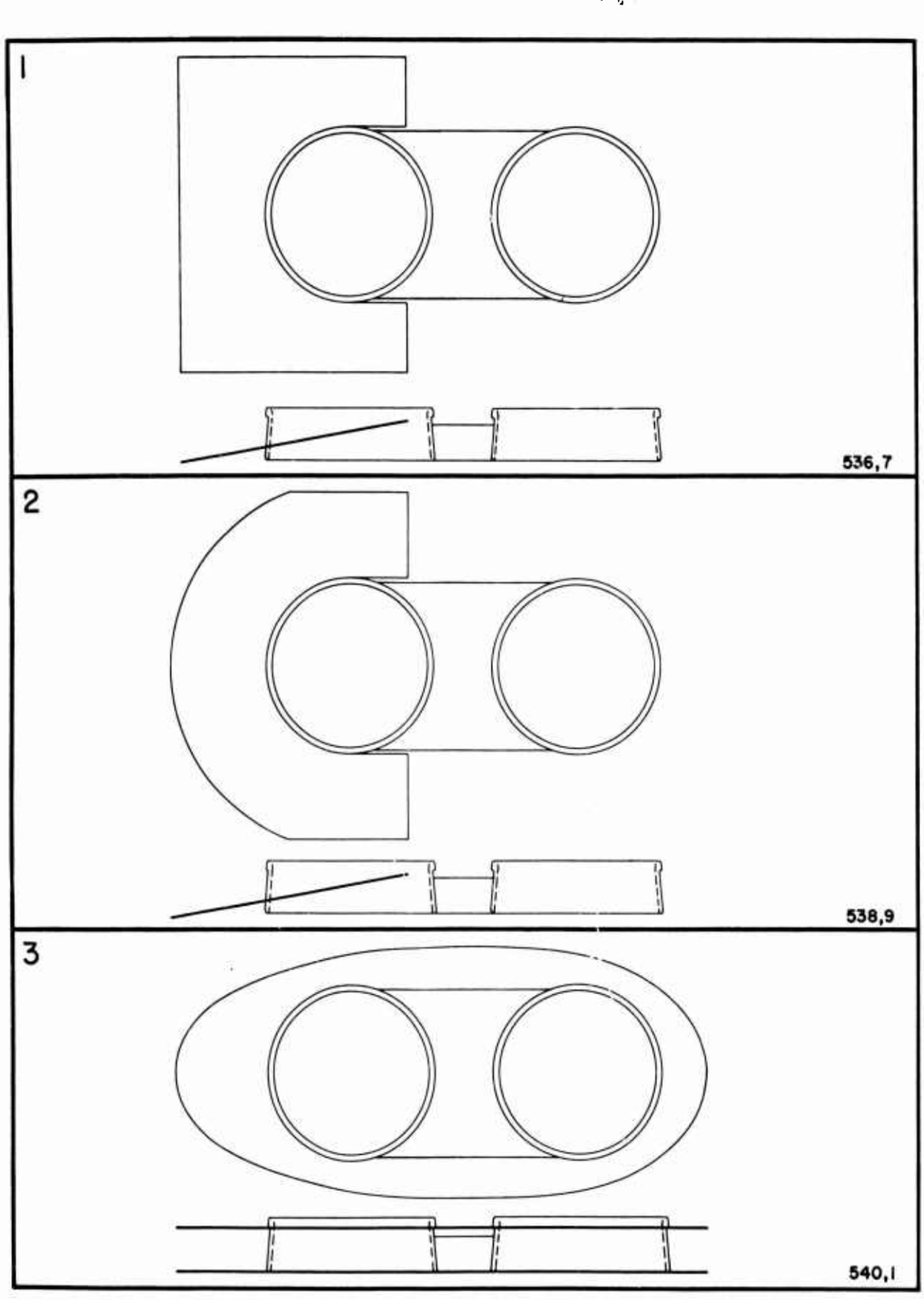

Figure 15. Schematic Drawings of Configuration Tested with External Plates

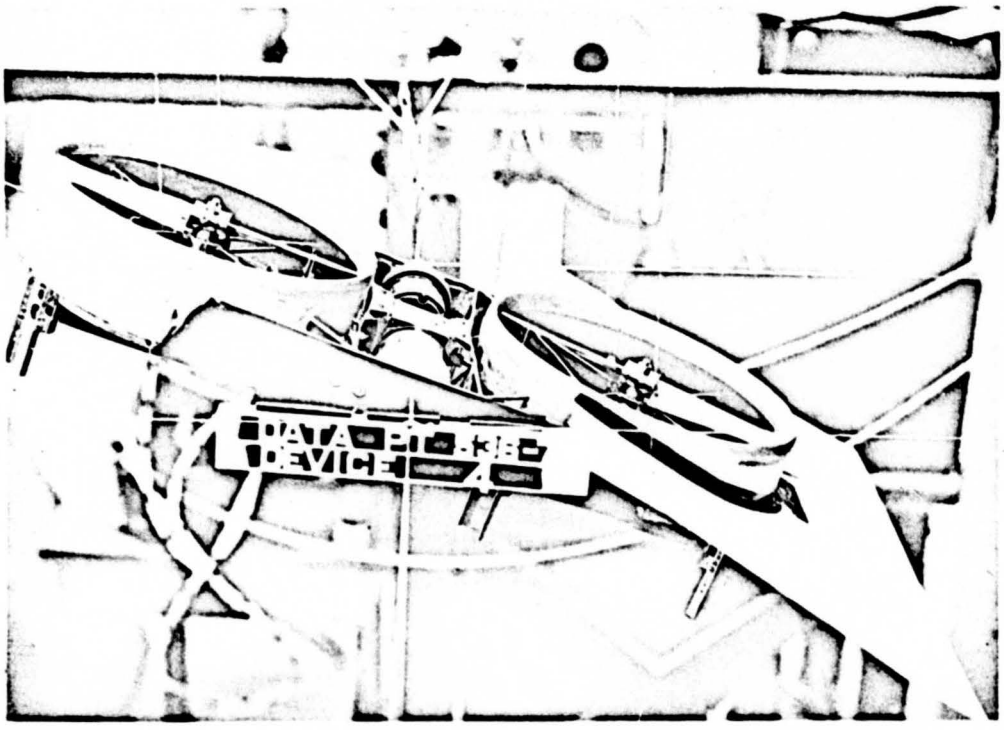

Figure 16. Photograph of Configuration Drawn in Figure 15-(1)

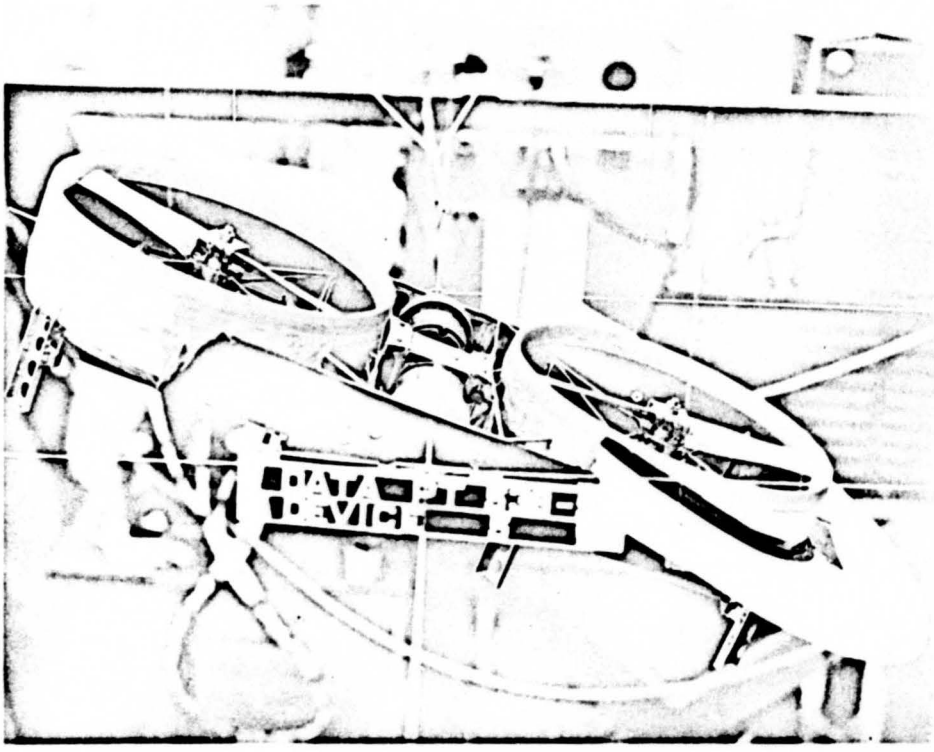

Figure 17. Photograph of Configuration Drawn in Figure 15-(2)

1. ⟵ DIRECTION OF FLIGHT.
2. CASCADE IN FRONT SHROUD IN ALL CASES.
3. CASCADE SLOPE AT -6° UNLESS OTHERWISE INDICATED.

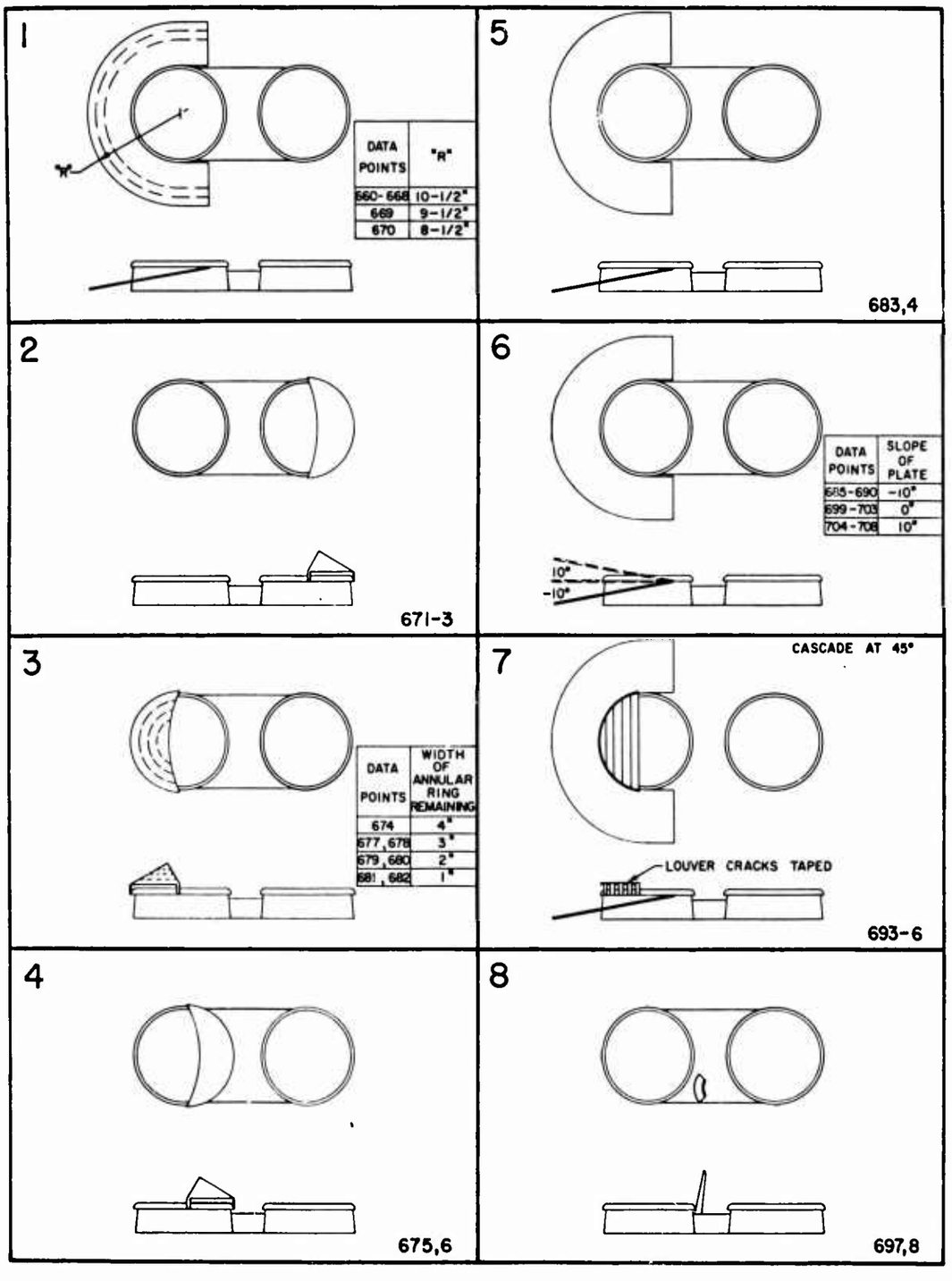

Figure 18. Schematic Drawings of Additional Moment Reducing Schemes Tested

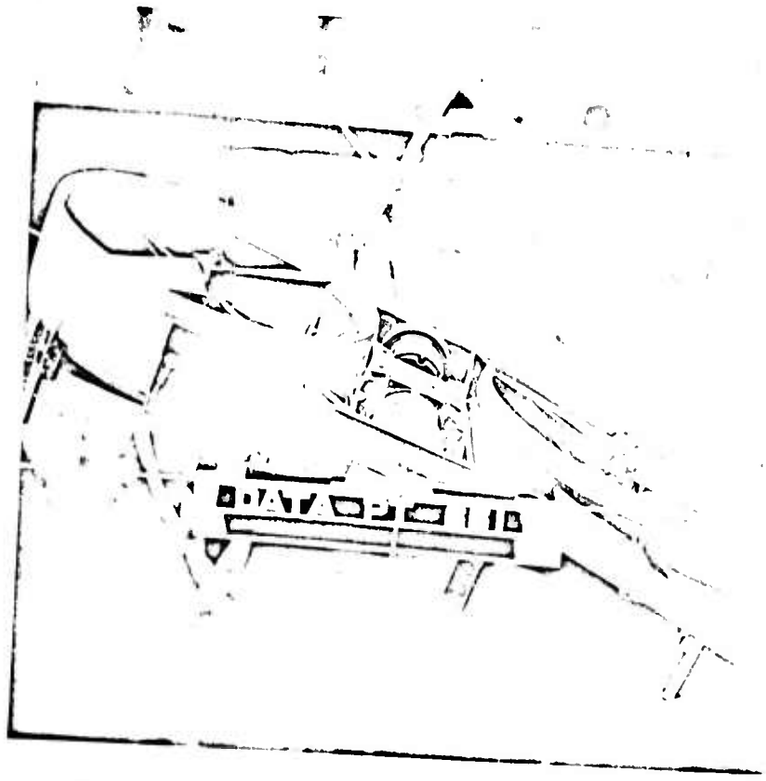

Figure 19. Photograph of Configuration Drawn in Figure 18-(1)

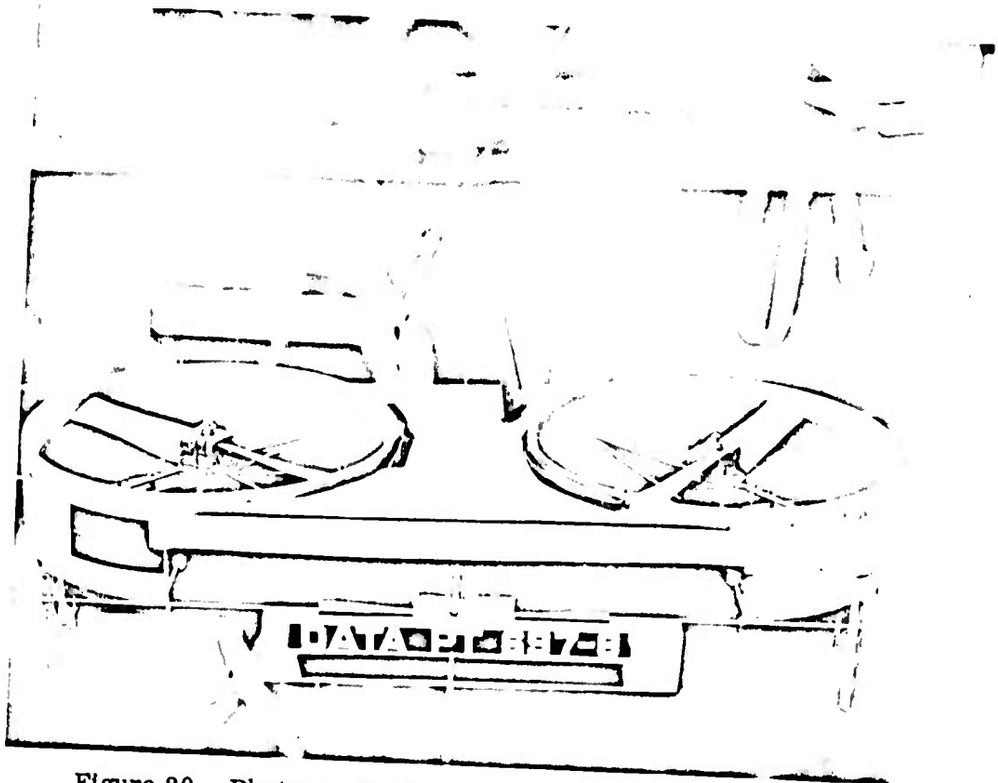

Figure 20. Photograph of Configuration Drawn in Figure 18-(8)

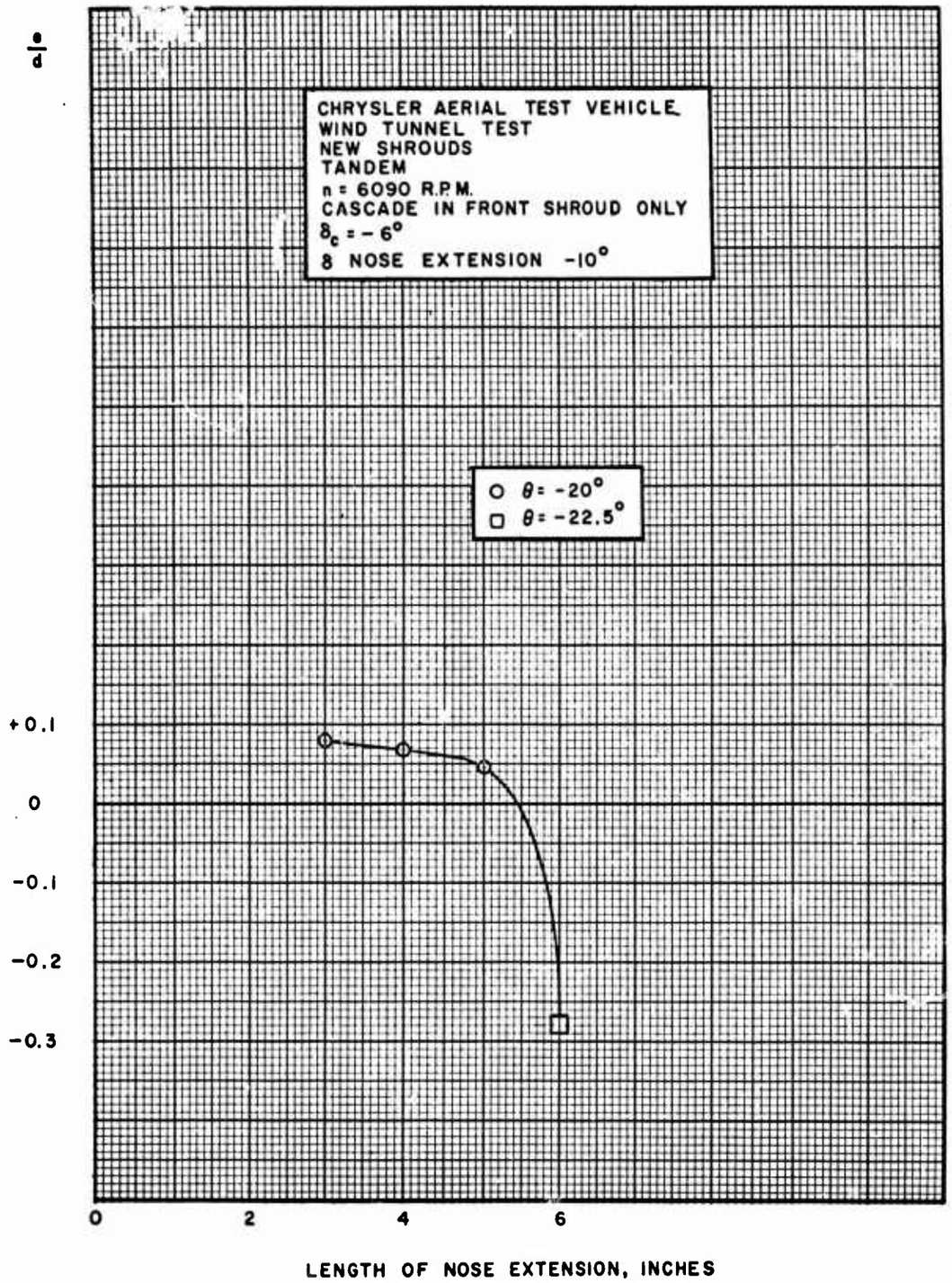

Figure 21. Graph of e/d vs Length of Nose Plate Extension

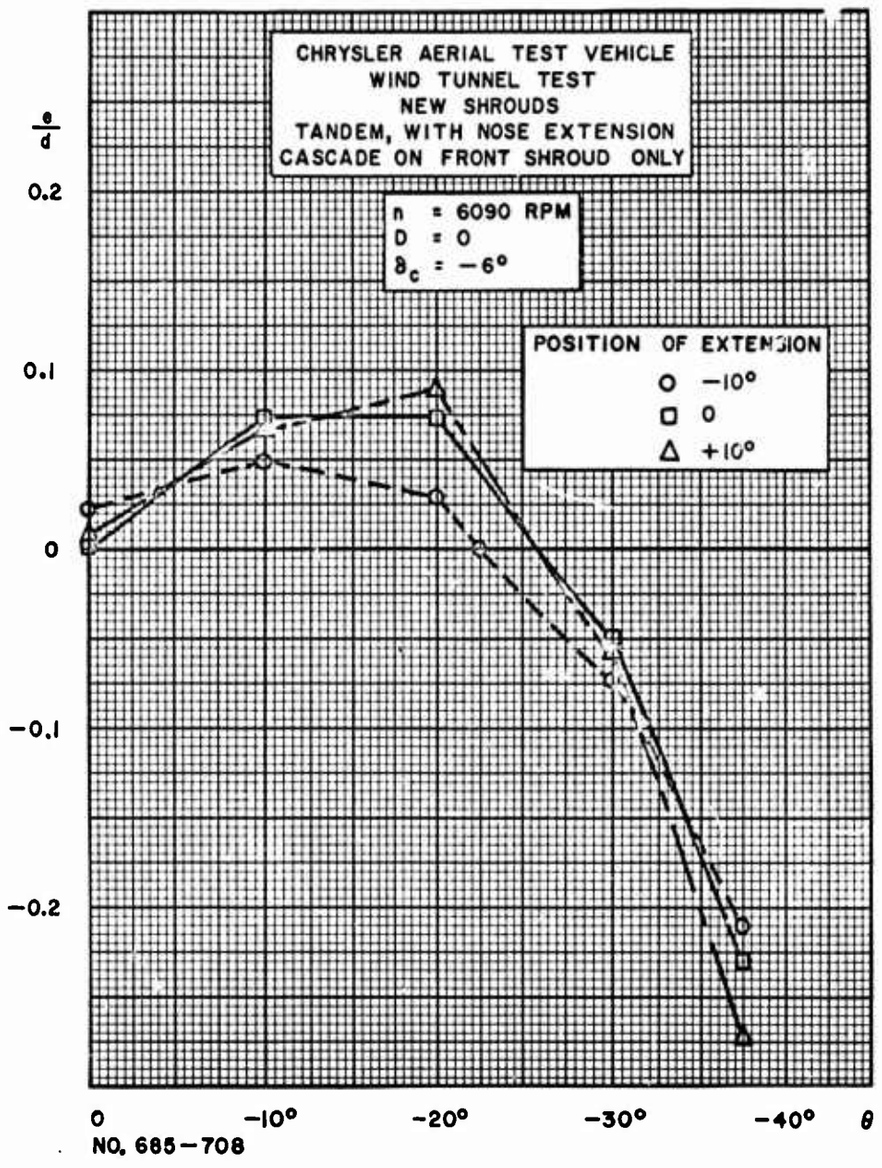

Figure 22. Graph of e/d vs θ for Several Nose Plate Inclinations

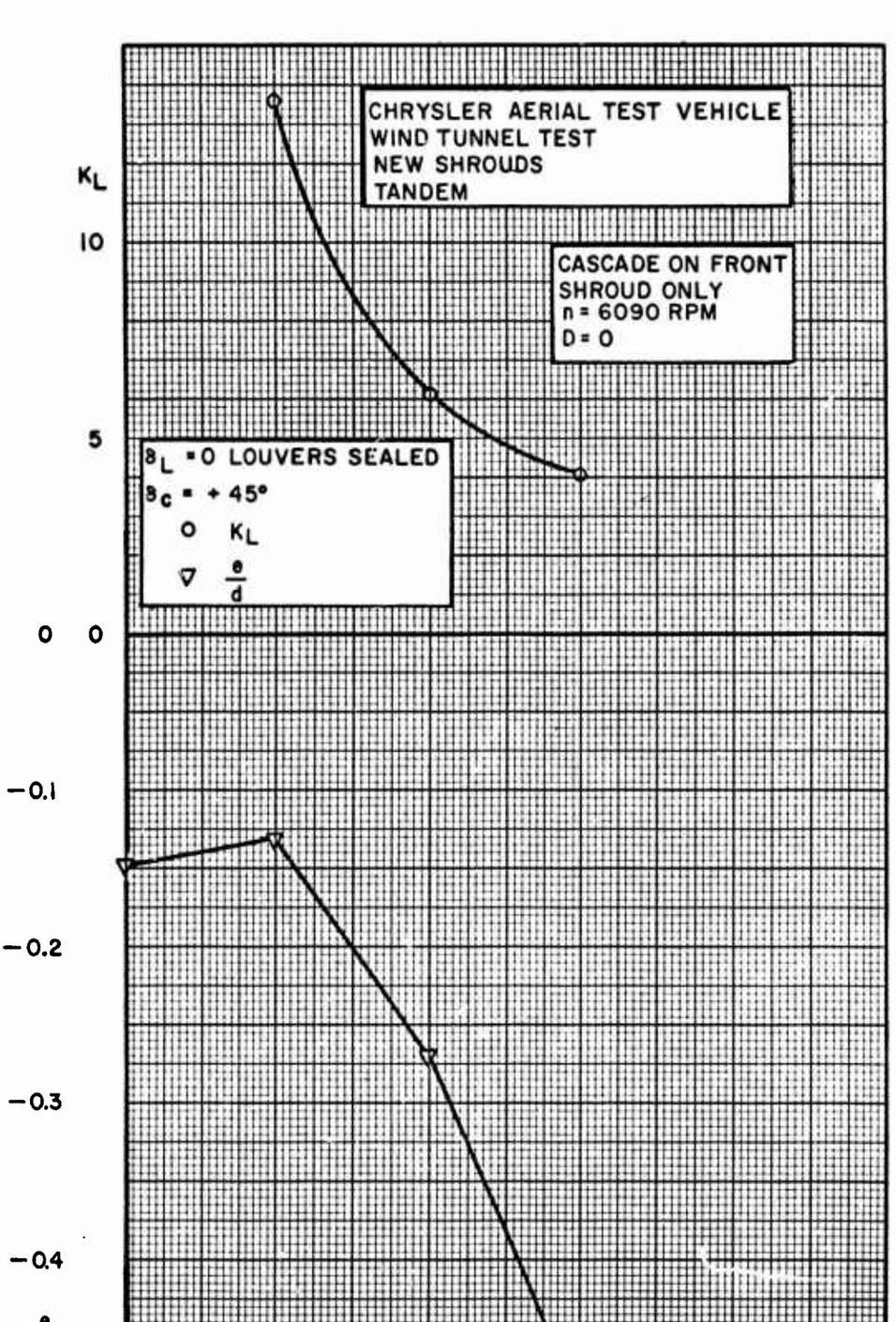

Figure 23. Graph of e/d and K_L vs θ for δ_L = O and δ_e = +45°

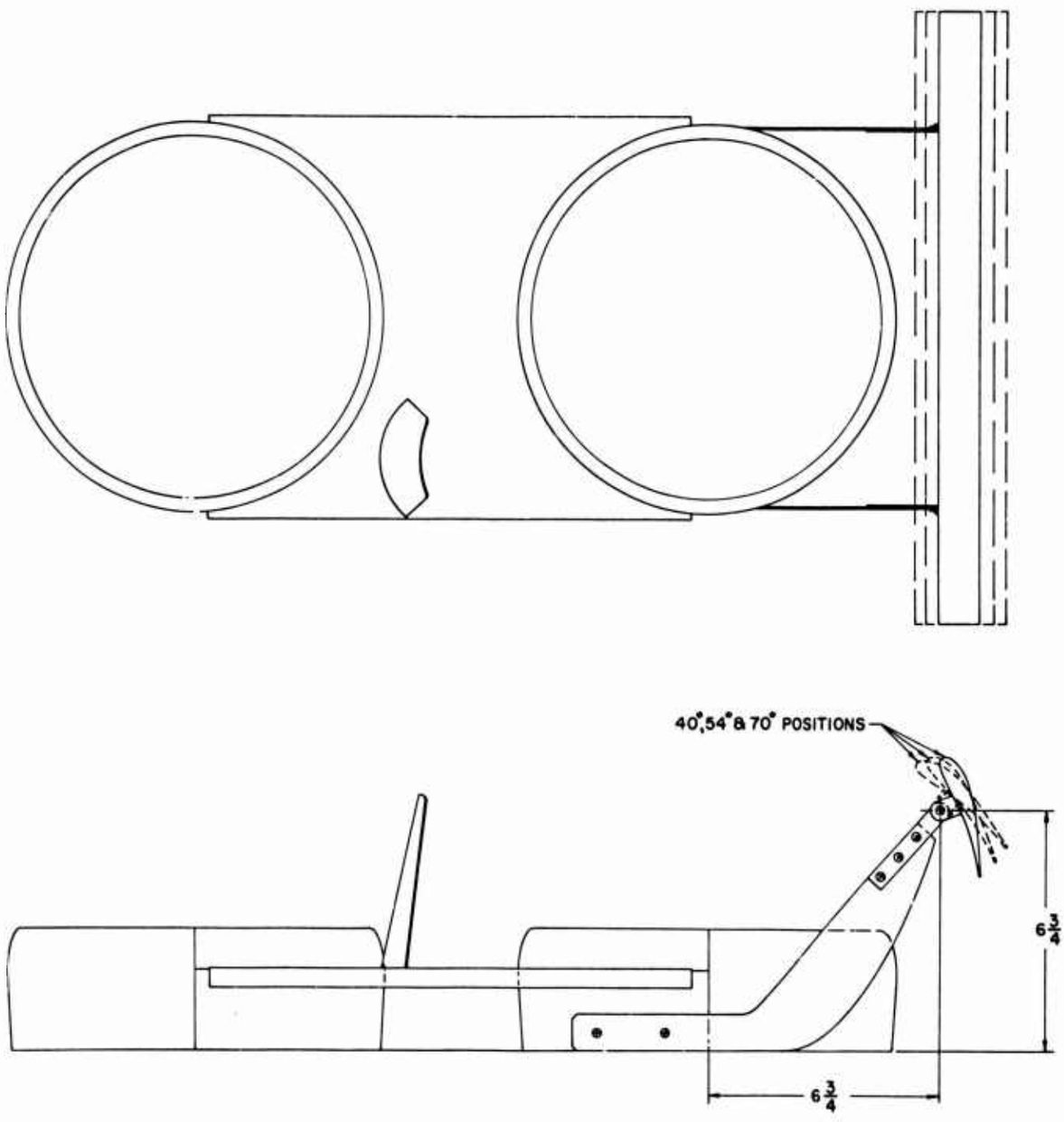

Figure 24. Detail Drawing of the Configuration with a Large Vane Above the Rear Shroud

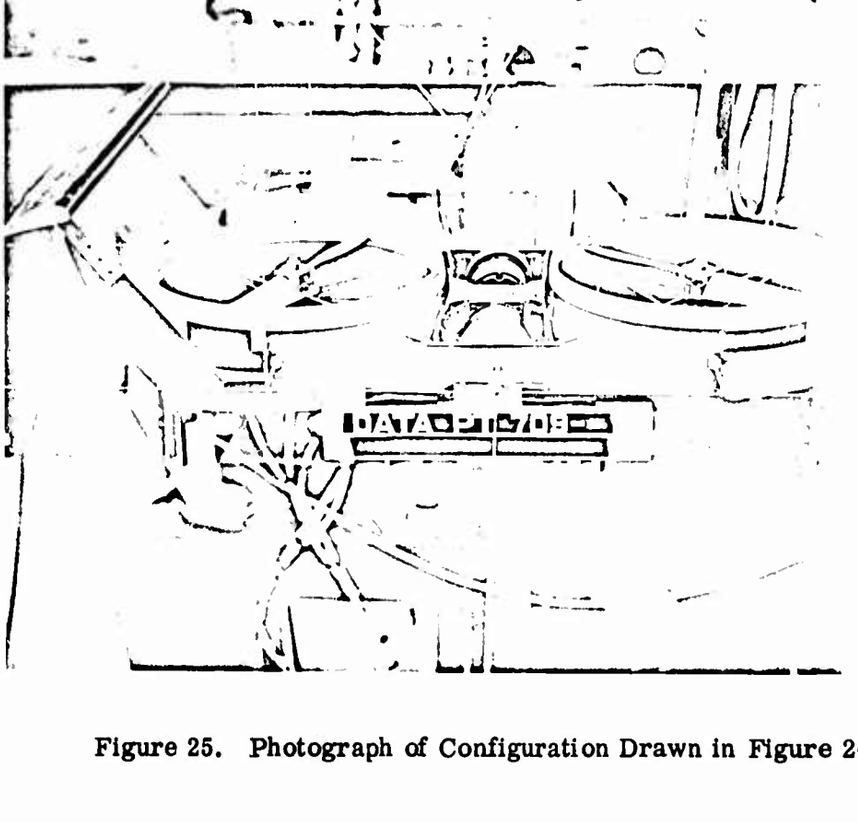

Figure 25. Photograph of Configuration Drawn in Figure 24

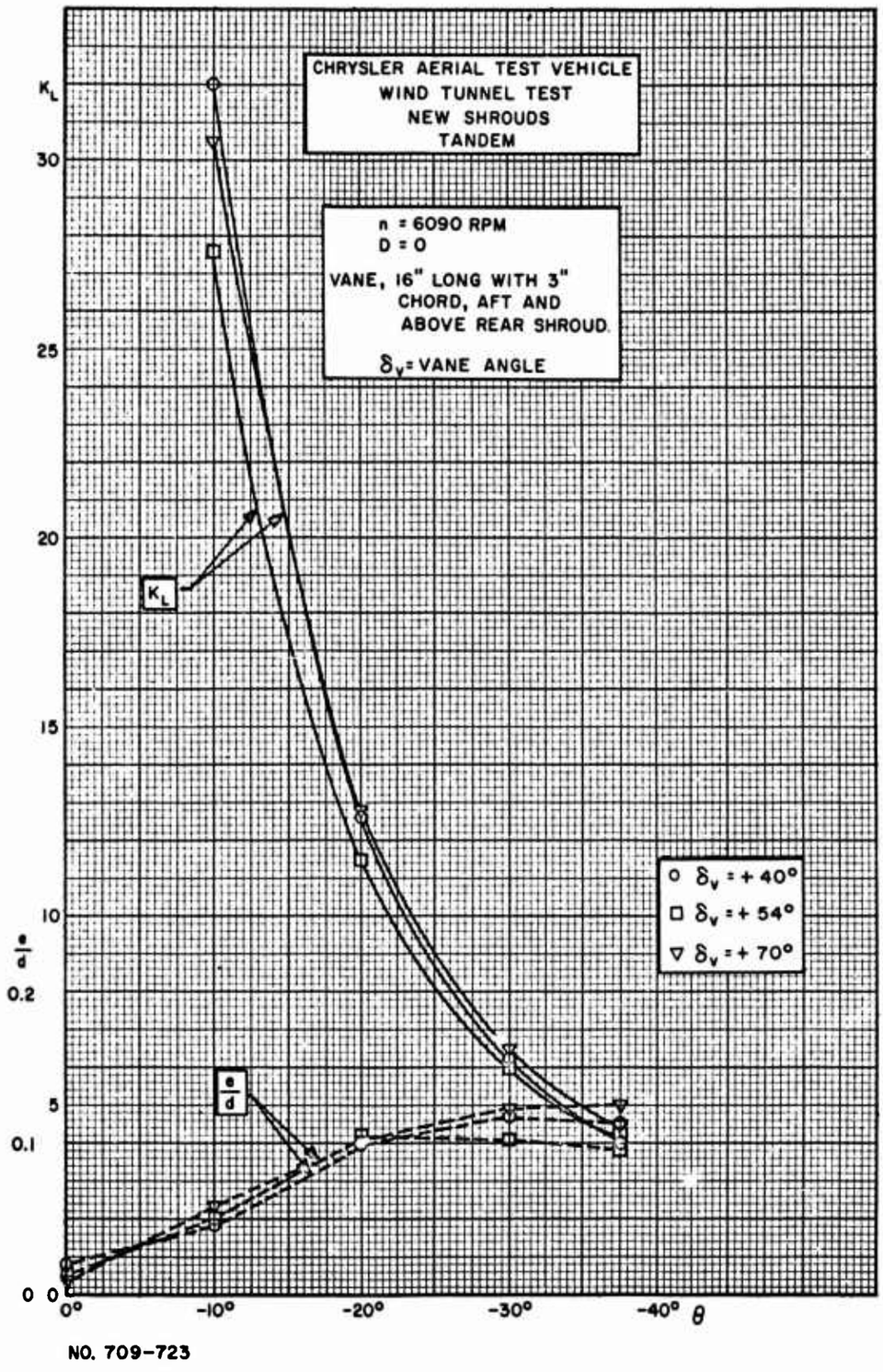

Figure 26. Graph of K_L and e/d vs θ for Several Settings of Large Vane

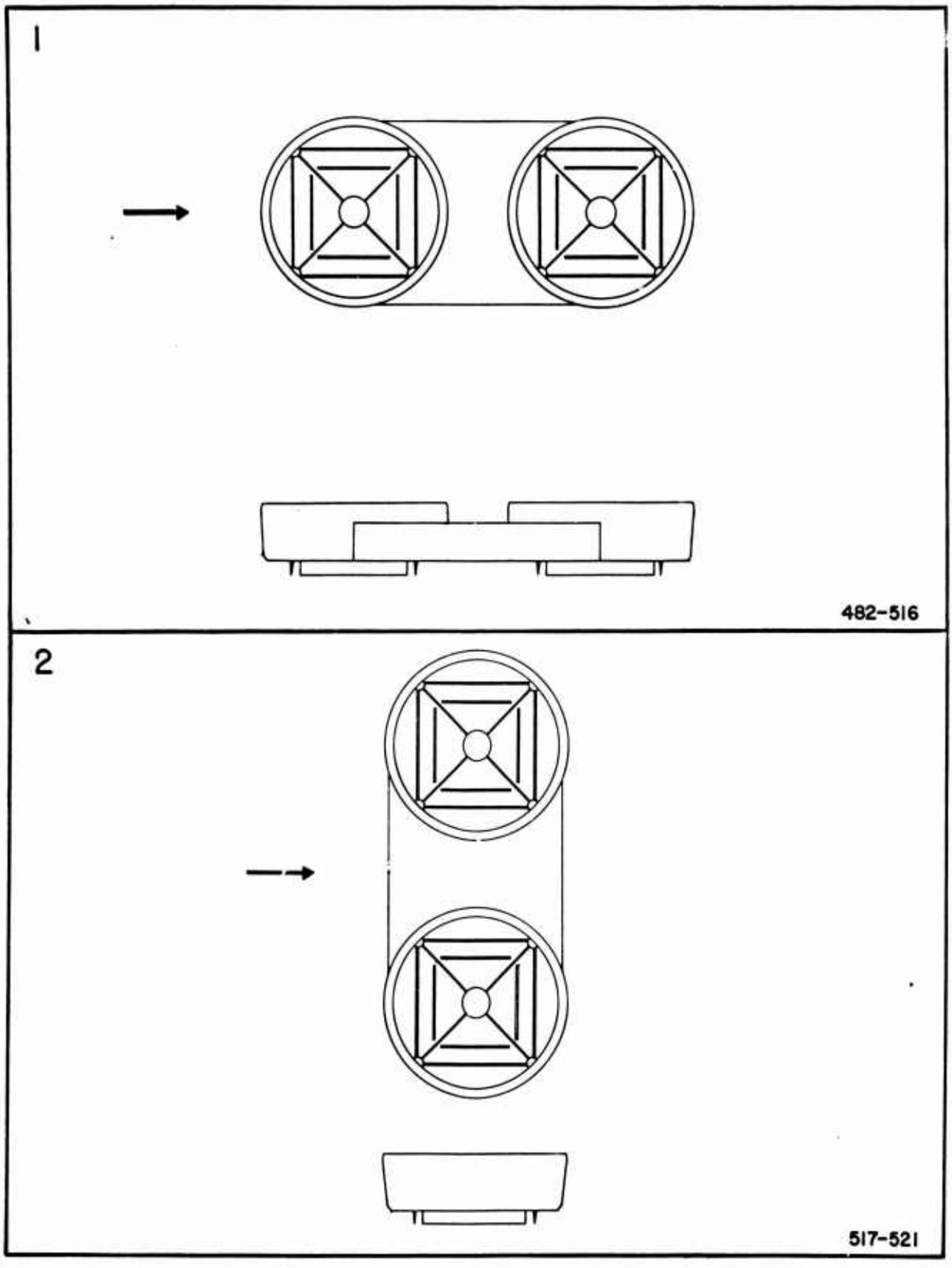

Figure 27. Schematic Drawing of Model in the Tandem and in the Abreast Attitude

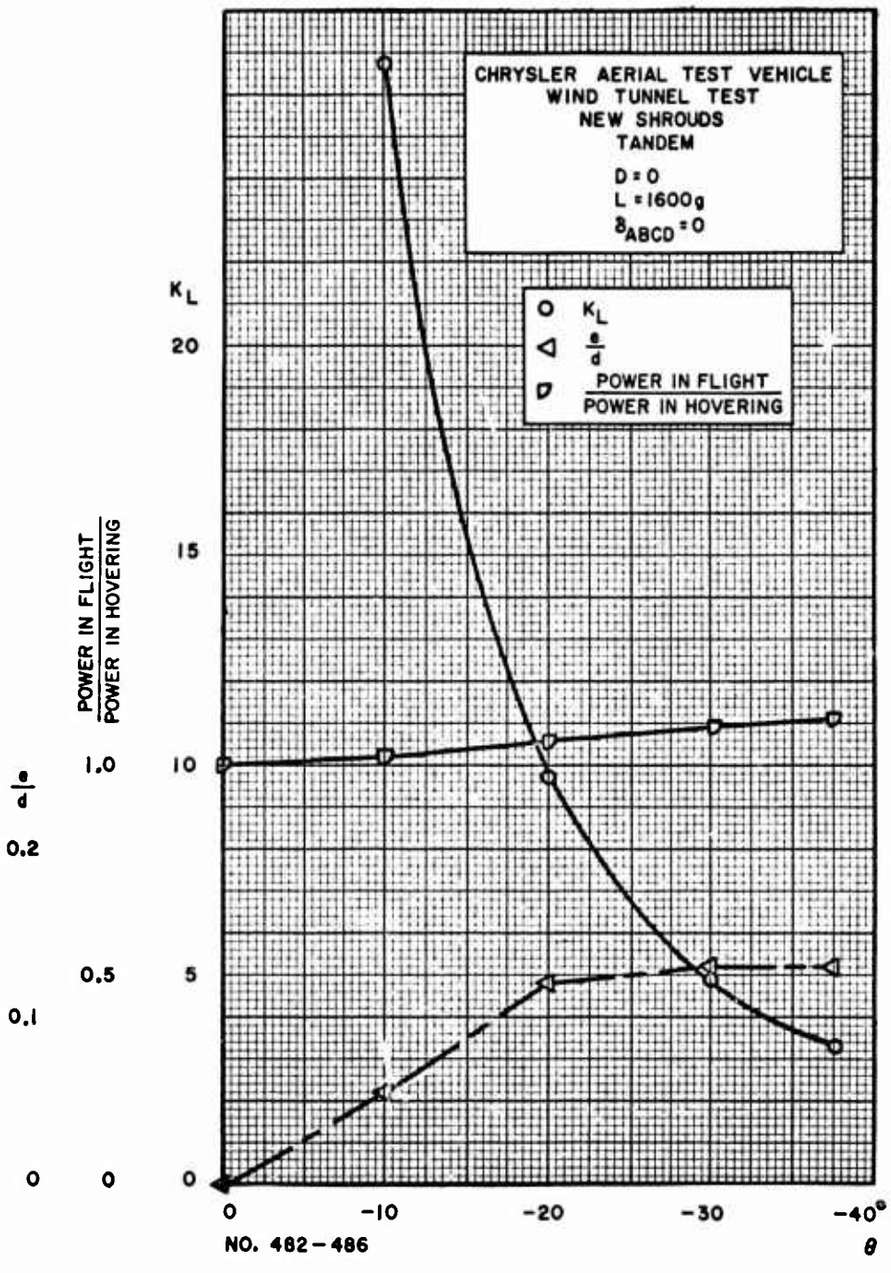

Figure 28. Graph of Performance Curves for the Model in Tandem

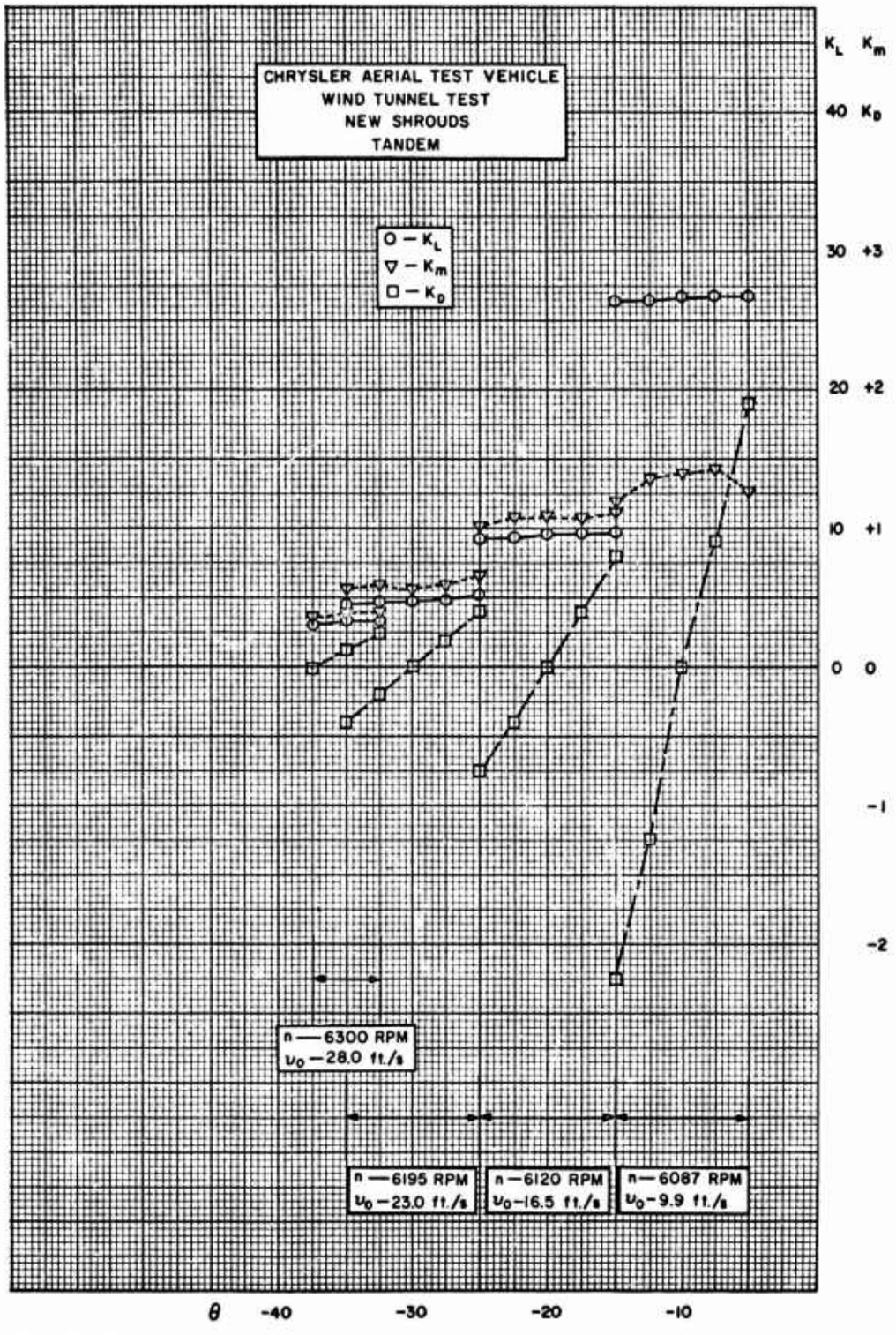

Figure 29. Graph of K_L and K_m vs θ for Stability Work

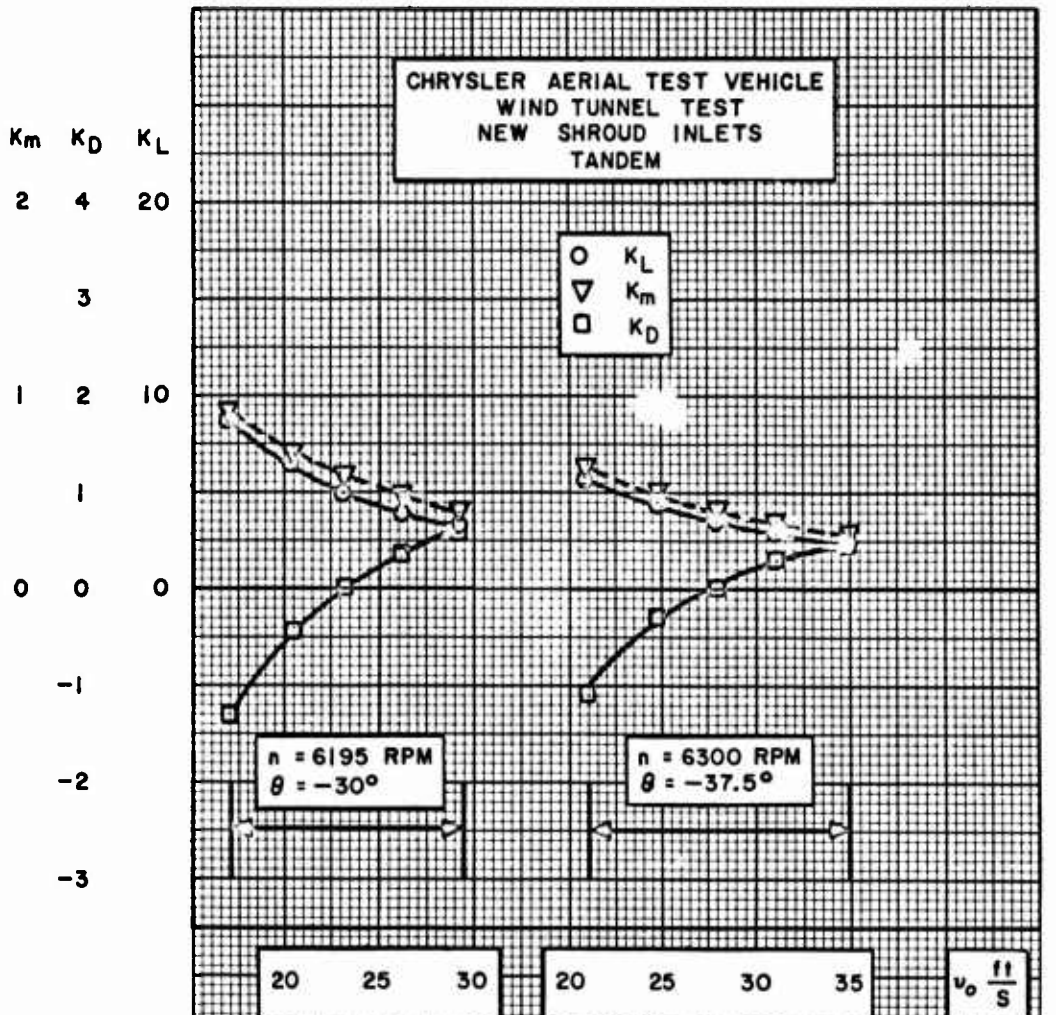

NO. 483-486
501-516

Figure 30. Graph of K_L, K_D and K_m vs v_o and $v_o/n'd$ for Stability Work

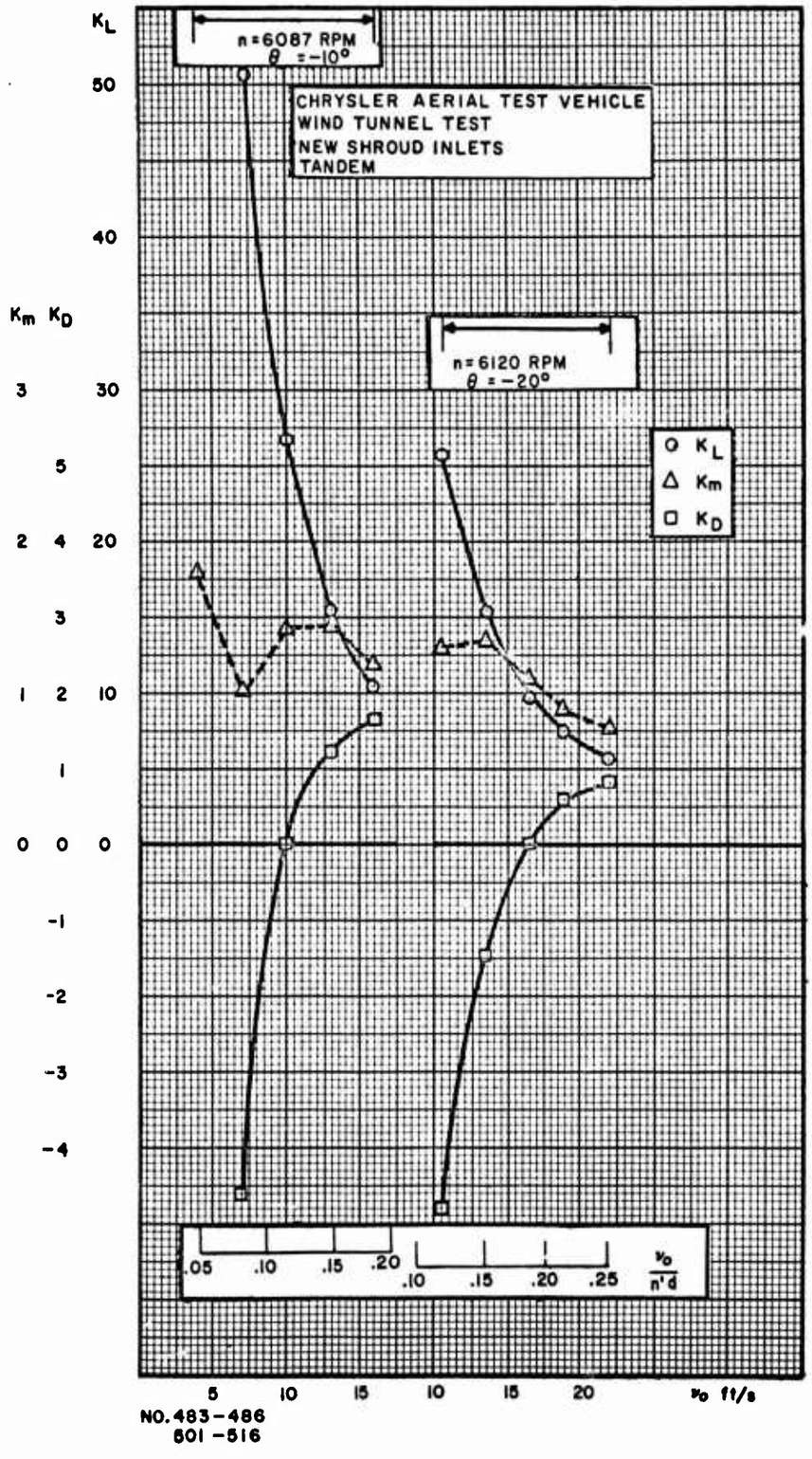

Figure 31. Graph of K_L, K_D and K_m vs v_o and $v_o/n'd$ for Stability Work

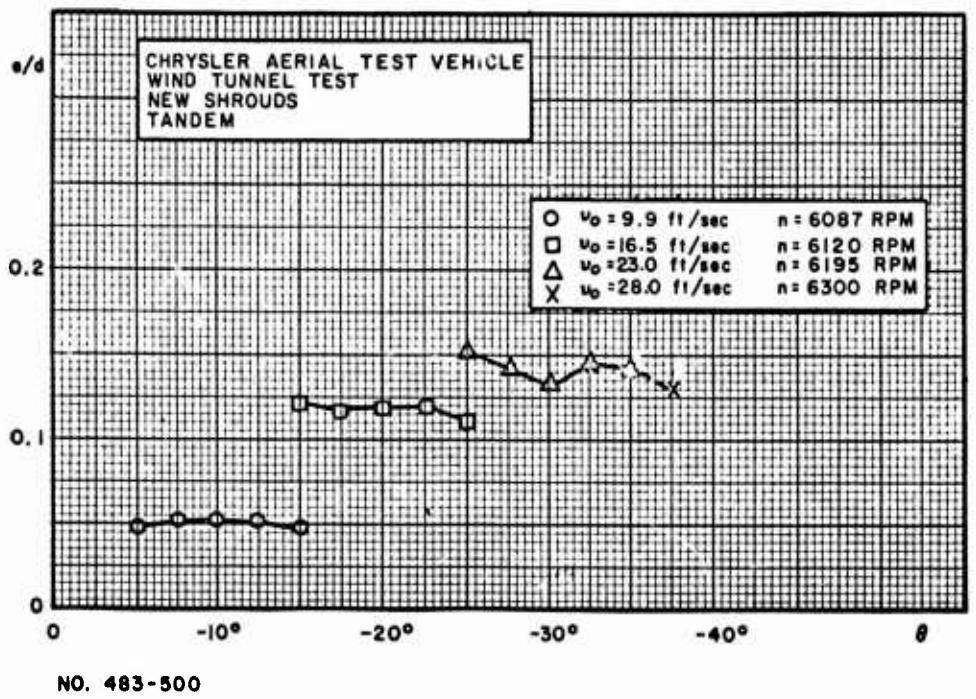

Figure 32. Graph of e/d vs θ for Stability Work

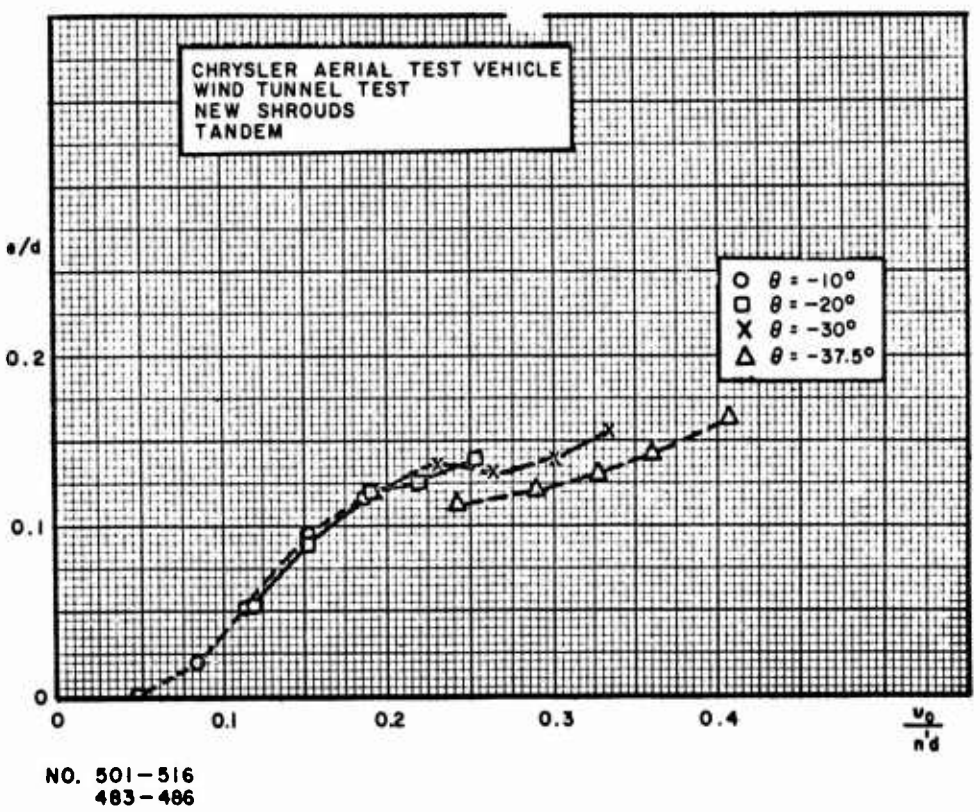

Figure 33. Graph of e/d vs $v_0/n'd$ in Stability Work

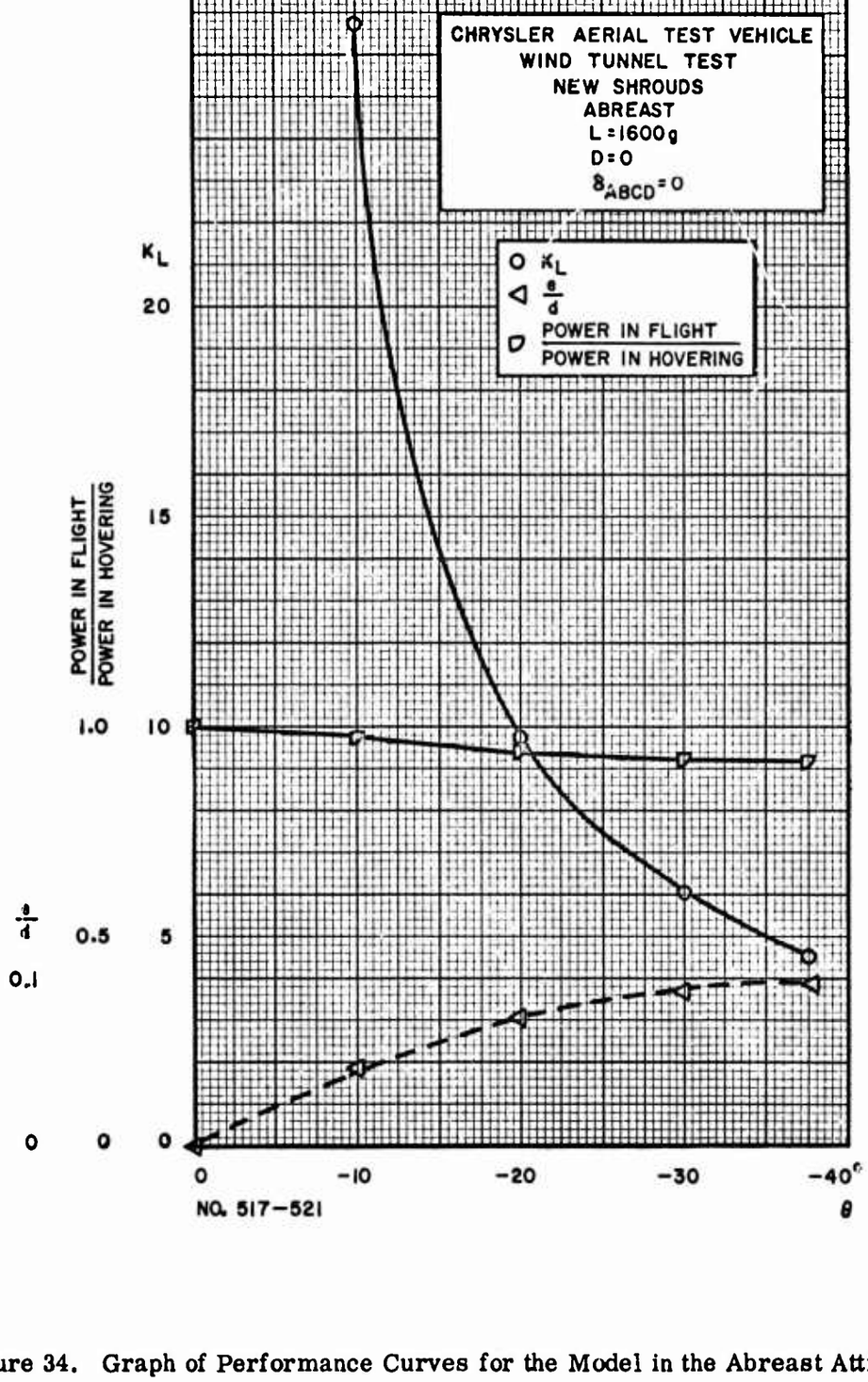

Figure 34. Graph of Performance Curves for the Model in the Abreast Attitude

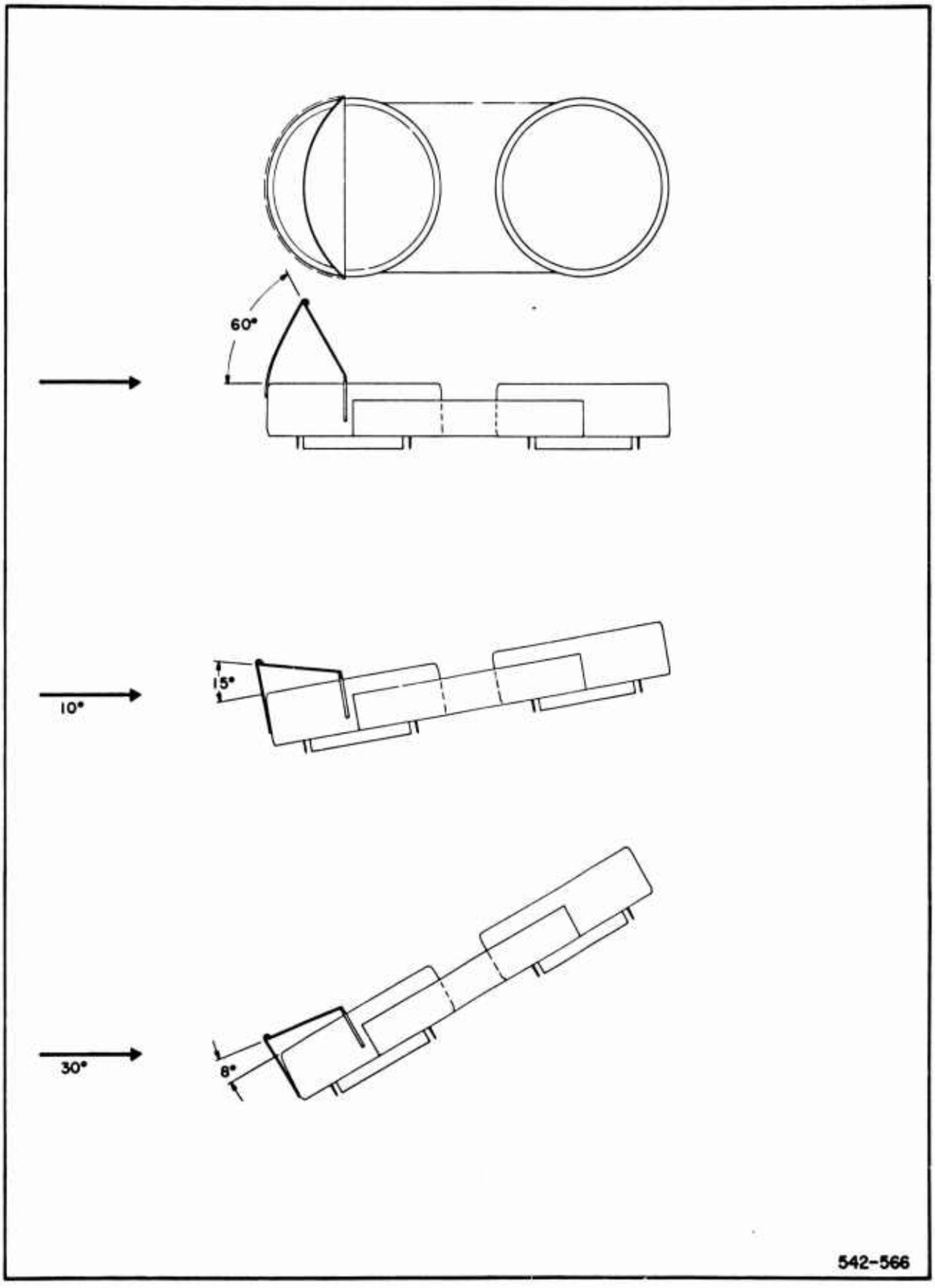

Figure 35. Schematic Drawing of Model in Several Attitudes with a Flap Trim Device

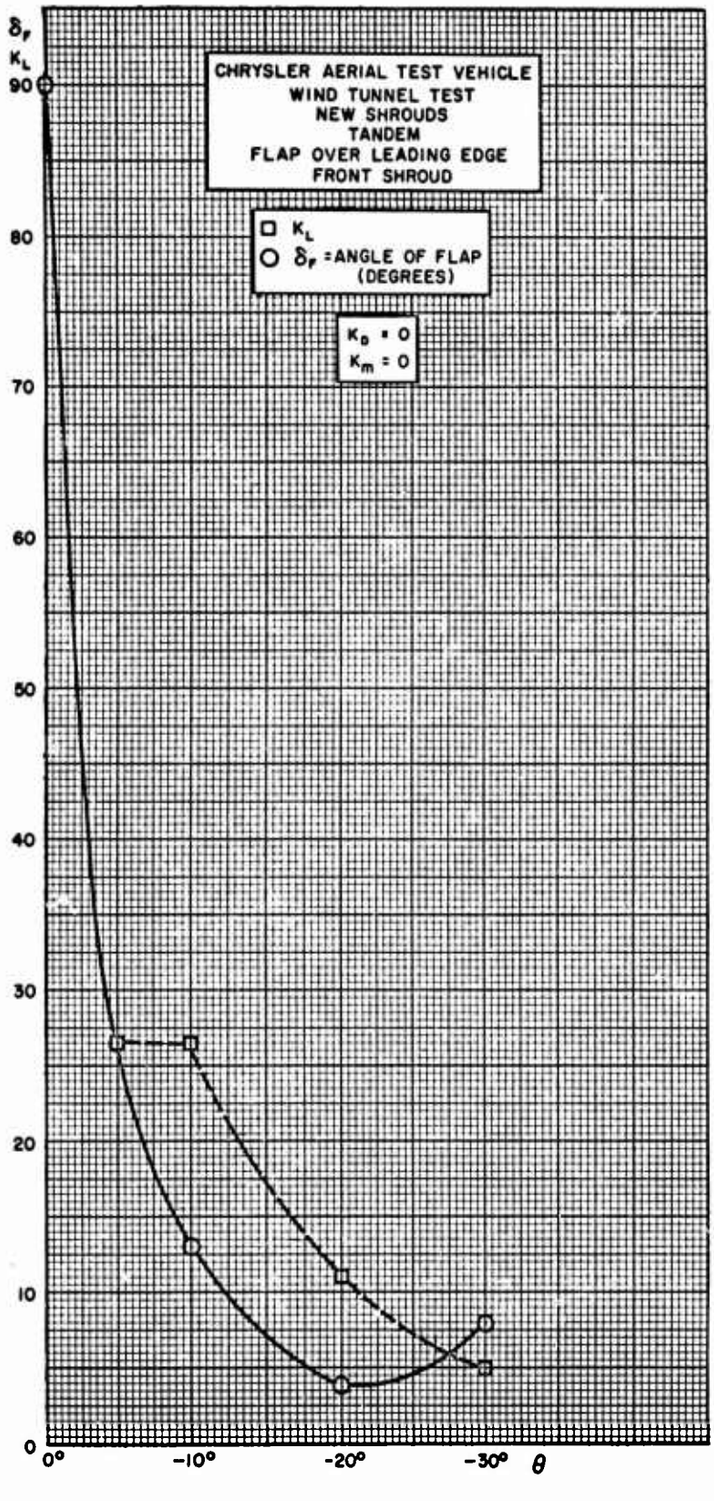

Figure 36. Graph of δ_F and K_L vs θ for the Model in Trim

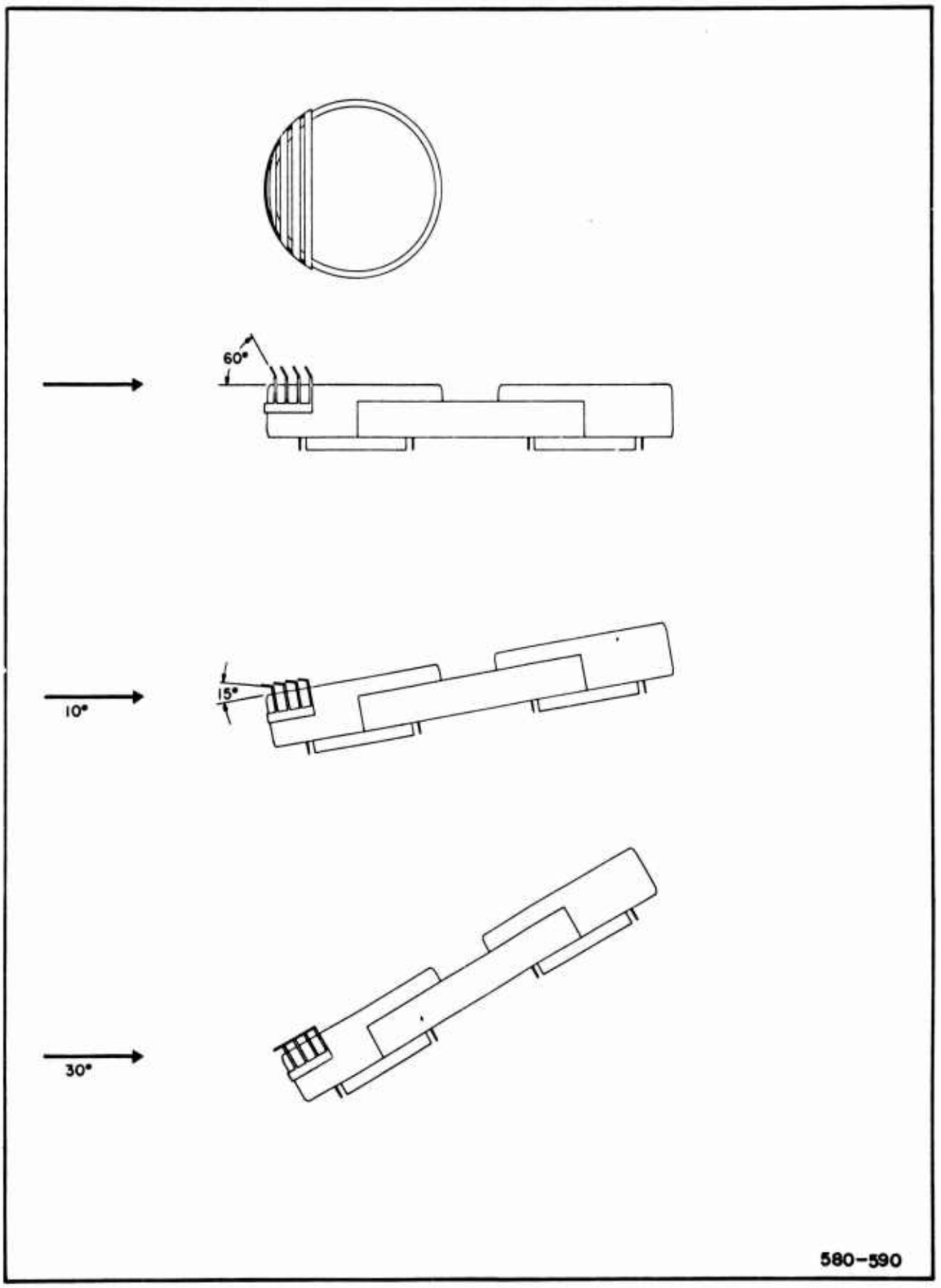

Figure 37. Schematic Drawing of the Model in Several Attitudes with Louvers as Trim Devices

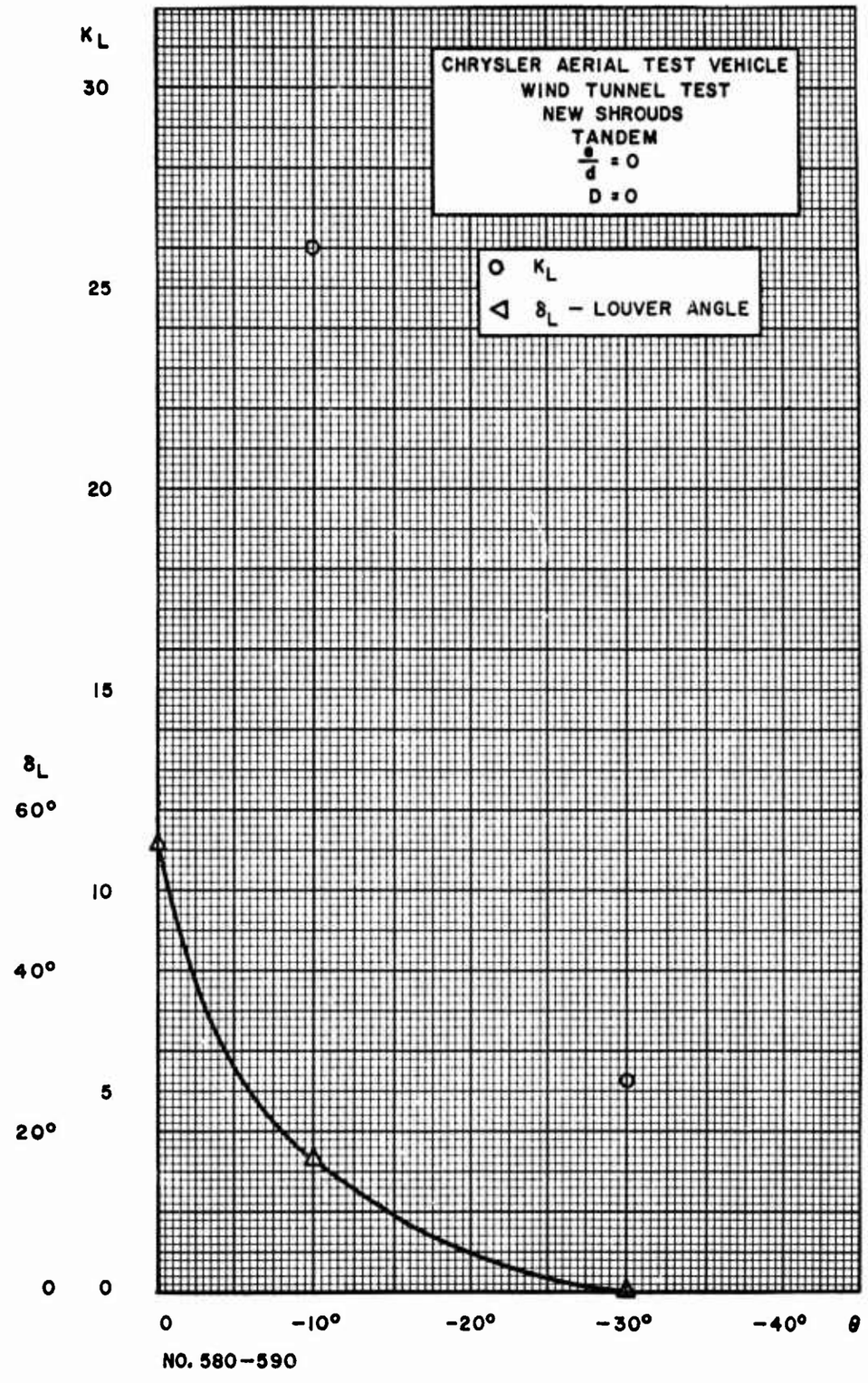

Figure 38. Graph of K_L and δ_L vs θ for e/d = O

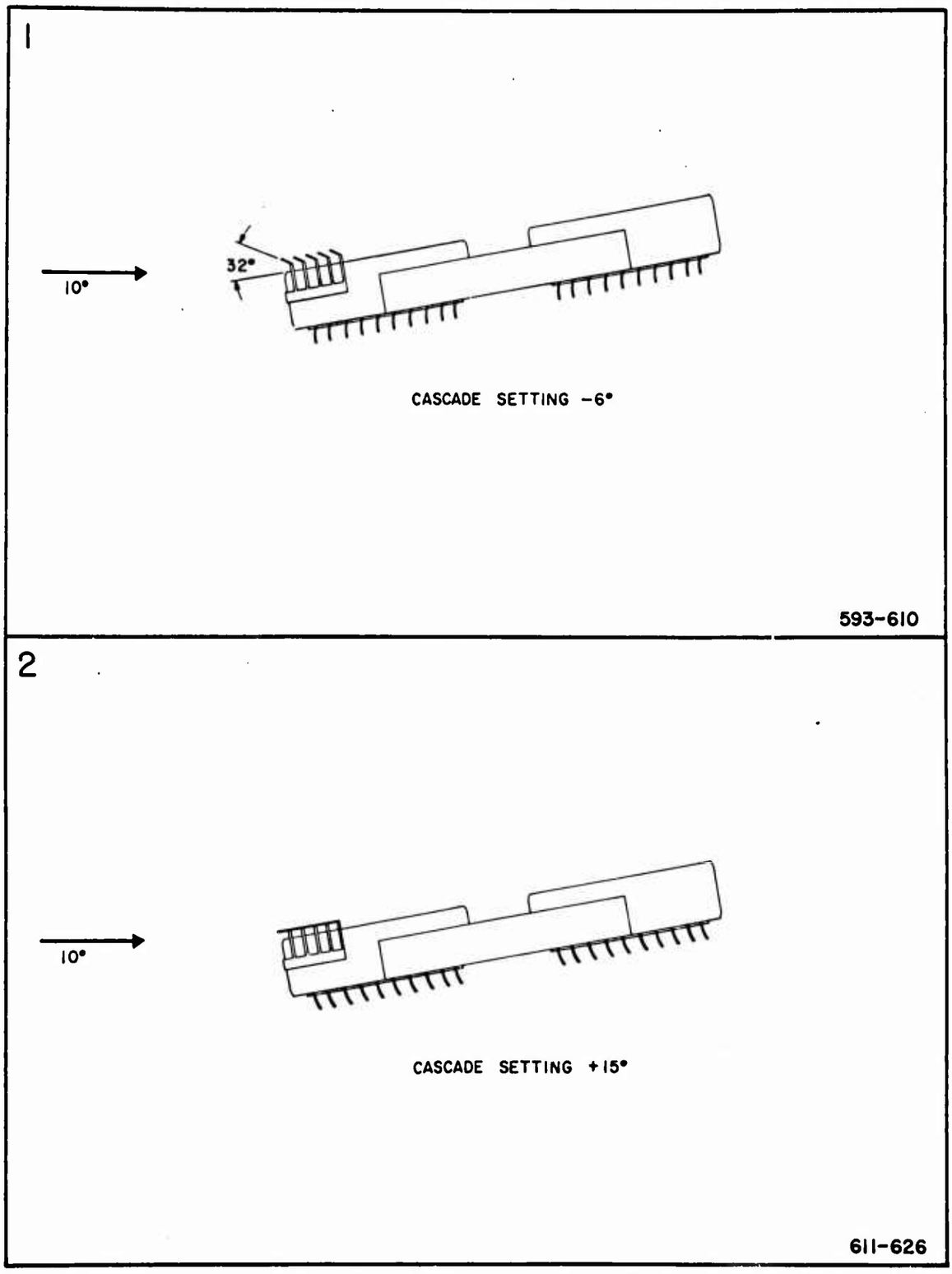

Figure 39. Schematic Drawing of Model in Typical Attitudes with Louvers and Cascades

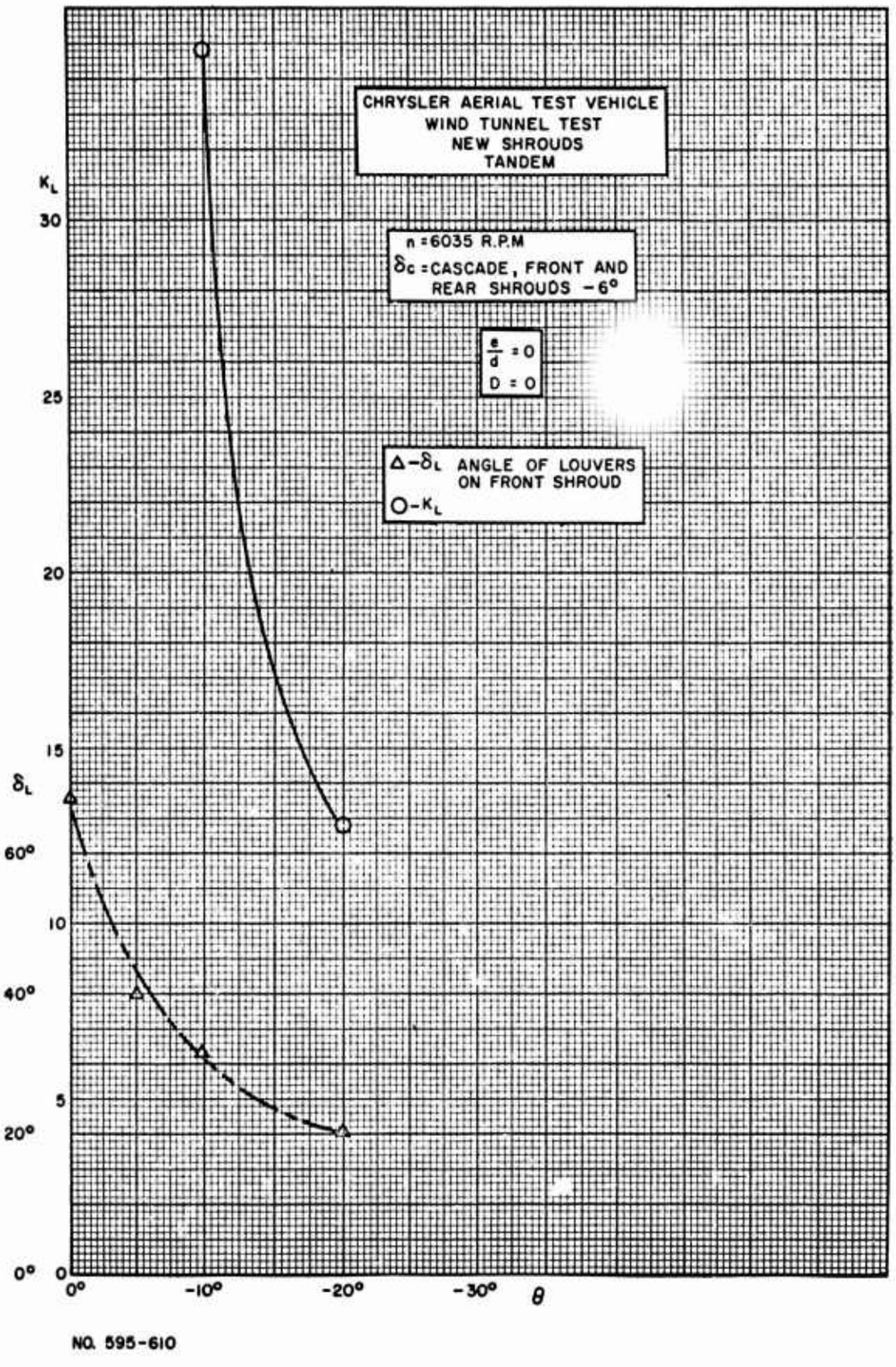

Figure 40. Graph of K_L and δ_L vs θ for e/d = 0 with Cascades

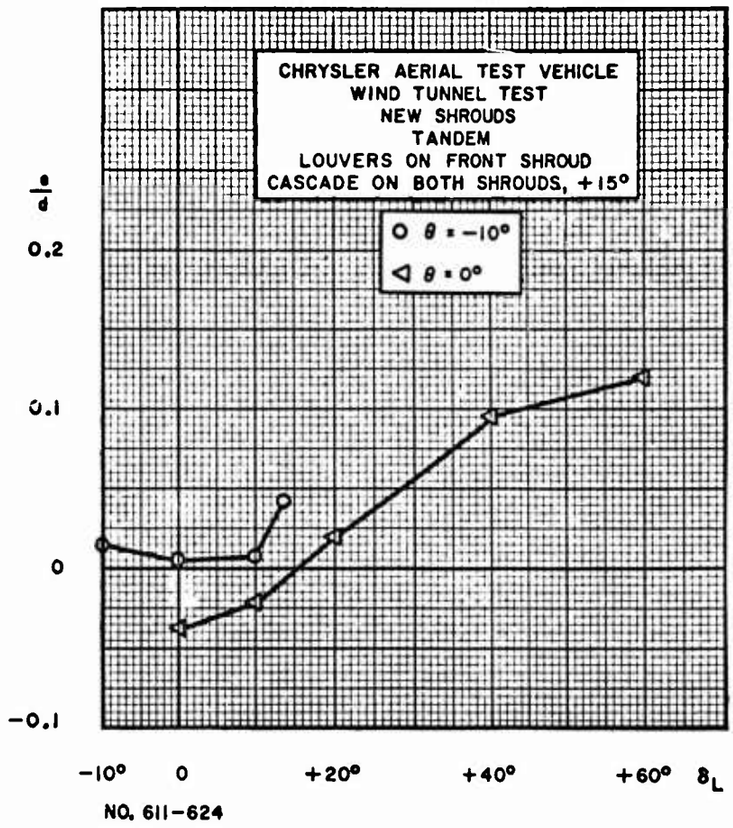

Figure 41. Graph of e/d vs δ_L for Model at 0° and -10° and δ_c

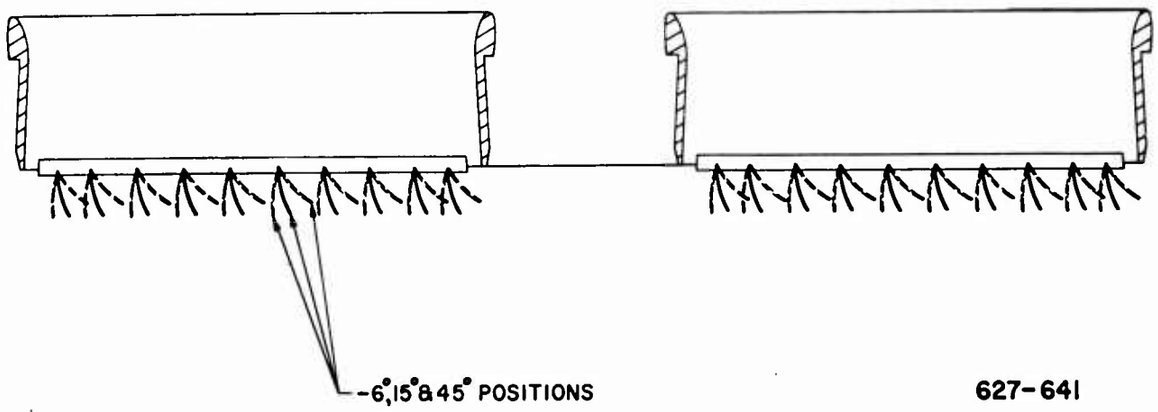

Figure 42. Cross-Section Drawing of Model Showing Various Cascade Settings

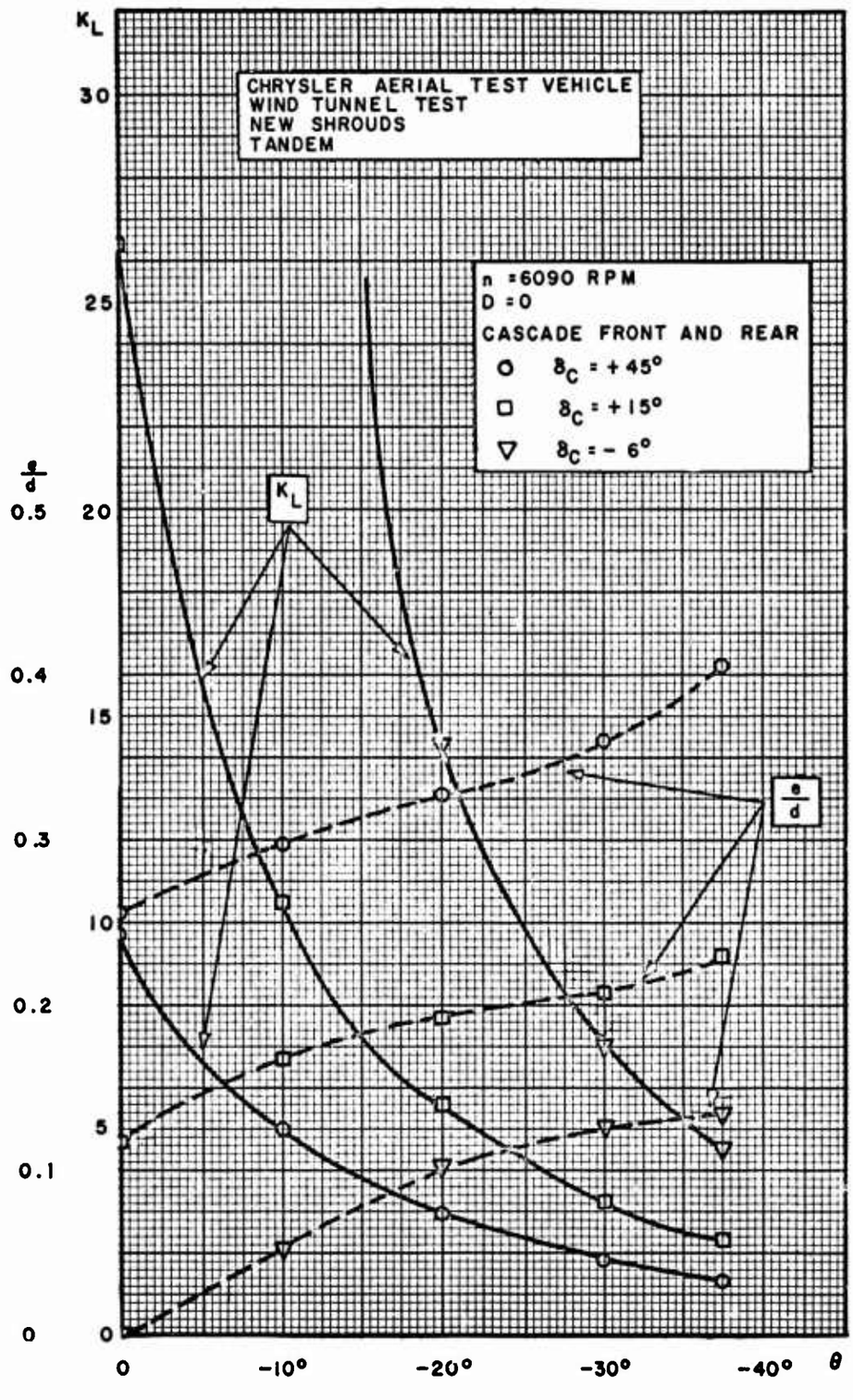

NO. 627-641

Figure 43. Graph of e/d and K_L vs θ for Three Cascade Settings (Cascades in front and rear)

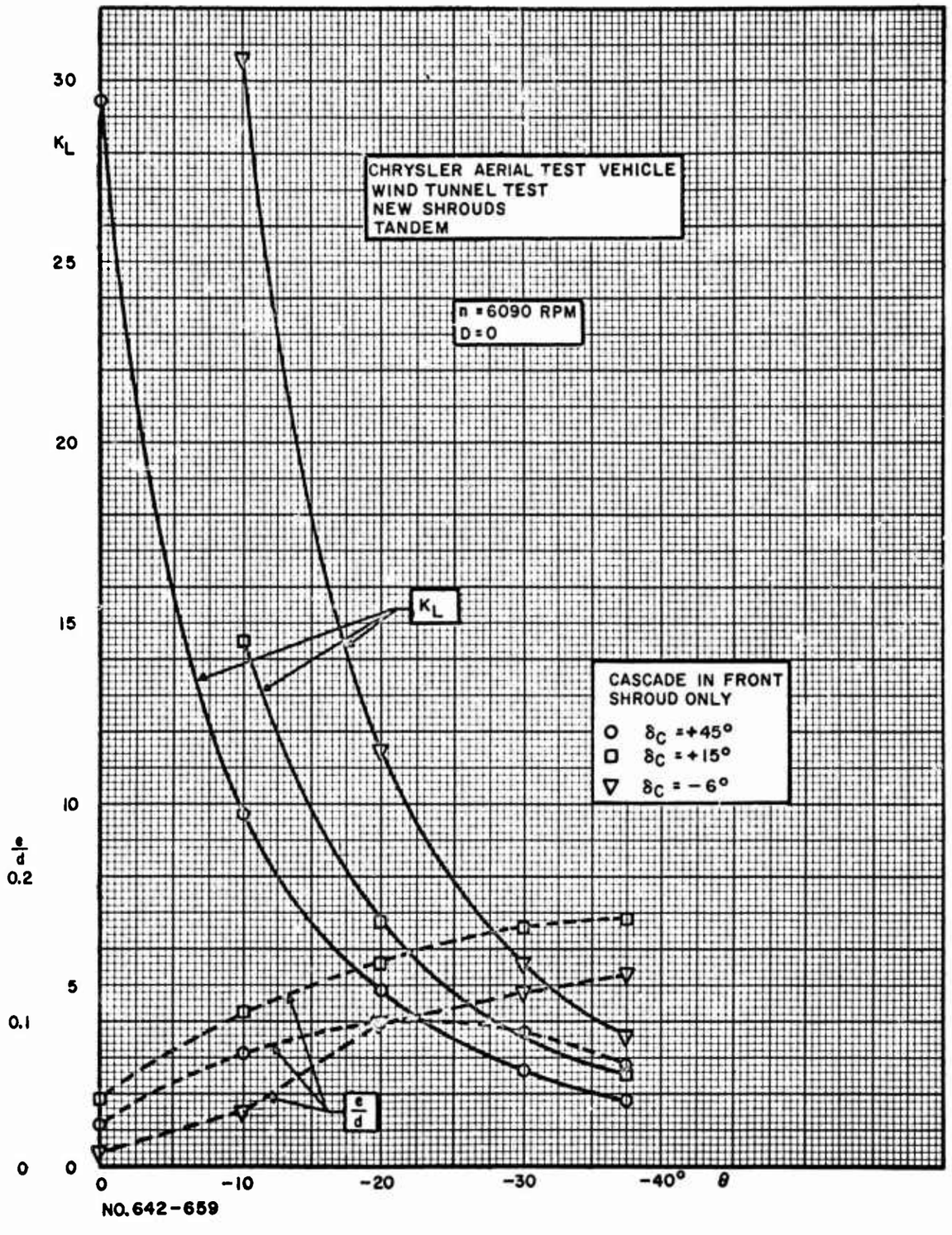

Figure 44. Graph of e/d and K_L vs θ for Three Cascade Settings (Cascades in front only)

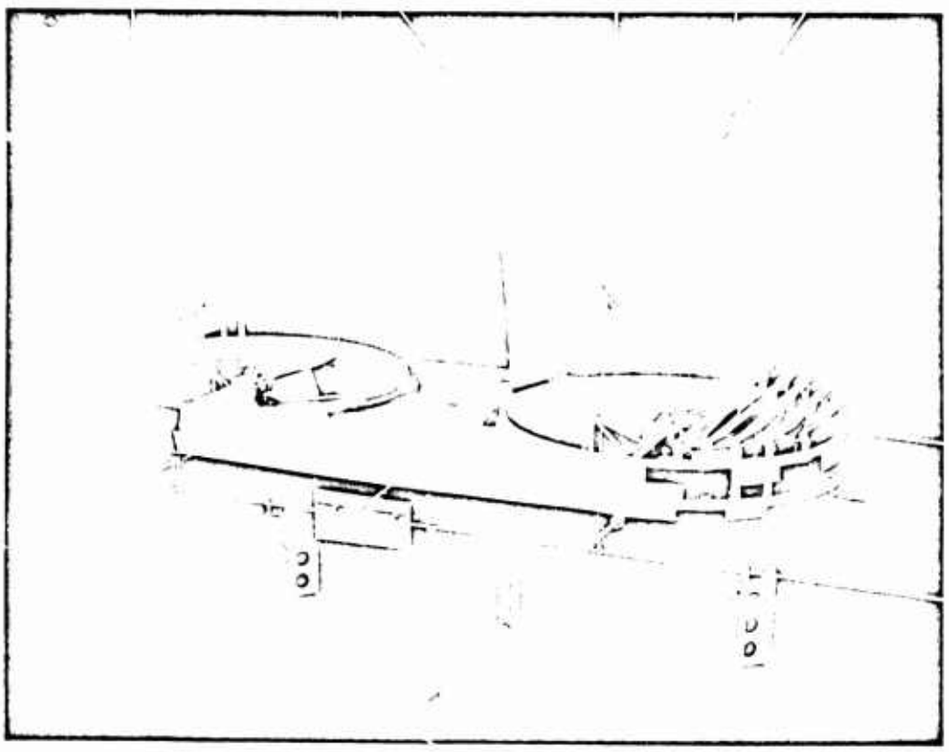

Figure 45. Photograph of Configuration Used to Obtain the Final Set of Performance and Stability Curves

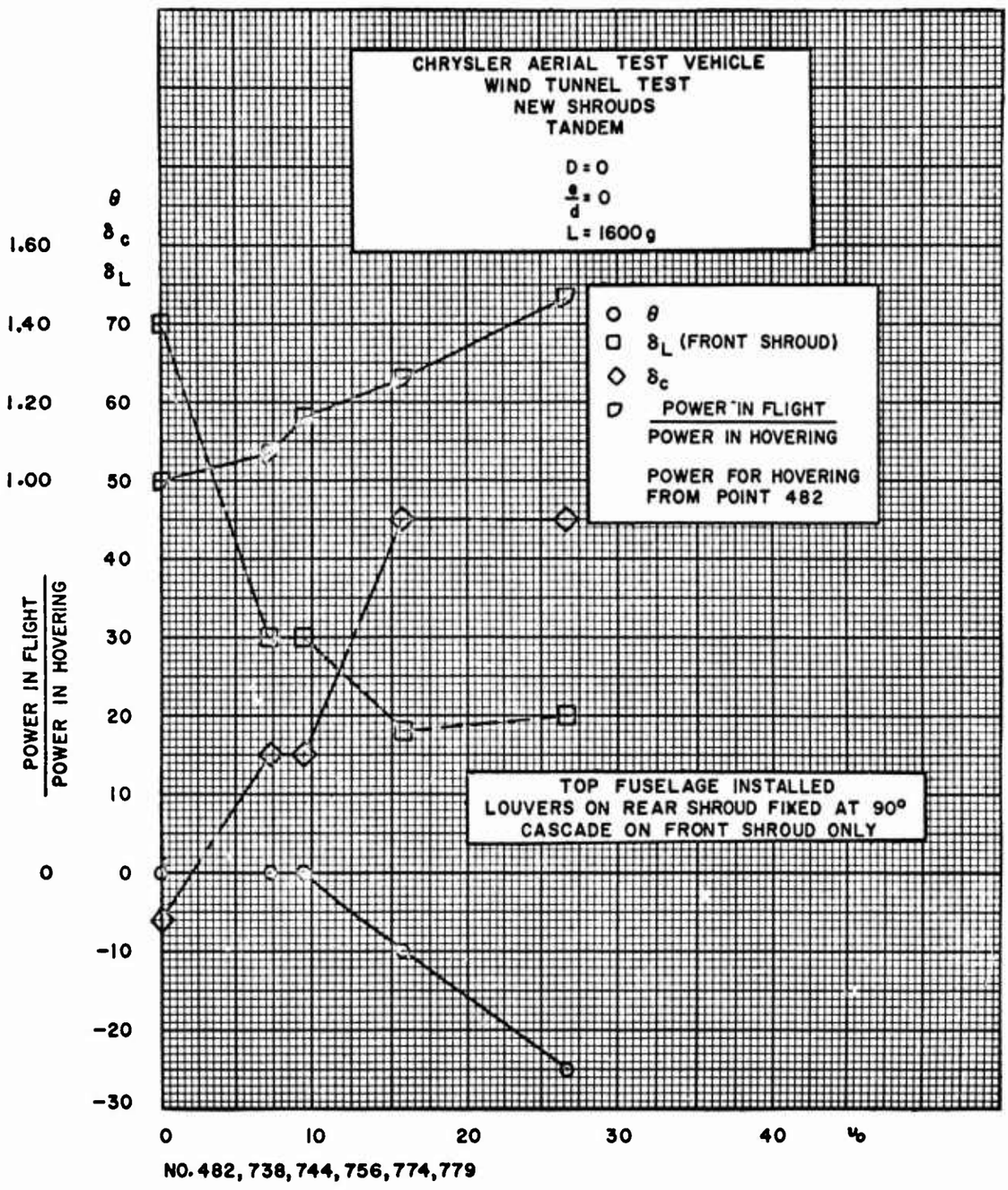

Figure 46. Graph of Performance Points for Transition from Hovering to Maximum Forward Speed

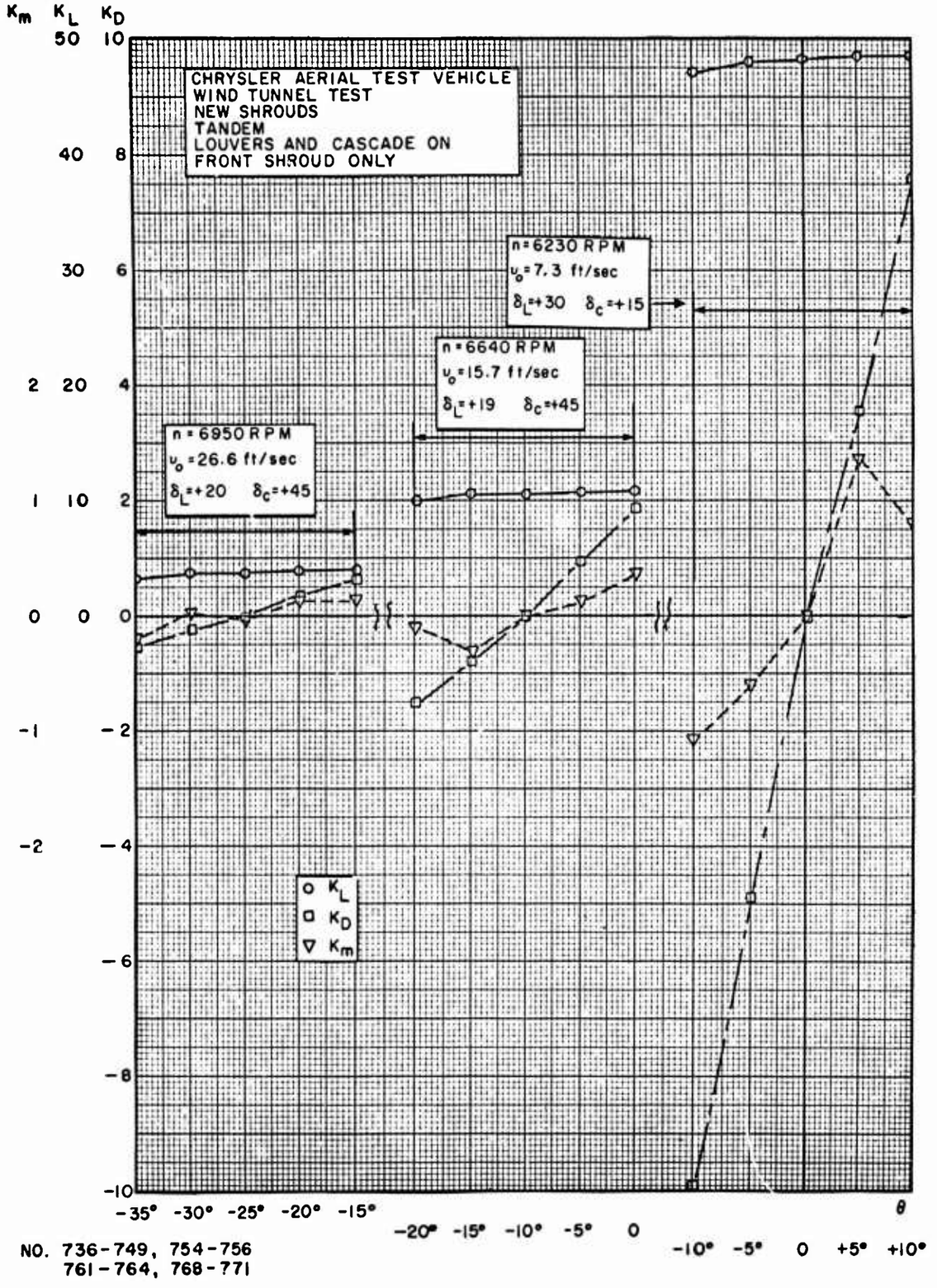

NO. 736-749, 754-756
761-764, 768-771

Figure 47. Graph of Variation of K_m, K_L, and K_D with θ for Stability Work

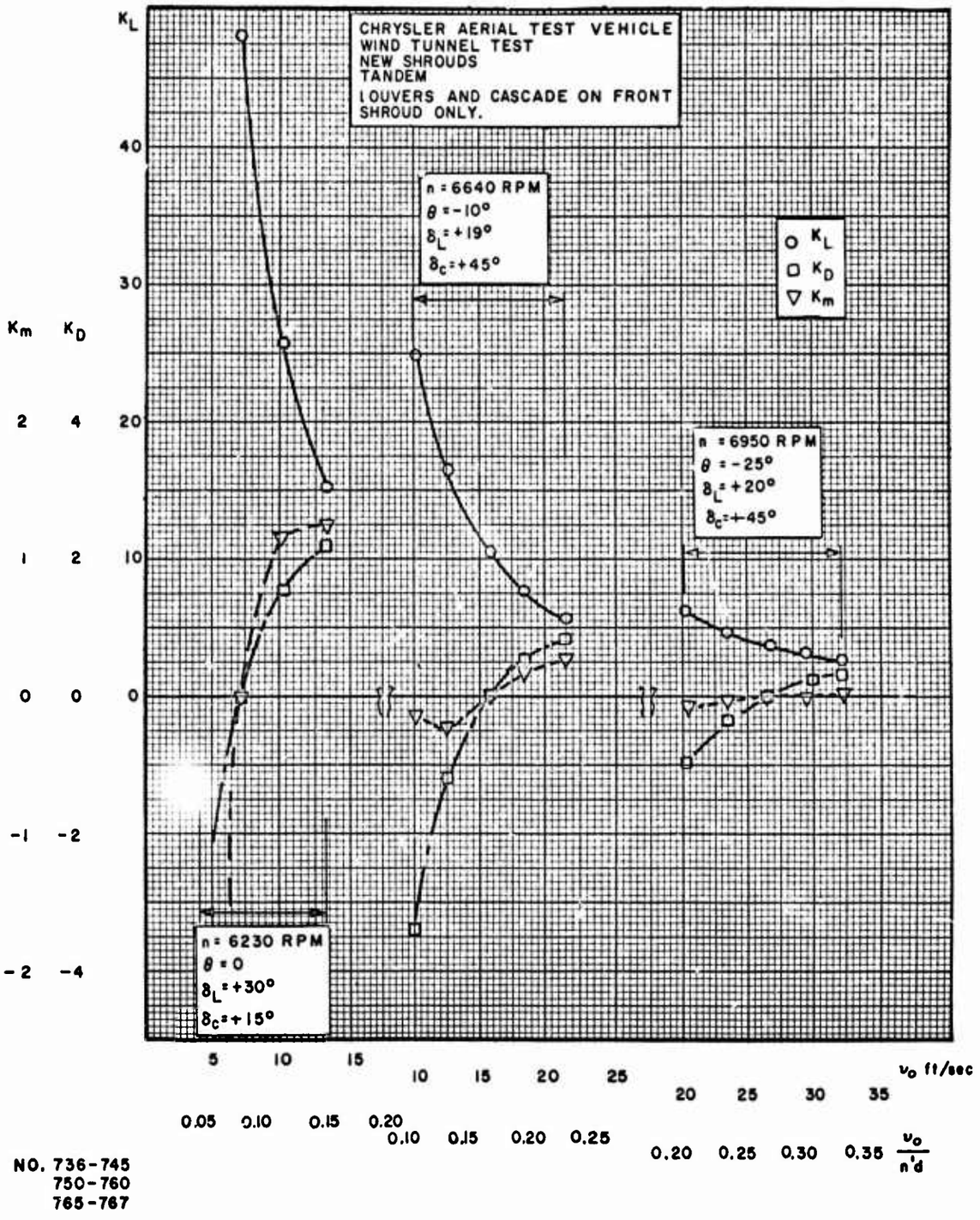

Figure 48. Graph of Variation of K_m, K_L, and K_D with v_o for Stability Work

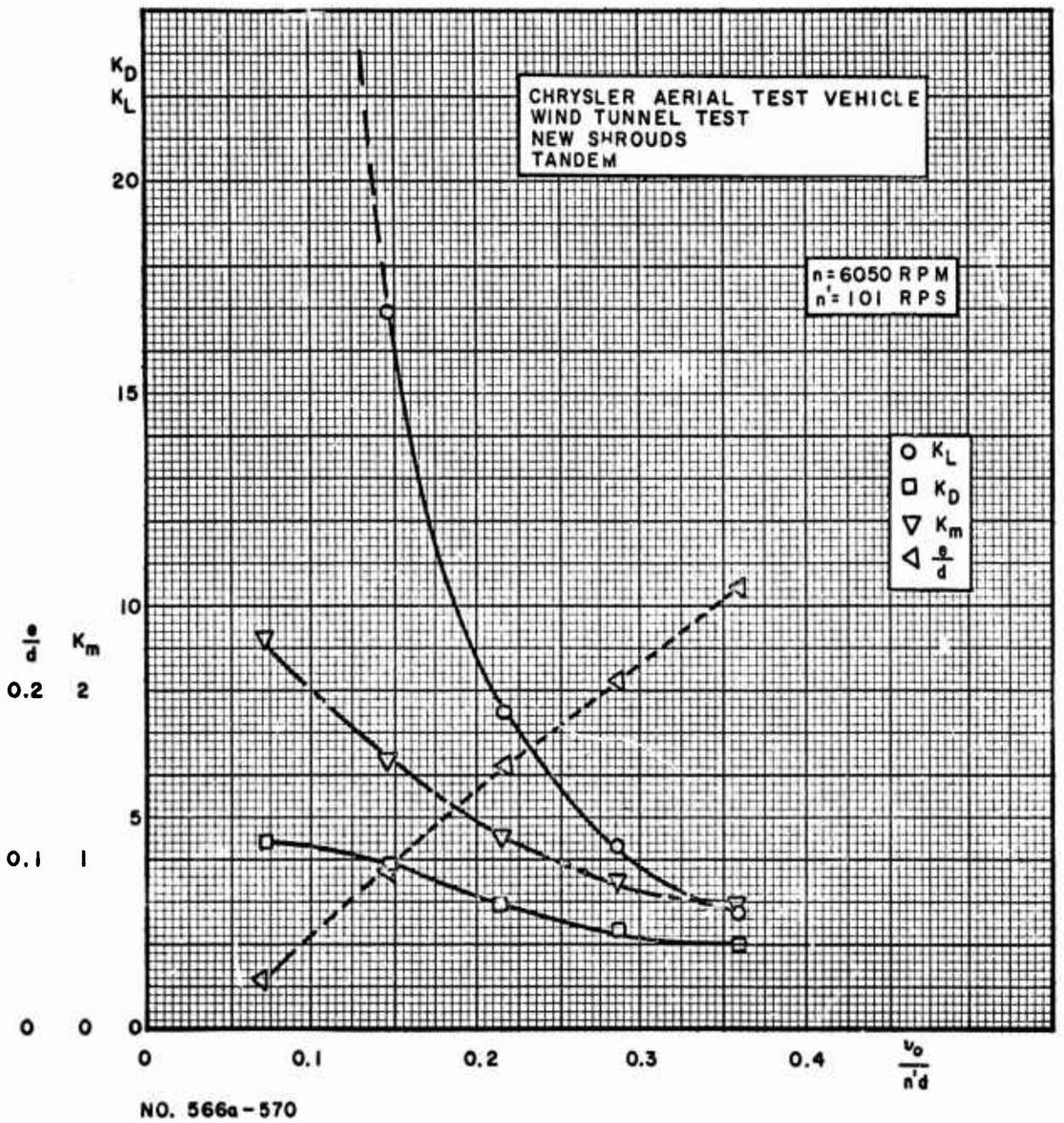

Figure 49. Graph of K_L, K_D, K_m, and e/d vs $v_o/n'd$ for $\theta = 0°$

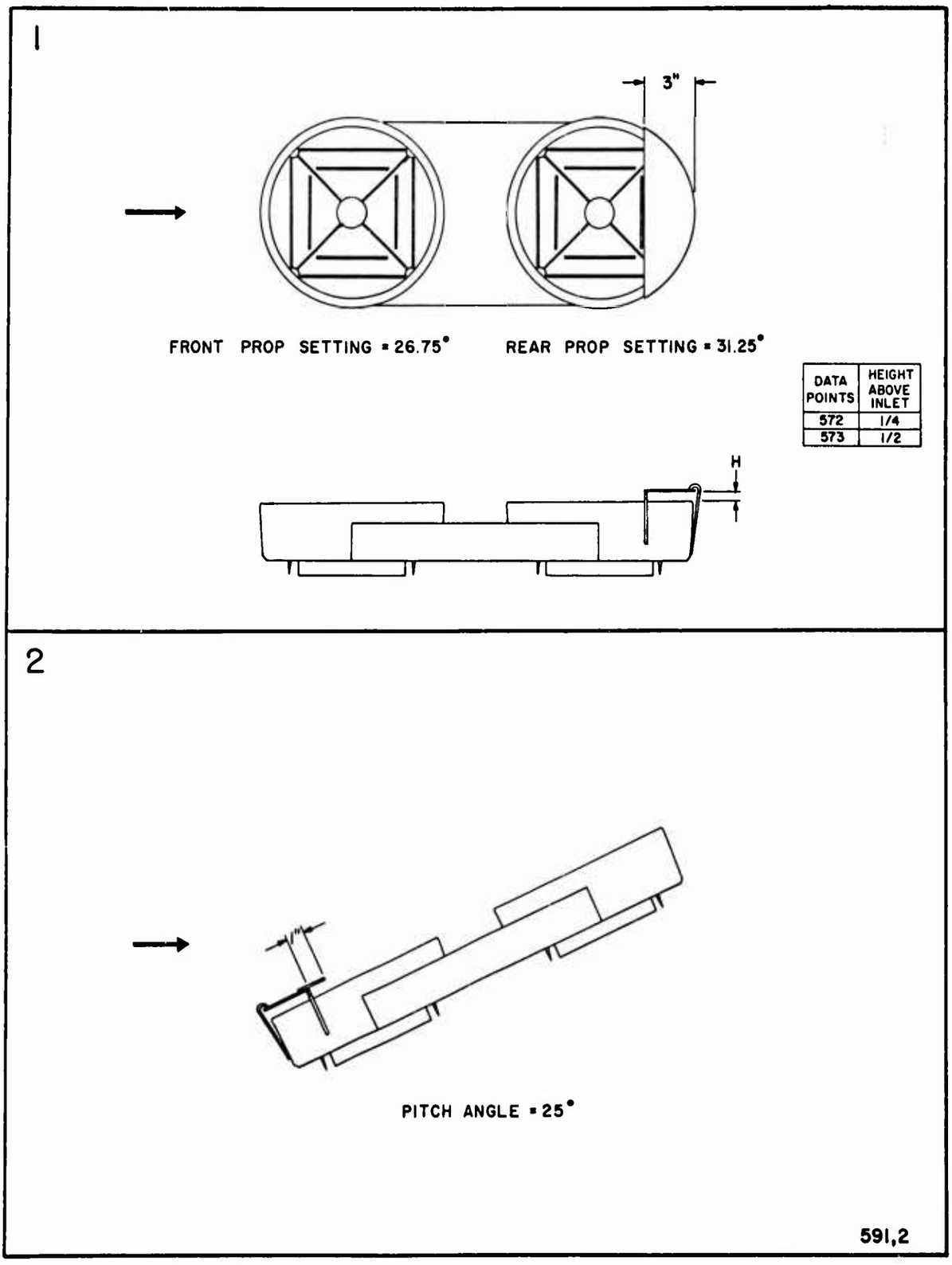

Figure 50.
(1) Schematic Drawing of Model in Hovering with Differential Pitch Adjustments
(2) Schematic Drawing of Model for 50% Overcontrol Tests

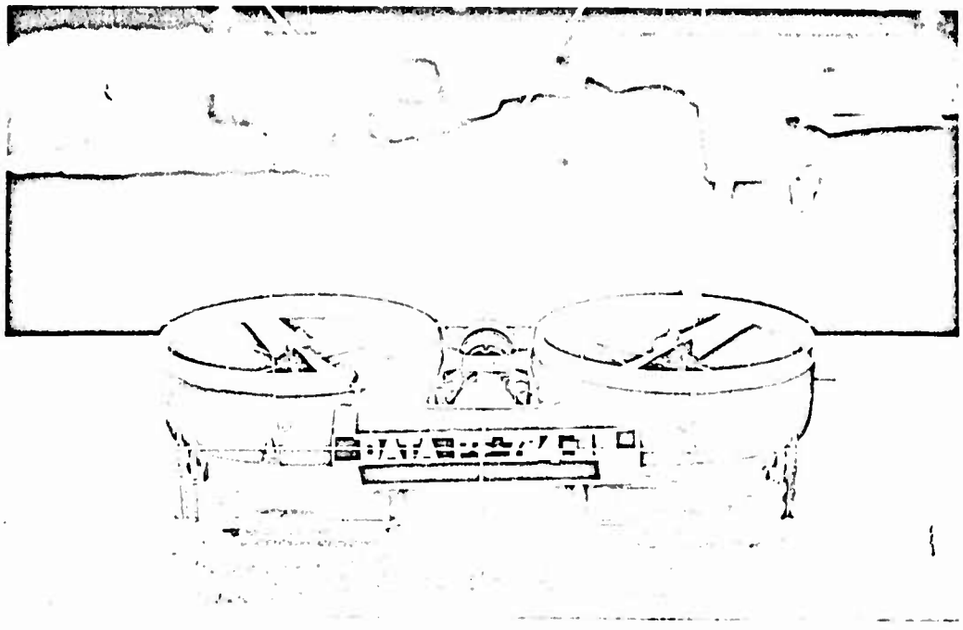

Figure 51. Photograph of Model During Ground Effects Tests

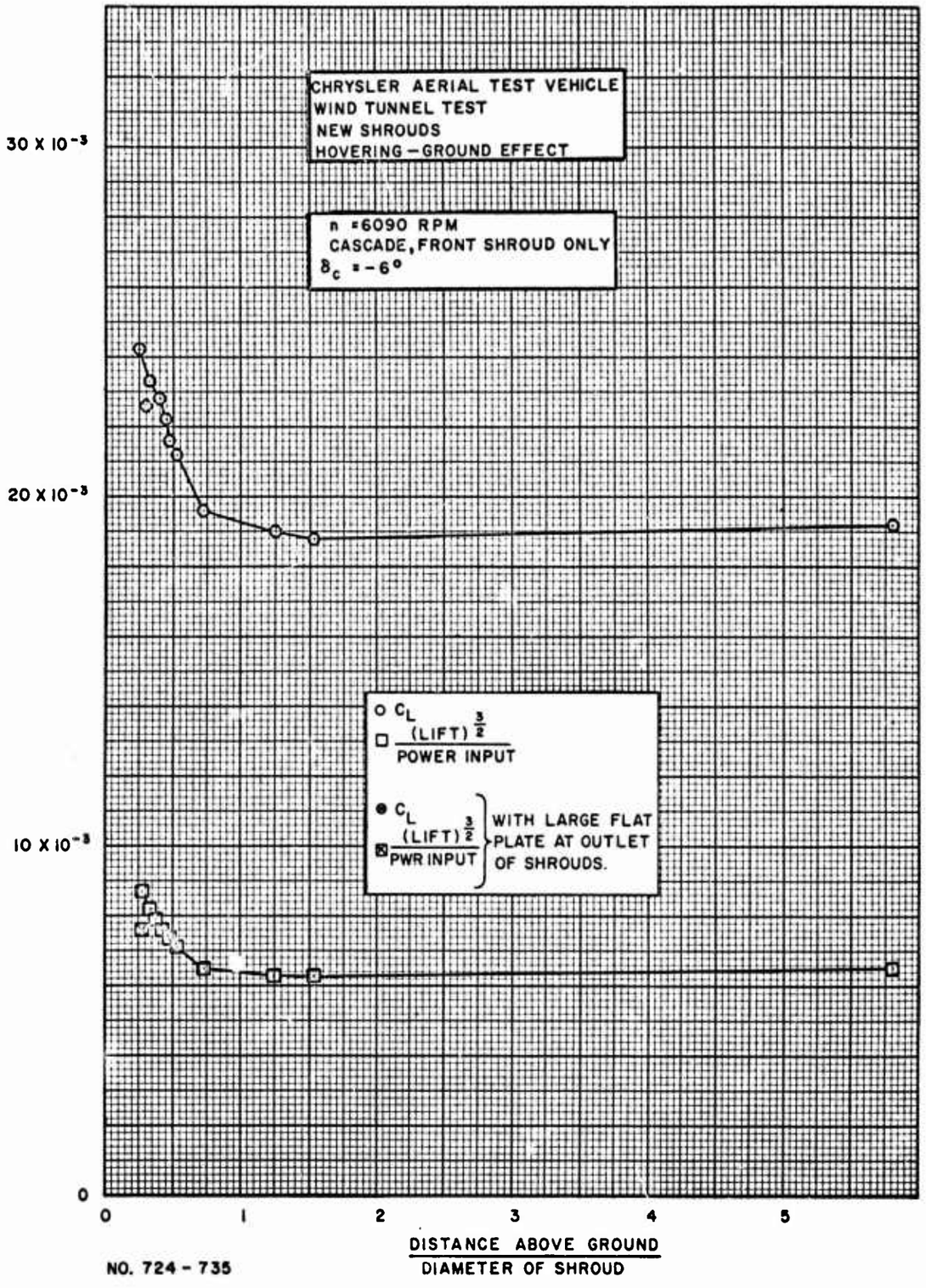

Figure 52. Graph of C_L and $\frac{\text{LIFT } 3/2}{\text{POWER INPUT}}$ vs Height Above Ground

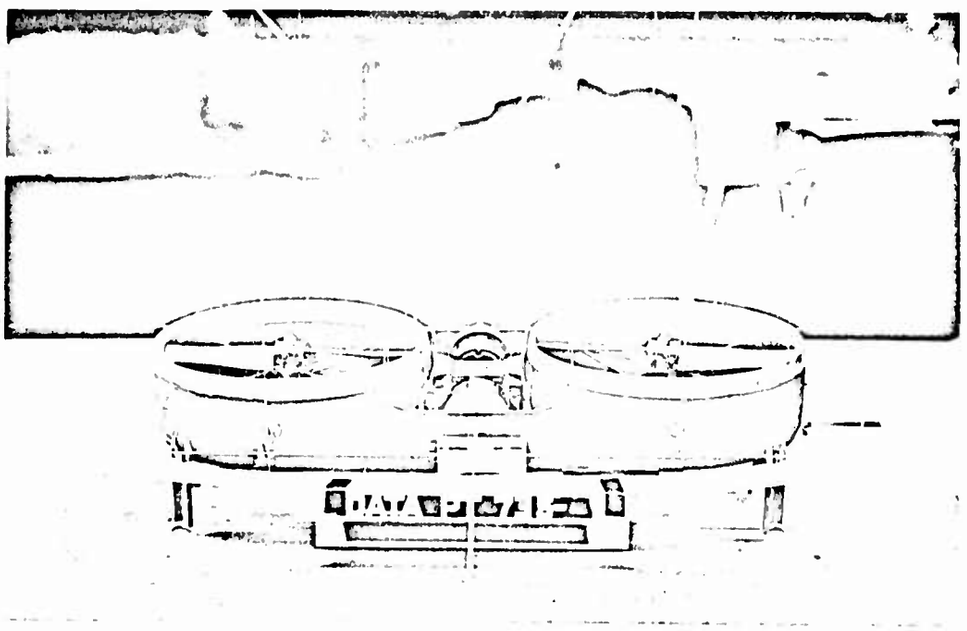

Figure 53. Photograph of Model During Ground Effects Tests with Flat Plate Added in Exit Plane

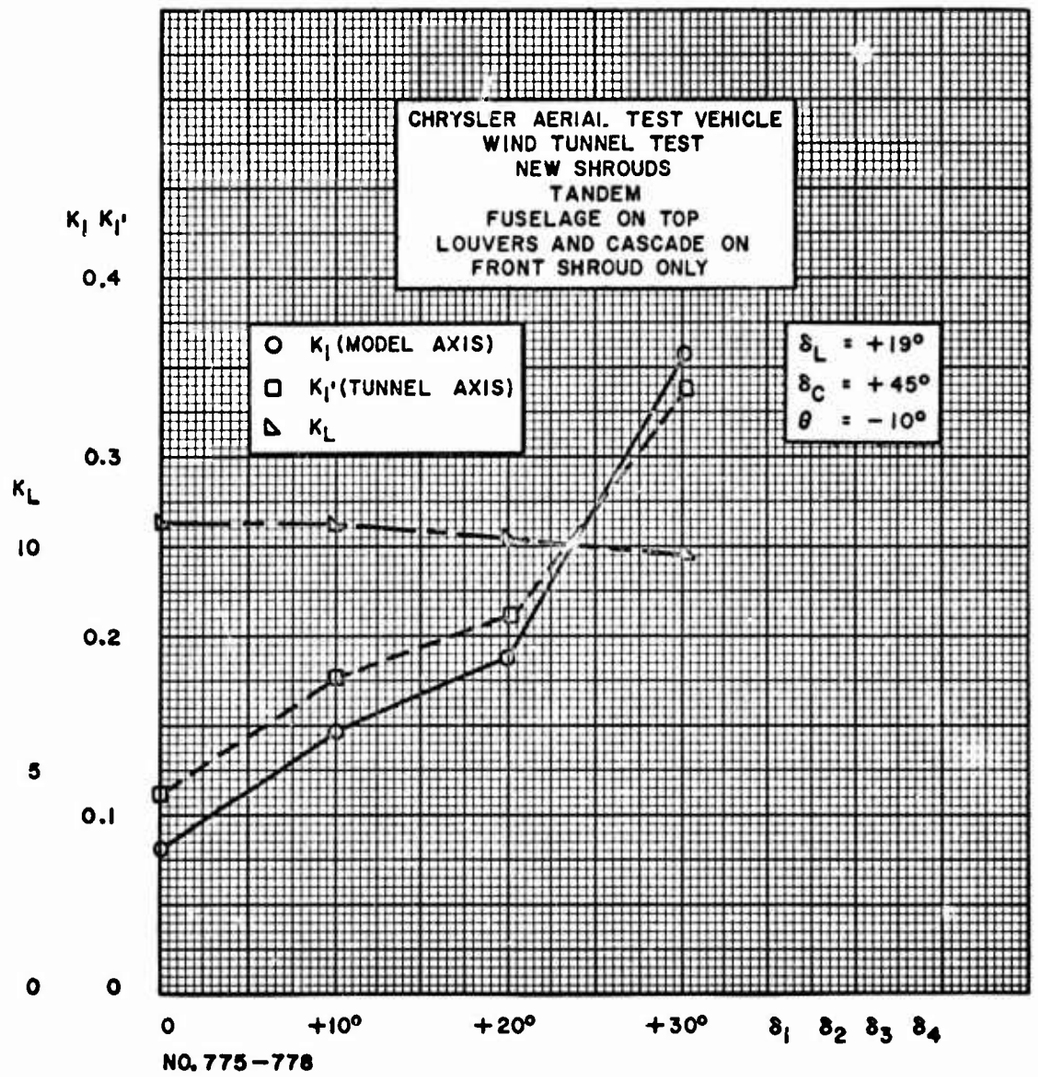

Figure 54. Graph of Roll Vane Effectiveness in Forward Flight

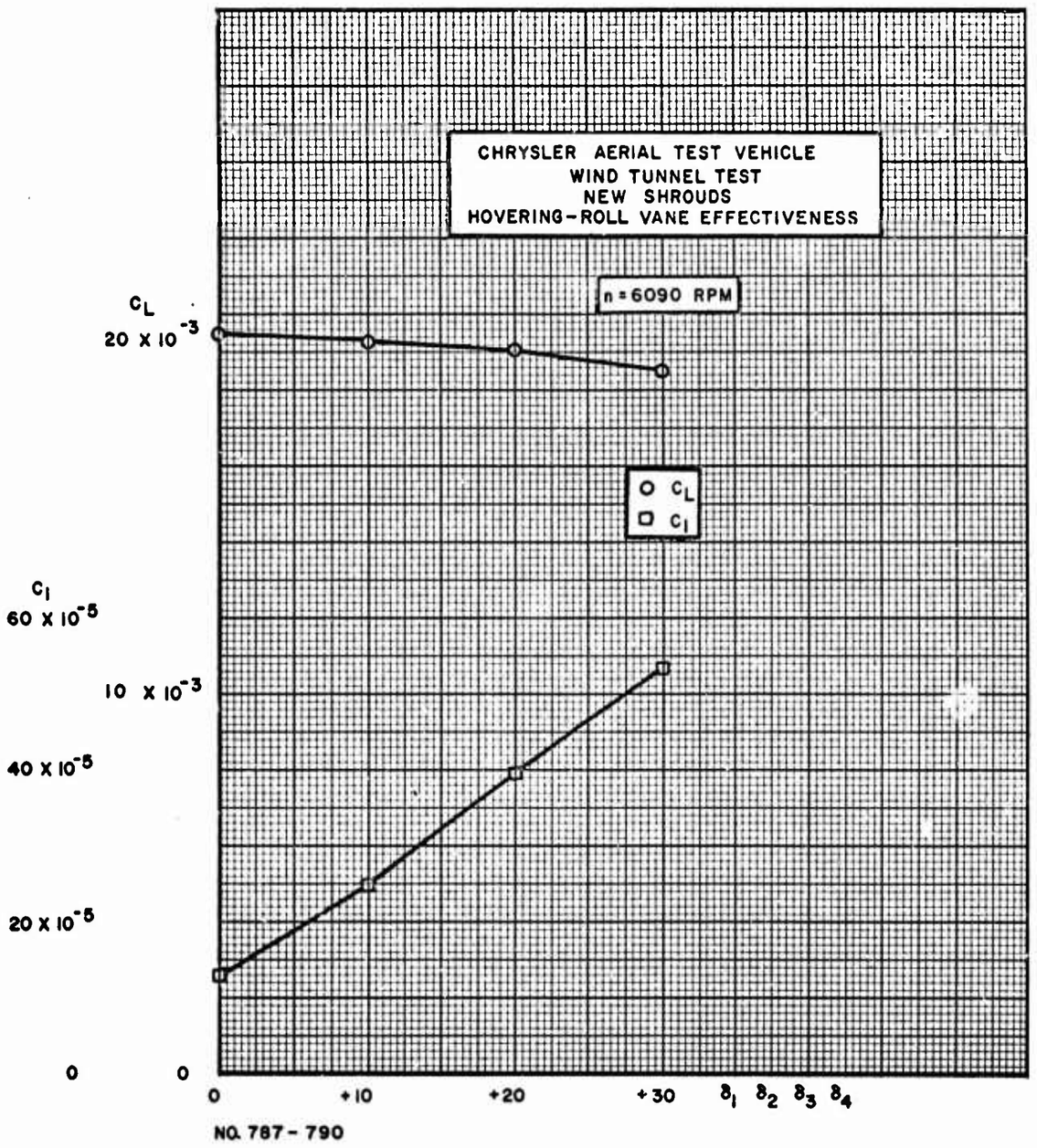

Figure 55. Graph of Roll Vane Effectiveness in Hovering Flight

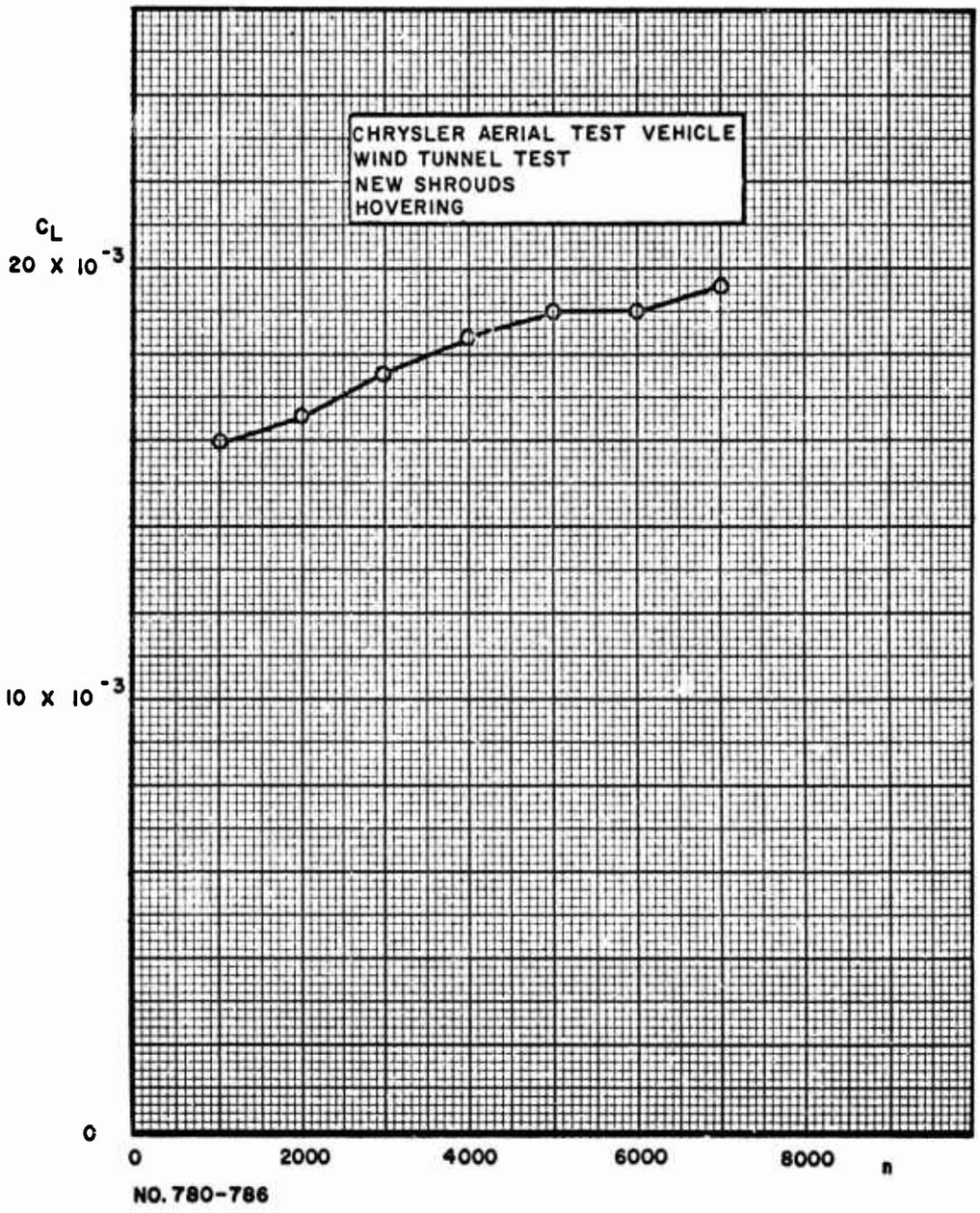

Figure 56. Graph of Variation of C_L with Speed

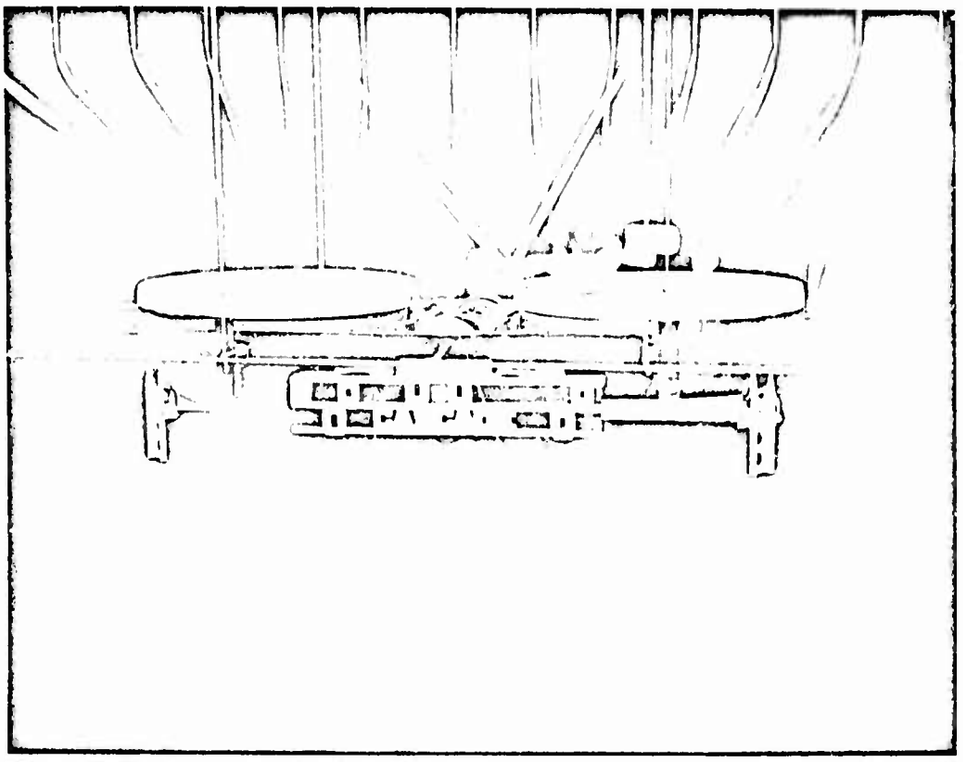

Figure 57. Flow Visualization Photograph

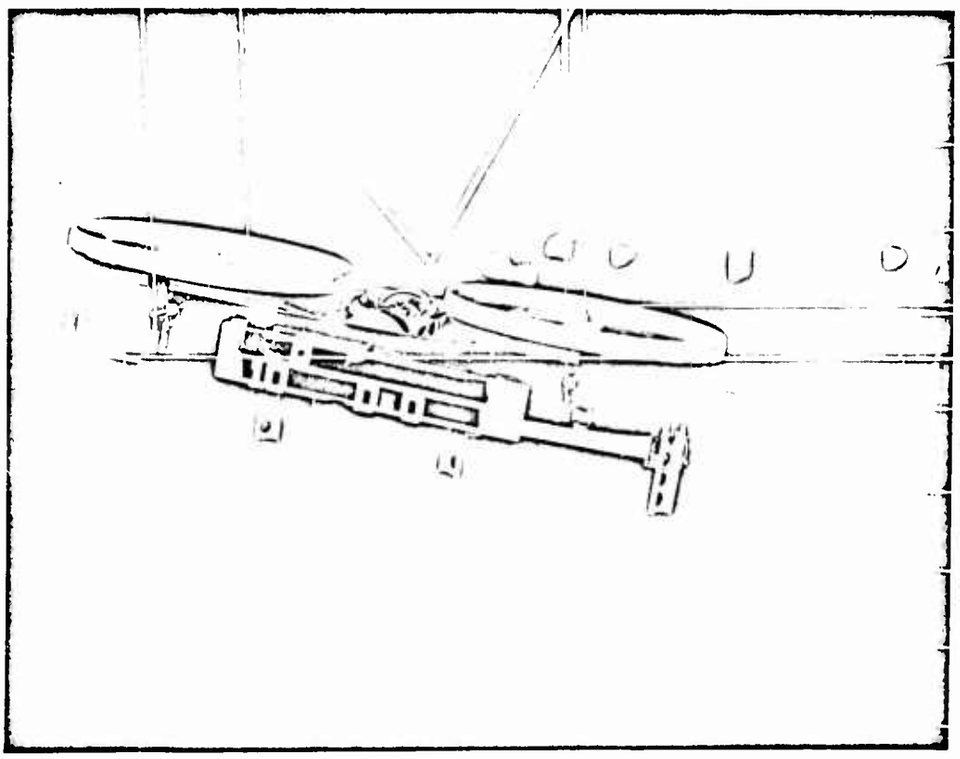

Figure 58. Flow Visualization Photograph

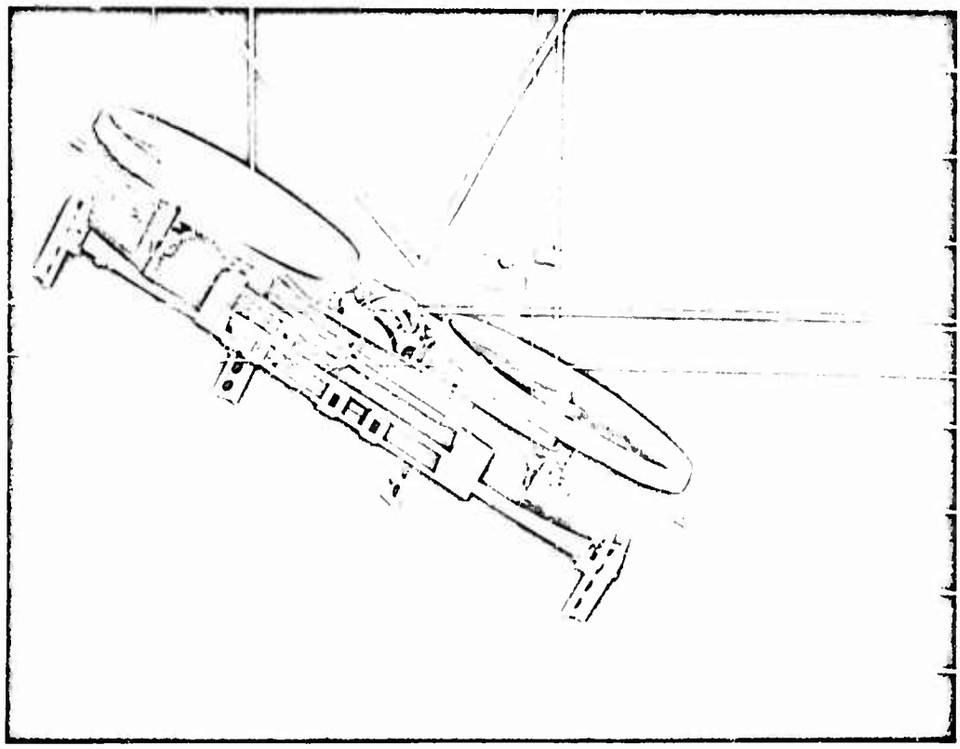

Figure 59. Flow Visualization Photograph

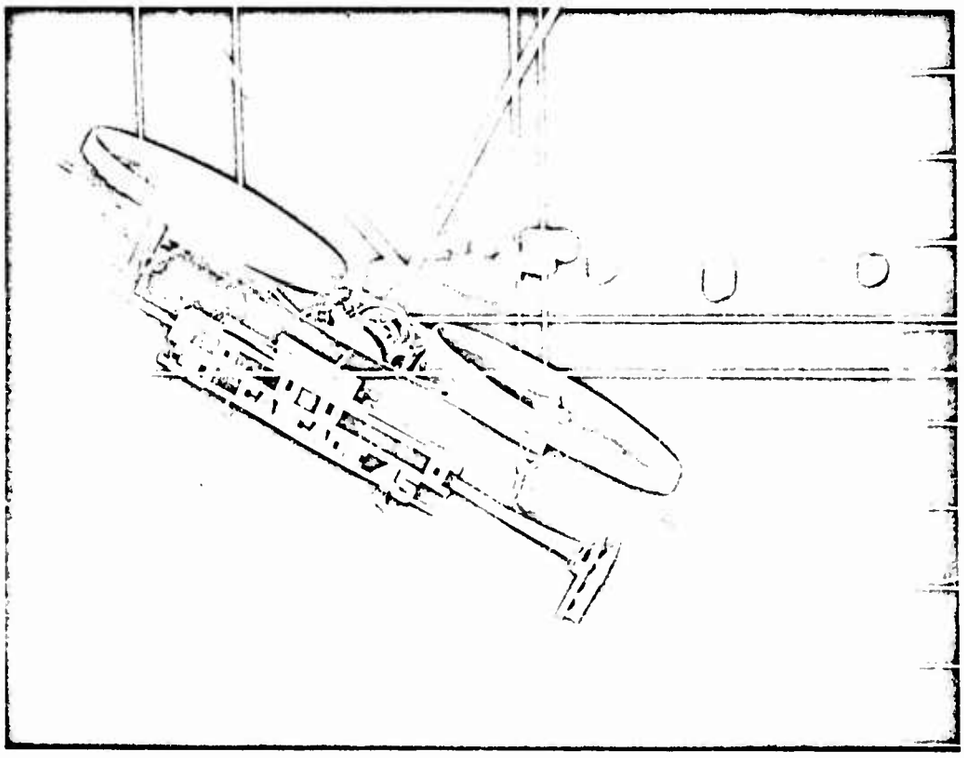

Figure 60. Flow Visualization Photograph

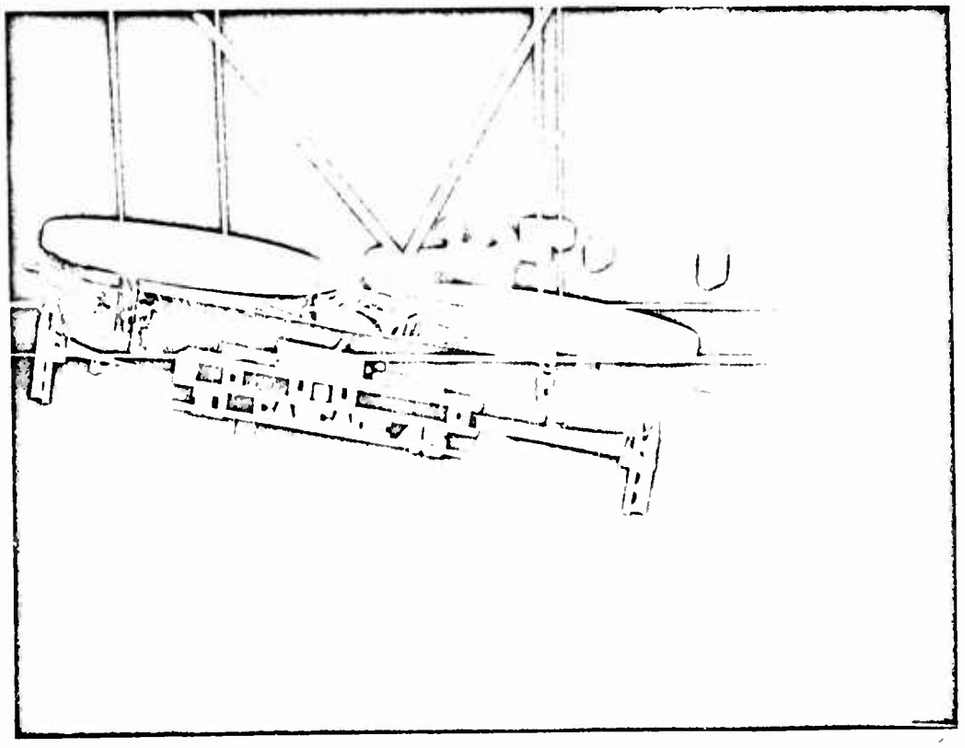

Figure 61. Flow Visualization Photograph

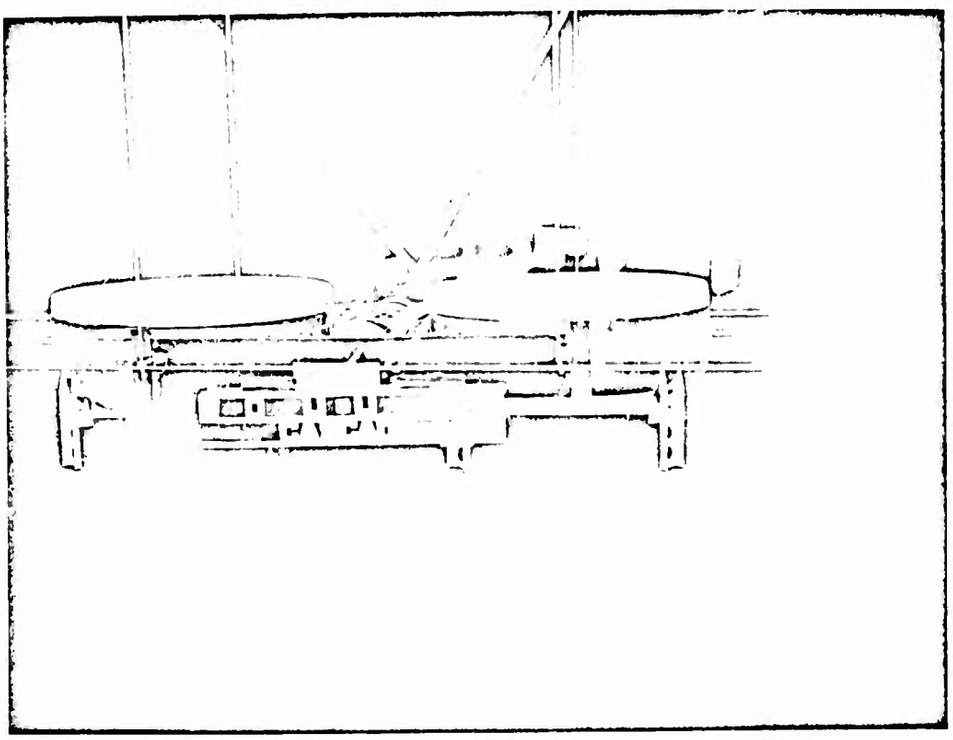

Figure 62. Flow Visualization Photograph

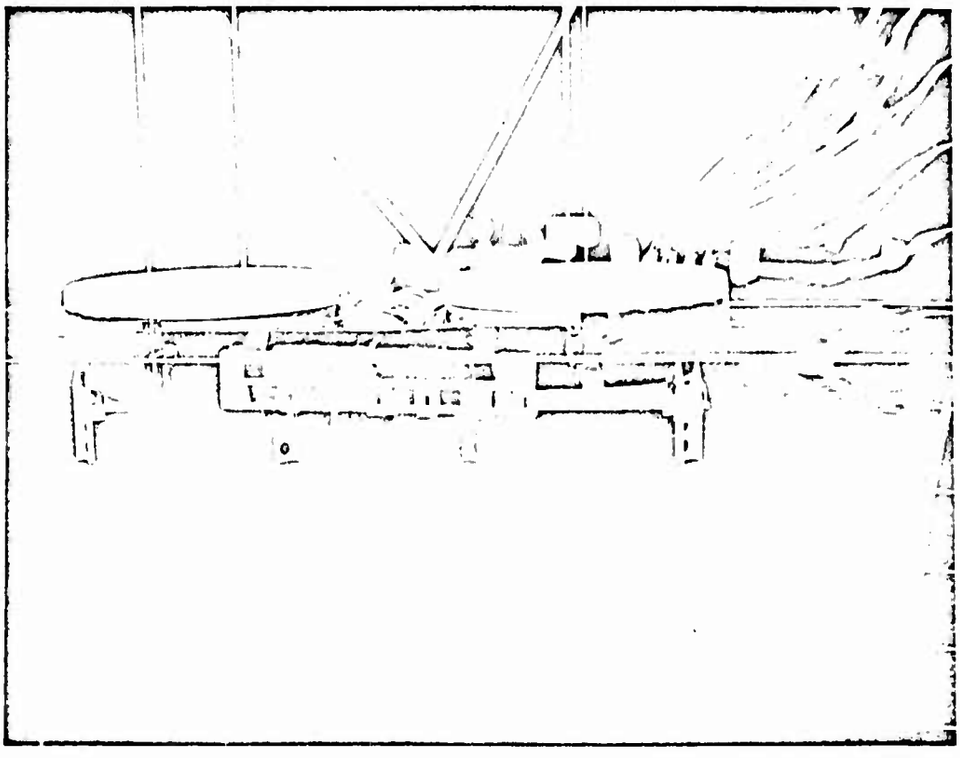

Figure 63. Flow Visualization Photograph

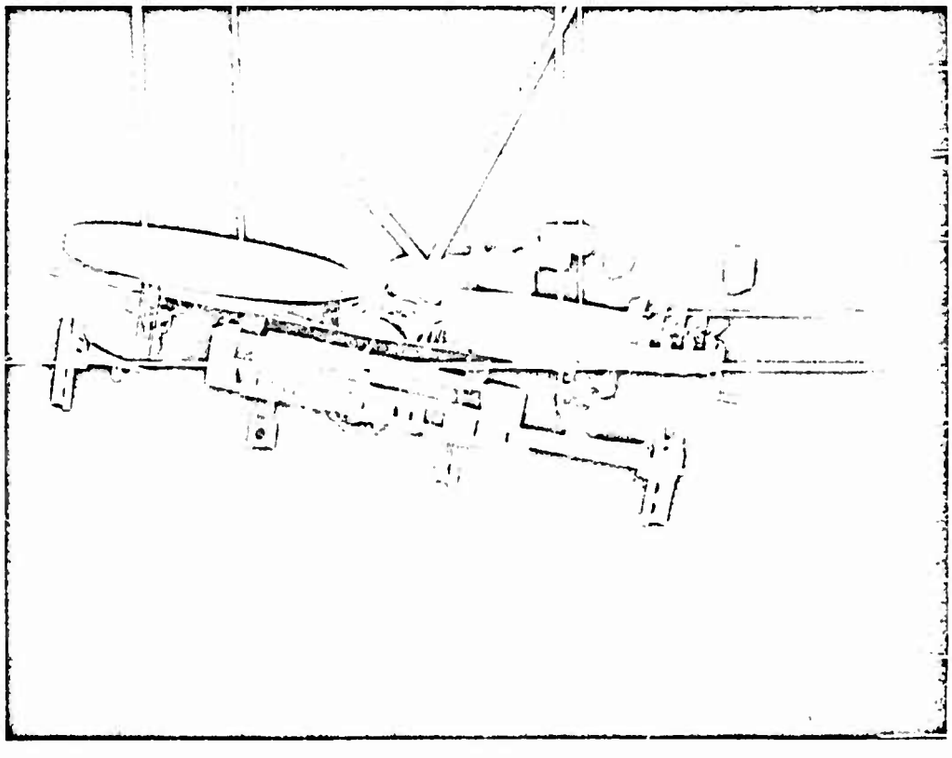

Figure 64. Flow Visualization Photograph

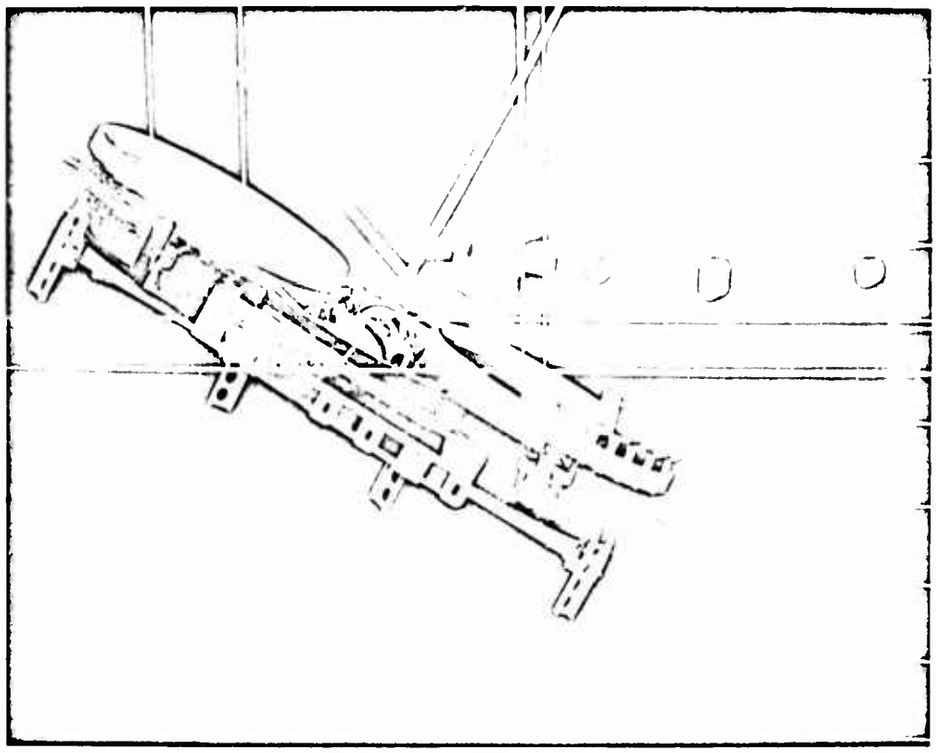

Figure 65. Flow Visualization Photograph